
UNIVERSITY
OF LATVIA

FACULTY OF PHYSICS, MATHEMATICS AND OPTOMETRY
INSTITUTE FOR MECHANICS OF MATERIALS

**Olga Bulderberga**

# DEVELOPMENT AND DETERMINATION OF PROPERTIES OF DAMAGE VISUAL INDICATION SYSTEM FOR POLYMER COMPOSITE STRUCTURES

Doctoral Thesis

Submitted for the degree of Doctor of Physics
Subfield of Physics of Materials

Supervisor:
Dr. Sc. Ing. Andrey Aniskevich

Riga, 2021

The doctoral thesis was carried out at the Chair of Institute for Mechanics of Materials, Faculty of Physics, Mathematics and Optometry, University of Latvia, from 2013 to 2020.

The thesis contains the introduction, 3 chapters, conclusions, and reference list.

Form of the thesis: dissertation in the field of Physics and Astronomy, Subfield of Physics of Materials.

Supervisor: Dr. Sc. Ing., LU MMI leading researcher, **Andrey Aniskevich**.

Reviewers:

1) **Māris Knite**, Dr.habil.phys, Professor, Riga Technical University;
2) **Jānis Vārna**, Professor, Luleå University of Technology, Sweden;
3) **Mikhail Zheludkevich**, Professor, University of Kiel, Germany;

The thesis will be defended at the public online session of the Doctoral Committee of Physics and Astronomy, University of Latvia, at 15.00 on February 26, 2021.

The thesis is available at the Library of the University of Latvia, Raiņa blvd. 19.

Chairman of the Doctoral Committee Dr. Phys Andris Jakovičs

Secretary of the Doctoral Committee Annija Stūrmane

**TABLE OF CONTENTS**

# ANNOTATION

The new concept of structural health monitoring of composite parts during its assembling, transportation, and exploitation is presented. This concept is realized by the developed Damage Visual Indication System (DVIS). The system visually indicates the place of a composite structure where the applied load has overcome the safety threshold. Proposed DVIS includes a mixture of microcapsules with dye and colour activator fixed on a fabric substrate. The idea of the DVIS is based on the approach, that shells of microcapsules burst under external loads, dye and colour activator get in contact, and chemical reaction is accompanied by the change of colour. For the fixation and protecting microcapsules from the unwanted effects of external factors, a polymer adhesive and lamination process were suggested.

The DVIS was studied out at different structural levels. At the micro-level, the mechanical and physical properties of an individual microcapsule were evaluated. At meso-level, the DVIS was studied as a whole element. The manufacturing technology of the DVIS was developed for different applications, and the durability of it was tested. At macro-level, composite structures containing the DVIS were investigated. The technology of the DVIS was developed in two ways, as the internal and as the external layers. The functionality of the DVIS was evaluated:

- The ability to be glued to the surface and to be replaced after using it for the DVIS as an external layer was confirmed;
- The effect of the integrated DVIS on the mechanical properties of the composite was evaluated;
- Kinetics of colour change after the applied load, the effect of storage temperature and durability of the DVIS were evaluated.

Presented approach for GFRP composites will allow to minimise the inspection time and simplify non-equipment permanent inspection of large surfaces, thus improving exploitation safety and simplifying the structural health monitoring process of polymer composites in constructions.

The doctoral thesis of Olga Bulderberga is presented in the form of dissertation in the field of Physics and Astronomy, Subfield of Physics of Materials.

The results of the research were published in 3 peer-reviewed scientific papers in journals indexed by Scopus, 8 international conference proceedings, and 2 patent applications. The results of the work were presented at 14 international conferences by the author. The thesis consists of an introduction, 3 chapters, and conclusions. The list of references contains 146 papers and internet sources.

Keywords: damage visual indication, polymer composites, structural health monitoring, microcapsules.

# ANOTĀCIJA

Darbā tiek piedāvāts jauns koncepts tehniskā stāvokļa monitoringam kompozītmateriāla elementiem to izgatavošanas, transportēšanas un ekspluatācijas laikā. Koncepta realizācijai tika izstrādāta 'Bojājumu Vizuālās Indikācijas Sistēma' (BVIS). Šī sistēma sastāv no auduma pamatnes, kas piesūcināta ar krāsvielu mikrokapsulu maisījumu, krāsu aktivatoru un aizsarg adhesīvu uz polimēra bāzes. Adhesīvs notur mikrokapsulas uz virsmas un aizsargā tās no apkārtējo faktoru ietekmes. BVIS darbības princips ir šāds: no pieliktas ārējas slodzes mikrokapsulu apvalks tiek sabojāts, to saturs nonāk kontaktā un ķīmiskās reakcijas rezultāta notiek krāsu izmaiņa. Šādi pieliktas slodzes vieta var tikt vizuāli identificēta.

BVIS tika pētīts dažādos līmeņos. Mikro līmenī tika noteiktas individuālo mikrokapsulu fizikālās un mehāniskās īpašības. Meso līmenī BVIS tika pētīts kā vesels elements. Tika izstrādāta BVIS izgatavošanas tehnoloģija, kas būs derīga dažādiem pielietojumiem, kā arī tika novērtēta BVIS izturība. Makro līmenī tika pētītas BVIS kompozītu struktūras. Pētījuma gaitā tika izstrādāti divi BVIS tehnoloģijas varianti: ar BVIS kā ārējo un kā iekšējo slāni. Pārbaudot BVIS funkcionalitāti tika noteikta:

- iespējamība pielīmēt BVIS kā ārējo slāni un pēc lietošanas to noņemt.
- kā BVIS ietekmē kompozīta mehāniskās īpašības, ja tas ir novietots kā iekšējais slānis.
- BVIS krāsu izmaiņas kinētika pēc pieliktas slodzes, uzglabāšanas temperatūras ietekme uz BVIS un BVIS izturība.

Piedāvātais BVIS koncepts ļaus samazināt ar stikla šķiedrām armēto kompozītmateriālu tehniskā stāvokļa pārbaudes laiku, vienkāršos lielu virsmu pārbaudi bez aparatūras. Šādi tiks paaugstināta ekspluatēšanas drošība un vienkāršots polimēru kompozītu iekšējās struktūras tehniskā stāvokļa monitoringa process.

Olgas Bulderbergas izstrādātais darbs ir prezentēts disertācijas veidā Fizikas un astronomijas zinātnes nozarē, Materiālu fizikas apakšnozarē.

Darba rezultāti ir publicēti 3 recenzētos zinātniskos rakstos indeksētos Scopus datu bāzē, 8 starptautiskos konferenču materiālos. Darba autore prezentēja rezultātus 14 starptautiskās konferences un līdzautorībā pieteica 2 patentus. Darbs sastāv no ievada, 3 nodaļām un secinājumiem. Literatūras sarakstā ir 146 zinātniskas literatūras un interneta avoti.

Atslēgvārdi: bojājuma vizuāla indikācija, polimēra kompozīts, tehniskā stāvokļa monitorings, mikrokapsulas.

## ABBREVIATIONS

| | |
|---|---|
| **AFM** | atomic force microscopy |
| **CC** shell | closed cylindrical shell |
| **CVL** | crystal violet lactone |
| **DVIS** | damage visual indication system |
| **E_1** | series 1 of water-based epoxy resin mixed with hardener samples |
| **GFRP** | glass fibre reinforced plastics |
| **ICR** | integral colour response |
| **MC** | microcapsules |
| **MF** | melamine formaldehyde |
| **NDT** | non-destructive testing |
| **PU** | polyurethane |
| **PVAc** | poly (vinyl acetate) |
| **PVAc_1** | series 1 of poly (vinyl acetate) samples |
| **RGB** | red, green, blue colours of visual responce |
| **SEM** | scanning electron microscope |
| **TT** ball | table tennis ball |
| **UV** | ultraviolet light |

# INTRODUCTION

Composites are widely used in various industries due to the specific combination of properties, but the main scientific challenges are related with polymer composites, especially, glass fibre reinforced plastics (GFRP) used as structural elements [1]. Structural health monitoring and damage diagnosis are most topical for aviation and aerospace, boats and marine, automobile and wind power industries, where constructions are subjected to high loads and have high costs. One of the most applicable ways to control structure condition during its manufacture and exploitation is to perform non-destructive testing (NDT). It is clear from the name that these tests are performed in a manner that does not affect the future use of the object or material. In other words, NDT allows parts and material to be inspected and measured without damaging them. Because it allows inspection without interfering with a product's final use, NDT provides an excellent balance between quality control and cost-effectiveness [2]. The existing methods of NDT allow one to assess the state of a structure during its operation through continuous monitoring, and not only locate a defect, but also to measure defect's size, shape, and orientation. Some of the most often used methods of NDT for composite structures are listed below [3-5].

Ultrasonic Testing - high-frequency sound waves are transmitted into a material to detect imperfections or to locate changes in material properties. For ultrasonic testing, a pulse-echo method is most common. Here waves are introduced into a test object and reflections (echoes) from internal imperfections returns to a receiver. Applying ultrasonic testing, defects like delamination [6] and porosity [7] could be detected in multi-layered composite materials.

Radiographic Testing involves using penetrating γ - or x-radiation on materials to look for defects or examine internal or hidden features. Depending on the thickness of the tested object low voltage radiography (for thin) and γ-rays (for thick) are used, while an x-ray is most useful when the parts are neither too thick nor too thin [8].

Acoustic Emission may be defined as a transient sound wave that is generated by a short, rapid release of energy, in the form of an elastic wave, produced by the movement of a dislocation or a change in the structural integrity of the material. The change in the structural integrity of a fibre reinforced composite could be caused by fibre breakage, matrix cracking, and debonding [9]. The main difference of this method, compared with other NDT, is that signals are emitting from the material, not from an equipment source. The main damage mechanisms can be ranked in ascending order of acoustic emission amplitude signal as following: matrix cracking, delamination and debonding, and fibre fracture [10]. The advantage of the present method is that internal change in the material integrity could be detected on a real-time not post factum like with other NDTs.

Infrared Thermography Testing, in general, is based on the detection and measuring of electromagnetic radiation emitting from the objects. It could be passive, an infrared camera detects only emitted electromagnetic radiation of the tested object and active when external heating sources are used [11]. In the case of composite structures, an active infrared thermography testing is applied. Thermal waves propagate through the sample, and in the case of defects, due to the thermal conductivity difference between the defects and the sample material, the diffusivity coefficient changes [12]. The advantages of this method are detection of different type of defects and damages, an inspection of a large area in a very short time, and the possibility to inspect objects with the various geometries. As well, any damage caused by impact could be detected online, due to the temperature change at the place of damage [13].

In general, all NDT methods mentioned above could be named as passive. A signal source is an external device, not a test sample. For each NDT measurement, specialised equipment, data analysis procedure, and trained personnel are required. Each technique has specific limitations mainly related to the shape of a tested sample. As well as a significant difference between NDTs methods is the time taken to set up the experimental device and to analyse the results [14], thus some progressive result in fast and user-friendly systems is required, both in equipment and data processing methods [15].

In contrast to the use of passive NDTs, composites with built-in sensors are created. In this case, active NDT is mainly realized by an *in situ* method, by embedding various sensors (detecting impact, delamination, or fatigue) in the design elements and the use of specialised equipment to decode these signals [16-20]. Obviously, embedding foreign objects in a system leads to the degradation of its mechanical properties. Therefore, the so-called self-reporting materials have become popular, where the size of the sensing elements embedded in a matrix is on nano- or micro-level. In this case, self-reporting is realized by incorporation into a structure conducting elements like carbon nanotubes, carbon nanoparticles, etc., thus implementing piezoresistivity. Forming a conductive network, deformation, or damage could be detected by the change in the electrical resistivity [21-23].

Despite a wide choice of NDT methods, the visual testing – the oldest and most common, is still actual for composite structures. It is, in many cases, quite informative and is the cheapest method of control. From the Visual inspection for aircraft - *"Visual inspection is defined as the process of using the eye, alone or in conjunction with various aids, as the sensing mechanism from which judgment may be made about the condition of a unit to be inspected"* [24]. However, due to the unchangeable form of composites after the damage, for the simplification of the visual inspection process, some improvements are required. Especially for the types of damages referred to as barely visible impact damage, where small indentation on the surface may lead to significant

delamination or other internal damages [25, 26]. Inspired by nature, some biomimetic approaches were already implemented in fabrics [27]. For example, like a bruise in the human body pointing out the place of microscopic tears in blood vessels under the skin [28], self-reporting composite with the inherent function of damage visualization could perform the same. This approach was described in several patents, and patent applications, where it is proposed to use fluorescent dye-loaded capsules [29], the film of thin skin with embedded microcapsules capable of being added onto the said substrate [30], foam expanded with a nontoxic, coloured gas [31], polymer coating, pressure-sensitive films and paints with incorporated one type of dye and one type of activator [32-37]. In all cases, when the material undergoes stress deformation, capsules burst and release the colour agent. For two-component colour agents, under the action of applied load shells of capsules burst, components come into the contact, and a chemical reaction following with colour change occurs, thus indicating the place of structure damage.

## Problem Statement

Despite the existing patents, in practice, this approach using the encapsulated dye or encapsulated dye and colour activator is not implemented convincingly enough [38-40]. The commercial solution – paints [41] is not suitable for all surfaces. It has not a sufficiently contrast visual response, and the current offers of encapsulated dye on the market [42-44] do not have specific solutions for polymer composite materials. Possible applications of microcapsules for structural health monitoring of various materials [45-47] are well presented in the scientific literature. However, there is lack of investigations dedicated to deep study of mechanical and physical properties of such microcapsules. Also, the durability under different environments of these microcapsules is not studied well [48]. For each application case, the complex study is needed, starting the study from the separate microcapsule and ending with a general system.

In this work, an attempt to adapt the existing NDT methods for fibre reinforced plastics and place microcapsules inside the material will be made. For these microcapsules, the complex study of the properties will be performed, including the examination of microcapsules and composite systems in different environments. **Two component's colour agent** will be selected – colour former (microencapsulated dye) and colour activator. Microencapsulation ensures that the components get in contact above a certain level of the applied load that will damage the shell of the microcapsule.

Obviously, before the damage, the surface colour must be neutral and different from that after the damage. For this, the leuco dye is a proper choice. Leuco dye molecules can acquire two forms, one of which is colourless. An example of leuco dye is the crystal violet lactone. This dye while in its lactone form is typically colourless, but in conditions of low pH, as it is protonated, it

shows the colour that is intense violet [49]. For the protection of leuco dye from the pH of the surrounding matter, usually, a microencapsulation process is applied.

Analysing the existing solutions for self-reporting materials and proceeding from the listed NDT, alternative, proposed here NDT method for polymer composites should be **accessible** (equipment is not used), **understandable** (no special algorithm and data proceeding needed), **fast** (the visual response after material damage should be identified in some seconds), and **simple** (no specialised training is needed to identify the damaged place).

Proposed **damage visual indication system (DVIS)** corresponds to the requirements put forward and will include:

1. Colour former - microencapsulated leuco dye.
2. Colour activator (in encapsulated or particle form).
3. Base - fabric to be coated with two components' colour agent (former + activator).
4. Substance / or method that holds the colour agent on the surface of the base.

The concept of the **damage visual indication system** and its components is presented in Figure 0.1.

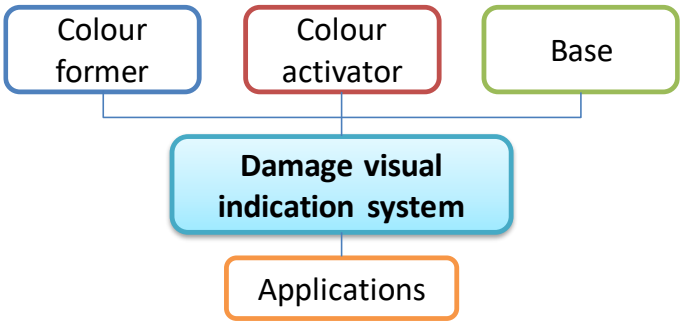


Figure 0.1. The concept of the DVIS.

## Aim and Main Tasks of the Research

The **general aim** of the study was to **improve exploitation safety** and **simplify structural NDT** process of polymer composites in constructions.

The **specific aim** of the study was to **develop a damage visual indication system** for polymer composites and **validate it**.

For this purpose, the following tasks were formulated.

T1: *Development and study of the microcapsules for the DVIS.*

Colourless microcapsules containing dyes should be synthesized in the laboratory and compared with the industrial ones. Physical and mechanical properties of microcapsules, used as a main component of the DVIS, should be estimated. Ability to change colour should be evaluated under different factors like ultraviolet irradiation, high temperatures.

T2: *Development and optimization of technology for manufacture of the DVIS.*

Technology to apply the colour agent on the base should be developed. The damage visual response measuring procedure should be developed for the verification of the DVIS.

T3: *Manufacture of a model composite with an integrated DVIS.*

Composite with an integrated DVIS should be presented as two demonstrators: a) DVIS as a separate layer, which could be placed on a surface of existing construction or element, b) DVIS integrated into a composite by vacuum bagging method.

T4: *Verification of the model composite with an integrated DVIS.*

Model composite should be tested by various methods. For example, the DVIS as an external layer should be tested on the ability to be glued on the polymer surface and removed from it. An effect of the DVIS integrated into the composite on the mechanical properties of the system should be evaluated by tensile tests. For both demonstrators, a visual response on applied load, the kinetics of colour change, and durability should be estimated.

## Concept of the Research

The concept of the research is based on the sequential, multidisciplinary study of the proposed DVIS on different structural levels starting from the micro to macro. **The general concept** of the work is presented in Figure 0.2.

- **Micro-level**

Microcapsules, as a part of the DVIS will be studied on the micro-level. Beginning from the synthesis of microcapsules, evaluation of the size and surface morphology will be studied, and further evaluation of mechanical and physical properties of microcapsule as a separate unit will be performed.

- **Meso-level**

The DVIS, as an integral object, will be studied on the meso-level. The manufacturing technology of the DVIS will be developed for different applications. For the qualitative (as a selection of the colour) and quantitative (determination of the necessary amount of microcapsules) characteristics of the DVIS, the methodology of the estimation of visual response on the applied load will be developed. For the use of the DVIS for various applications, the durability and stability of the DVIS under different environmental factors will be evaluated.

- **Macro-level**

On the macro-level, a composite structure containing the DVIS will be investigated. The manufacturing technology of the composite with integrated DVIS will be developed. The effect of integrated DVIS on mechanical properties of composite will be studied. The effectiveness of the DVIS will be evaluated for the structures with different rigidity.

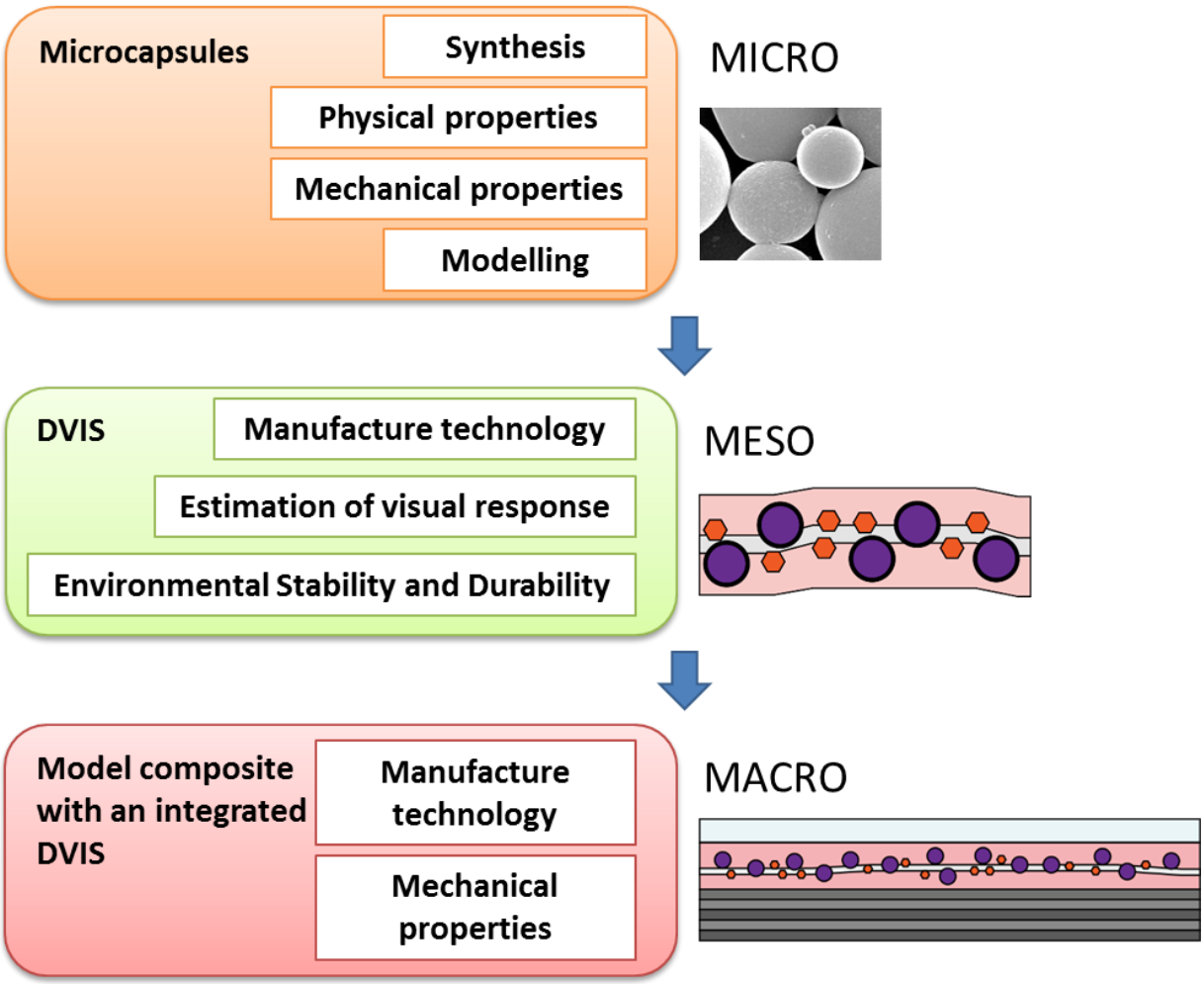


Figure 0.2. The concept of the work includes research from micro-level (microcapsule), meso-level (DVIS), and to macro-level – a composite structure containing the DVIS.

# 1 MICROCAPSULES FOR DAMAGE VISUALIZATION

Since microcapsules are one of the main components of the planned DVIS, some investigations of the microcapsule nature, physical, and mechanical properties were performed. Microencapsulation is defined as a process of enclosing micron-sized particles of solids or droplets of liquids or gasses in an inert shell, which in turn isolates and protects them from the external environment [50]. The result of this process could be microcapsules, microspheres, or microparticles depending on morphology and with a size ranging from 2 to 2000 μm. The main difference between a microcapsule and a microsphere is that the first one has an inner core and outer shell, while the other is a matrix with an active ingredient dispersed inside [51, 52]. Various types of microcapsules exist, where size, structure and the shape of the microcapsules depends mostly on the materials used for production and on the process of production. According to morphology, they could be classified as 1) matrix; 2) mononuclear; 3) irregular; 4) multiwall; 5) polynuclear; 6) assembly of microcapsules, and as well combination of them [53], see Figure 1.1.

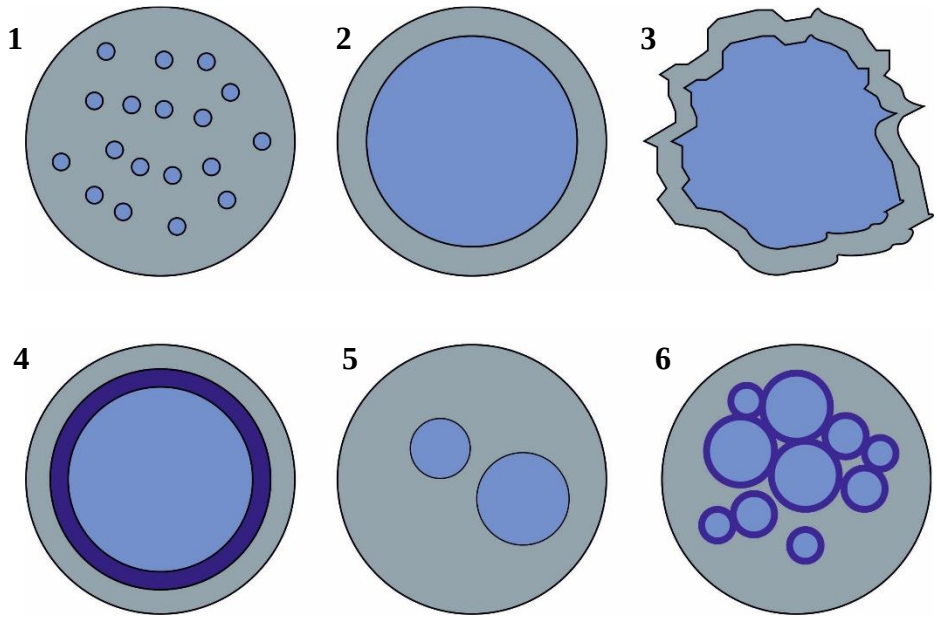


Figure 1.1. Morphology of different types of microcapsules: matrix (1); mononuclear (2); irregular (3); multiwall (4); polynuclear (5); assembly of microcapsules (6).

In the present work, only mononuclear microcapsules (MC) were studied. Such capsules are of micrometre size (>1 μm) and have a spherical shape. The structure of microcapsules can be divided into two parts, namely the core and the shell. The schematic of microcapsule type studied in the present work is presented in Figure 1.2. The core (the intrinsic part) contains the active ingredient (e.g., a hardener or a biocide). In contrast, the shell (the extrinsic part) protects the core permanently or temporarily from the external atmosphere [54].

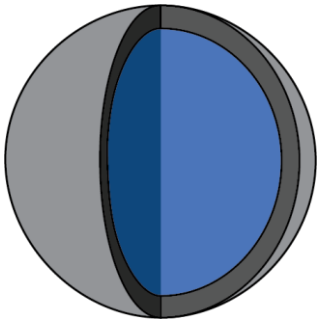

Figure 1.2. Schematic of the mononuclear microcapsule.

Due to the ability of microcapsule to keep core substance isolated and unmodified for an extended period and be released only upon specific conditions, they are widely used in many applications for improving the performance of products. Applications of microcapsules are very diverse; some of the examples listed below. In the food industry, encapsulation of functional ingredients is used to improve flavour, colour, and texture properties and to extend the shelf-life of products, as well ingredients that have functional health benefits, such as antioxidants and probiotics. In a pharmaceutical industry for controlled release of drugs [55]. In the textile industry, intelligent textiles are developed with encapsulated moisturisers, therapeutic oils, and insecticides incorporated into fabrics [56]. For cosmetics and personal care products, experimental results showed that microencapsulation could be an alternative for the transdermal delivery of some active components. Thus microcapsule allows delivering of active components through several layers of the skin [57].

For the use of **microcapsules as a part of the damage visual indication system**, examination of the microcapsule as a main functional and structural element of DVIS is a requirement. The scheme of the study of the microcapsules is presented in Figure 1.3.

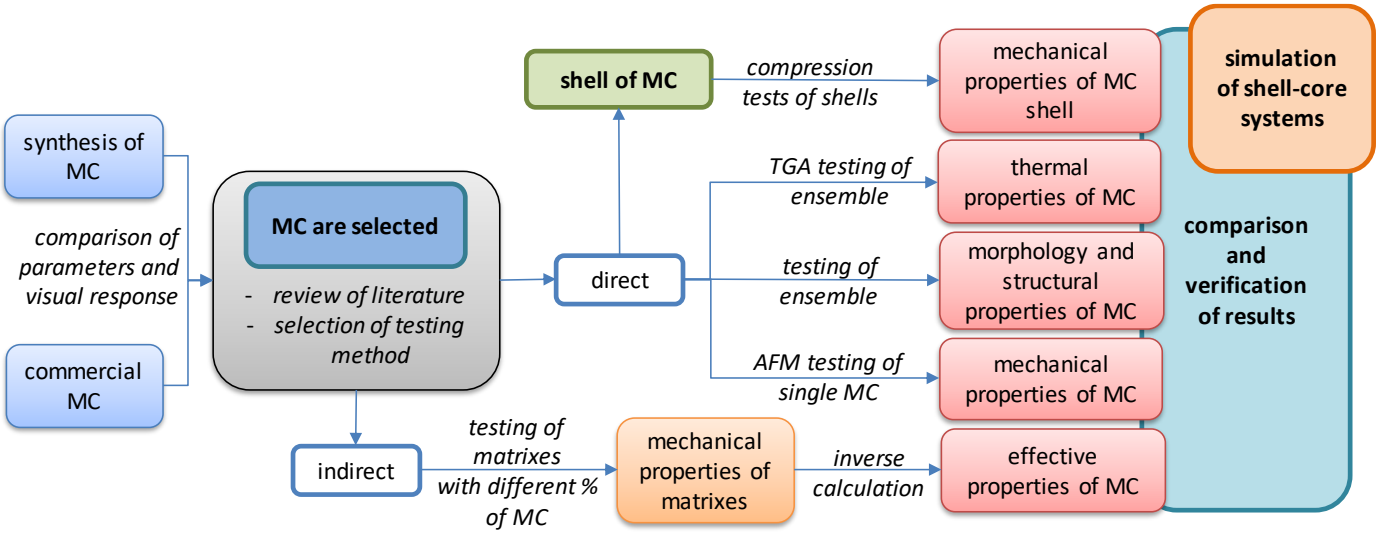


Figure 1.3. Scheme of the study of the microcapsules.

As the first step microcapsules were synthesized in a laboratory. Such synthesis, in a case of its success, allows changing different parameters of capsules, like wall thickness or size. On the other hand, to produce commercial capsules, a well-established procedure is applied and resulting capsules all the time are expected to be the same. Synthesized and commercial capsules were compared by parameters like the regularity of the shape and size, capsules purity (lack of excess material after synthesis). Properties of selected microcapsules were unknown; thus, the literature review was done. The search for data was performed based on the information of materials used for capsule synthesis. Based on the review, the most suitable types of testing to get properties of selected capsules were defined. Furthermore, data about mechanical properties of microcapsules with the same shell material were summarized from the literature. To obtain mechanical properties of selected microcapsules, it was decided to test microcapsule directly by various methods like thermogravimetric analysis, atomic force microscopy, and optical microscopy, and to test shell of microcapsules by mechanical tests. As a second way of microcapsule testing, an indirect method was selected; microcapsules were placed into a matrix and then tested, from the data obtained by inverse calculation, effective properties of microcapsules were defined. Results from the direct and indirect testing were compared and applied for modelling.

## 1.1 Synthesis of microcapsules

In the present work, two groups of microcapsules were compared: commercially available microcapsules made for Carbonless copy paper and microcapsules synthesized in the laboratory. For the selection of the most suitable microcapsules for the DVIS, several requirements were outlined: bright colour response after the damage of the microcapsules' shell, regular size, and spherical shell. Since the synthesis process is similar for the two-component colour agent, here the synthesis process for the one component colour agent is presented.

Two types of capsules were prepared via *in situ* polymerization [58]; with polyurethane (PU) [59] and melamine-formaldehyde (MF) [60] shell materials. Synthesis process and analysis of microcapsule morphology were performed on a scanning electron microscope (SEM) (Hitachi SU-70) in the laboratory of Aveiro Institute of Materials, University of Aveiro, Portugal in collaboration with colleagues from CICECO. Microencapsulation via *in situ* polymerization could be performed in four steps, see Figure 1.4: 1) Emulsifying the core material in the aqueous phase (water, hydrophobic core material, protective colloid); 2) Addition of the wall former by condensation and phase separation through pH reduction; 3) Wall formation by encapsulating the emulsion droplets with wall material; 4) Cross-linking the wall material by addition of melamine and hardening through temperature increase [43].

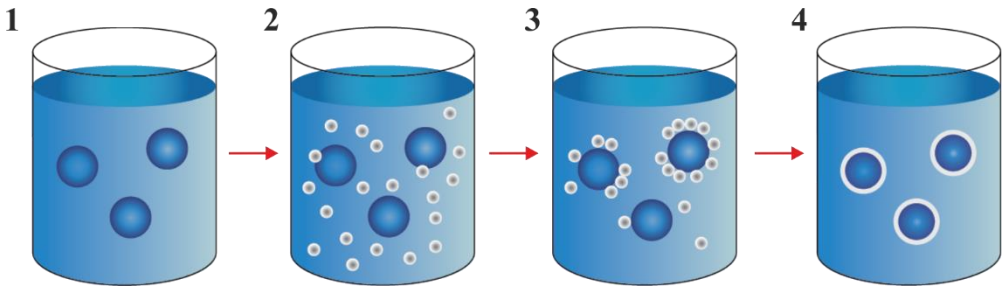


Figure 1.4. General scheme for microencapsulation via *in situ* polymerization: Emulsifying the core material in the aqueous phase (water, hydrophobic core material, protective colloid) (1); Addition of the wall former by condensation and phase separation through pH reduction (2); Wall formation by encapsulating the emulsion droplets with wall material (3); Cross-linking the wall material by addition of melamine and hardening through temperature increase (4).

For PU and MF microcapsules, a colour agent – Umbelliferone was used. Before the rupture of microcapsules, they are colourless, after the rupture the colour agent release and it could be observed in ultraviolet light (UV). In addition to the reference synthesis, for each type of capsule were synthesized samples with modified basic components. For the modification of microcapsules, two parameters were selected – wall thickness and microcapsule size diameter. During the synthesis, the wall thickness could be controlled by monomer amount for PU and by pre-polymer for MF, respectively increase of monomer/pre-polymer amount leads to thicker microcapsule wall and vice versa. Microcapsule size diameter could be controlled by surfactant amount for PU and MF, respectively decrease of surfactant leads to the bigger size of microcapsules [61, 62].

### 1.1.1 Synthesis of Polyurethane microcapsules

For the reference synthesis of microcapsules with PU shell material, an amount of used main components was **3 g of TDI**, **2 g of DETA**, **1 g of Span 85**. All used components are listed in Table 1.1. The synthesis process of PU microcapsule could be divided into two stages; 1) preparation of the water phase, and 2) preparation of the organic phase. This was followed by the mixing of both phases for 30 min. Then, without interrupting the mixing, the monomer was added to the solution drop by drop to avoid sticking and the formation of big pieces of material. For the completion of the process of forming microcapsules, the solution was heated to 60 °C with constant stirring. Suspension of capsules was washed with the water of the remains of the raw materials. The resulting microcapsules were separated from the liquid by the vacuum filtration method. Process of the reference synthesis of microcapsules with PU shell material is presented in Figure 1.5. After the reference synthesis, some modifications were introduced to the reference composition; the amount of used monomer and surfactant was changed to produce microcapsules with different walls thickness and different size. During the synthesis, two methods of stirring were tested to find the optimal solution for a deagglomeration of microcapsules; with a magnet capsule and using a high-speed mixer. Besides, the stirring speed directly affects the size of the

resulting microcapsules – speed increases lead to size reduction [63]. Summary of the used components and modifications of synthesised PU microcapsules are presented in Table 1.2. After filtration resulting capsules were visually evaluated, in the case of not successful synthesis - big agglomerates, solid pieces of undefined material were not explored. Synthesis N.9 and N.10 were not successful (highlighted in Table 1.2.). In the case of the uniform material, it was observed in SEM. It was noticed, that stirring using a magnet gave better results compared with the use of a mixer. During the testing on SEM, it was observed, that capsules are covered with the remaining materials of synthesis or not separate enough from each other. To address this, capsules were "washed" with 10% solution of ethanol in distilled water. Results of the SEM testing with some comments are presented in Table 1.3. After “washing” procedure, capsules were observed on SEM again, see Figure 1.6 and Figure 1.7.

Table 1.1. List of the used components for the PU microcapsules synthesis.

| **Name** | **Designation in the scheme** |
|---|---|
| Span 85 | Span 85 |
| Polyvinylpyrrolidone | PVP |
| Tolylene-2,4-diisocyanate | TDI |
| Cyclohexane | CH |
| Umbelliferone | UMB |
| 1-Butanol, 99% | Butanol |
| Diethylenetriamine, 99% | DETA |
| Distilled water | water |
| Acetone | acetone |

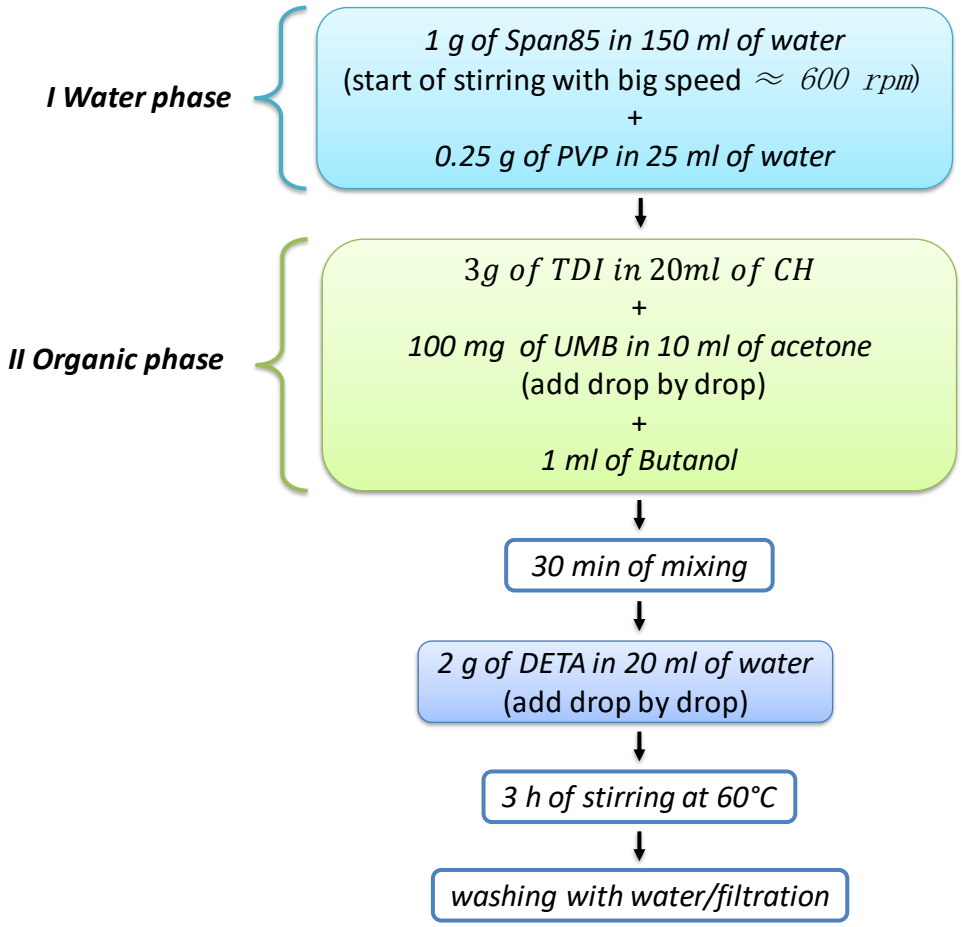


Figure 1.5. The protocol of the reference synthesis process of microcapsules with PU shell material.

Table 1.2. List of synthesised PU microcapsules.

| Microcapsules with PU shell material | | | | | | | |
|---|---|---|---|---|---|---|---|
| **№** | **Modifications** | **TDI, g** | **DETA, g** | **Span85, g** | **Stirring** | **T, °C** | **Time, h** |
| 1 | **Reference_1** | **3** | **2** | **1** | with magnet | 60 | 3 |
| 2 | (½) of monomer | 1.5 | 1 | R | | | |
| 3 | Reference_2 | R | R | R | | | |
| 4 | (×2) of monomer | 6 | 4 | R | | | |
| 5 | (×5) of monomer | 15 | 10 | R | | | |
| 6 | (1/10) of surfactant | R | R | 0.1 | | | |
| 7 | (1/5) of surfactant | R | R | 0.2 | | | |
| 8 | (×5) of monomer | 15 | 10 | R | mechanical | | |
| 9 | Reference_3 | R | R | R | | | |
| 10 | (×2) of monomer | 6 | 4 | R | | | |
| 11 | Reference_4 | R | R | R | | room conditions (≈ 22) | 24 |
| 12 | (1/10) of surfactant | R | R | 0.1 | | | |
| 13 | (1/5) of surfactant | R | R | 0.2 | | | |

Table 1.3. Summary of the SEM analysis of PU microcapsules.

| № | Modifications | Expected morphology | SEM Image | Comments |
|---|---|---|---|---|
| **Shell material - Polyurethane** | | | | |
| 1 | Reference – regular synthesis | Spheres with size diameter of 100-1000 nm |  | Two different “populations”; one small as expected and other very big. |
| 2 | (½) of monomer | Thinner microcapsule wall | 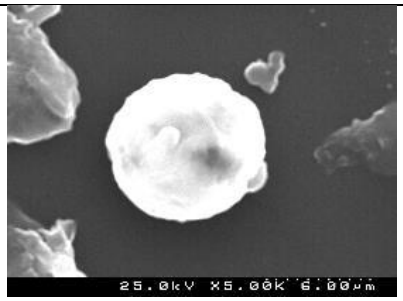 | Capsules larger than expected. |
| 3 | Reference 2 | Spheres with size diameter of 100-1000 nm | 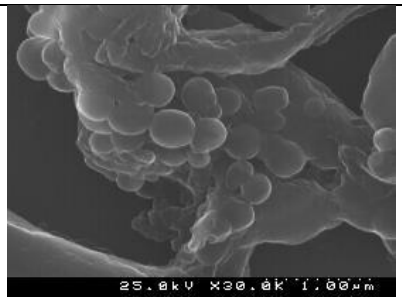 | Expected size, but they were very agglomerated. |
| 4 | (×2) of monomer | Thicker microcapsule wall | 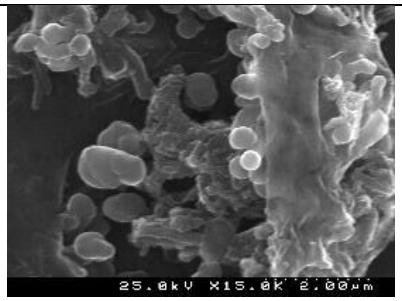 | Correct size, but there was an excess of “polymer” around. |
| 5 | (×5) of monomer | Thicker microcapsule wall |  | Correct size, but there was an excess of “polymer” around. |

| | | | | |
|---|---|---|---|---|
| 6 | (1/10) of surfactant | Much bigger size diameter | 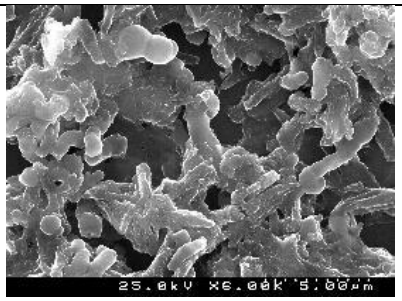 | Larger size than expected, but only a few capsules were observed in the middle of an immense amount of polymer. |
| 7 | (1/5) of surfactant | Bigger size diameter | 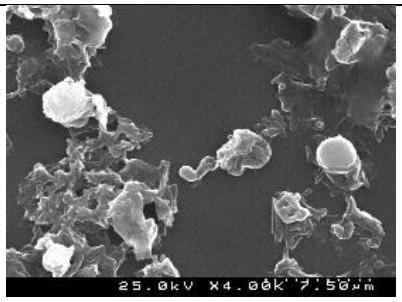 | There is something resembling capsules but in a minimal amount. |
| 8 | Repetition of N. 5<br>- with mechanical stirring | Thicker microcapsule wall | 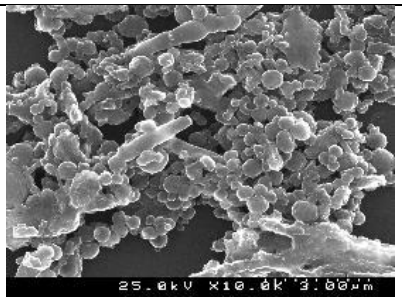 | Size and size distribution seem acceptable; some polymer between capsules is observed. |
| 11 | Reference 4<br>- with mechanical stirring (24 h) at room T | Spheres with size diameter of 100-1000 nm | 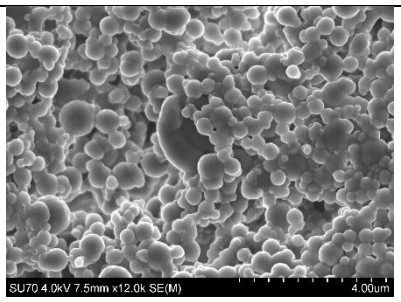 | Size and size distribution seem acceptable, but capsules are not separate. |
| 12 | Repetition of N. 6<br>- (1/10) surfactant amount;<br>- with mechanical stirring (24 h) at room T. | Much bigger size diameter | 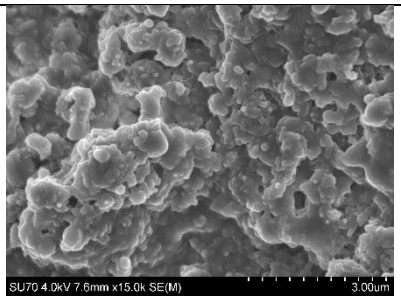 | Difficult to identify capsules. |
| 13 | Repetition of N. 7<br>- (1/5) surfactant amount,<br>- with mechanical stirring (24 h) at room T. | Bigger size diameter | 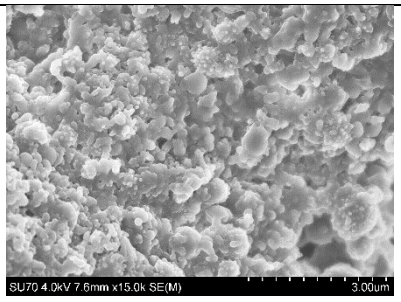 | Difficult to identify capsules. |

Capsules from the reference synthesis (№ 11), comparing them before and after "washing" looked similar, but they were not so agglomerated, see Figure 1.6. Capsules from the synthesis № 13 with a decreased amount of surfactant before and after "washing" have not changed. Capsules remained covered with unknown material, and it was difficult to identify separate capsules, see Figure 1.7.

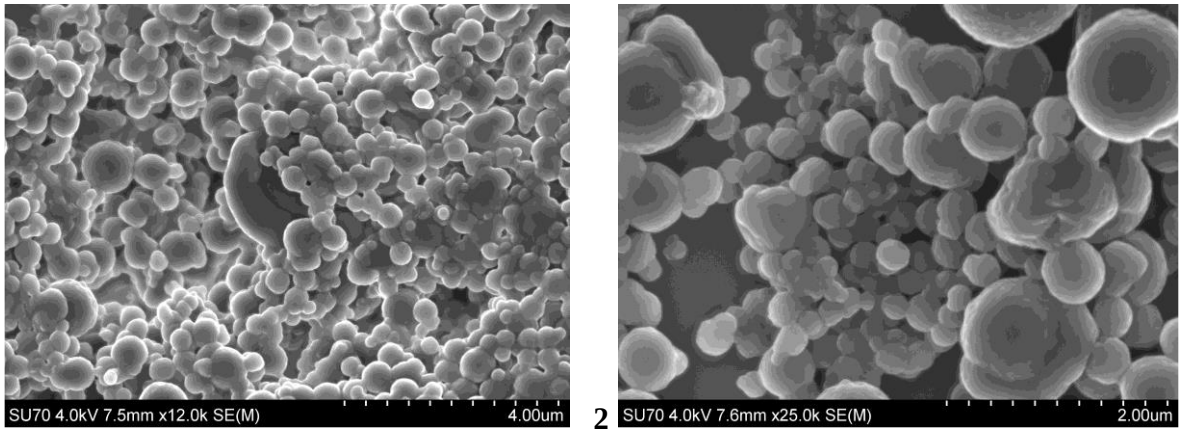


Figure 1.6. PU capsules obtained by the synthesis № 11; before (1) and after (2) “washing”.

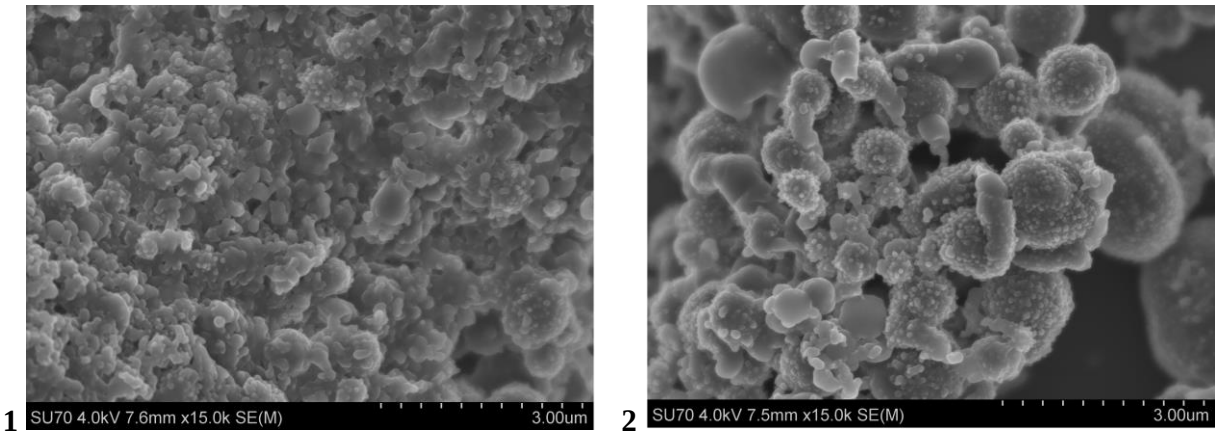


Figure 1.7. PU capsules obtained by the synthesis № 13; before (1) and after (2) “washing”.

Conclusions of the synthesis of capsules with PU shell materials could be following. Synthesis with the reference amount of the main components allows getting separate capsules. With the modification of the amount of monomer or surfactant, obtained capsules were covered with a significant amount of remaining material. With a mechanical stirring separate capsules were not obtained at all.

### 1.1.2 Synthesis of Melamine formaldehyde microcapsules

For the reference synthesis of microcapsules with MF shell material, an amount of main components was **75 ml of pre-polymer and 3.25 g of surfactant.** All used components are listed in Table 1.4. Synthesis of MF microcapsules was performed in three steps [64]; for the first step,

MF pre-polymer was synthesized, see Figure 1.8. For this purpose, melamine powder and formaldehyde solution in 250 mL distilled water were adjusted to pH 8.8 using sodium hydroxide solution. The MF was prepared by 1.5 hrs of stirring at alkaline conditions and temperature 90 °C. For the next step, sodium dodecyl sulphate surfactant was dissolved in 35 ml of distilled water, see Figure 1.9. The last step included the mixing of the organic phase and water phase with the later adding of MF pre-polymer, see Figure 1.10. A solution with the main ingredients of Cyclohexane and solvent as an organic phase was mixed up. The solvent was chosen according to the material, which was preferred to be stored in the final capsules. Here Umbelliferone was selected. The organic phase was mixed with 30% of sodium dodecyl sulphate. Due to the specific chemical structure of SDS, where one side of the molecule is hydrophilic, and other is hydrophilic, organic parts became trapped within the water phase. With the increasing temperature up to 40 °C and permanent mixing, MF pre-polymer was evenly distributed. For faster polymerisation, the temperature was raised to 85- 90 °C and catalyst Magnesium chloride hexahydrate was added. To obtain the necessary pH level (≈ 4) to finish polymerization, acetic acid was added. After 2 h of mixing at 90 °C, capsules were washed with water and filtered through the paper filter using the vacuum pump. With the experience from the PU synthesis, here only magnetic mixing was applied. The summary of the used components and modifications of synthesised MF microcapsules are presented in Table 1.5. A here similar procedure was applied: resulting capsules were visually evaluated, good ones were tested on SEM if required, capsules were additionally cleaned with a 10% solution of ethanol in distilled water. Results of the SEM testing with some comments are presented in Table 1.6.

Table 1.4. List of the used components for the MF microcapsules synthesis.

| Name | Designation in the scheme |
|---|---|
| Sodium dodecyl sulphate | SDS |
| Sodium carbonate | $Na_2CO_3$ |
| Cyclohexane | CH |
| Umbelliferone | UMB |
| Distilled water | water |
| Magnesium chloride hexahydrate | $MgCl_2 \cdot 6H_2O$ |
| Sodium hydroxide | NaOH |

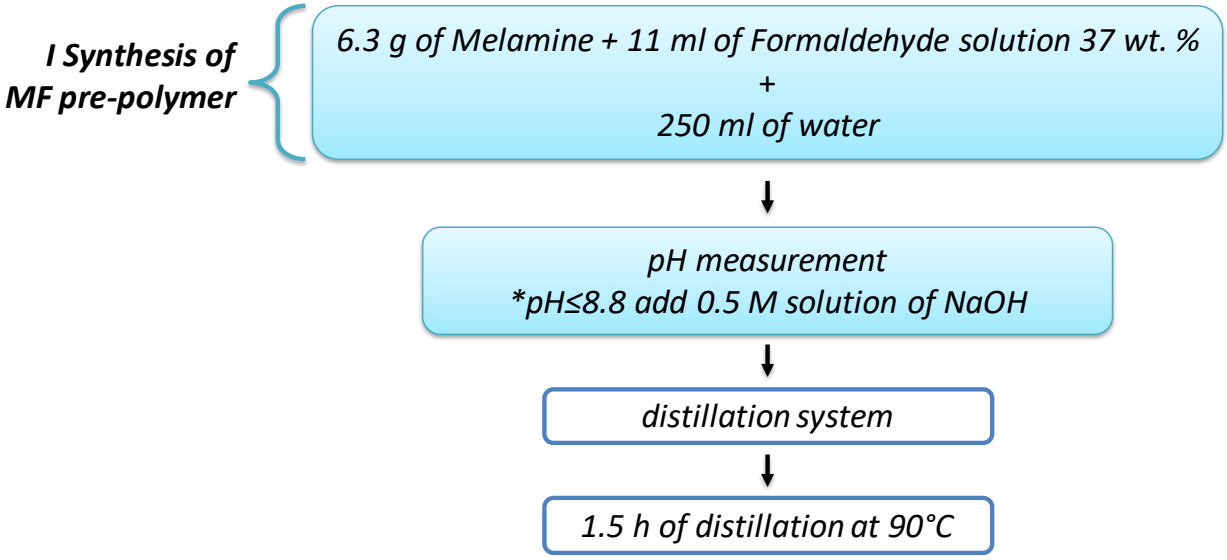


Figure 1.8. Preparation of MF pre-polymer.

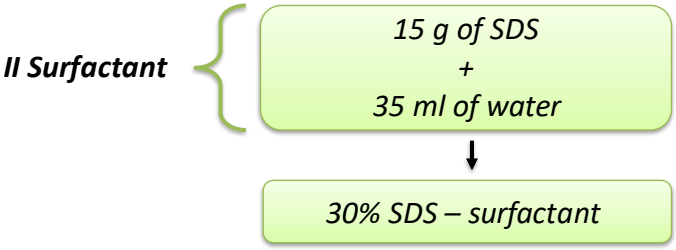


Figure 1.9. The protocol of the preparation of the surfactant.

Table 1.5. List of synthesised MF microcapsules.

| Microcapsules with MF shell material | | | | | | |
|---|---|---|---|---|---|---|
| **№** | **Modifications** | **Pre-polymer, ml** | **Surfactant, g** | **Stirring** | **T, °C** | **Time, h** |
| 1 | Reference | 75 | 3.25 | with magnet | 90 | 2 |
| 2 | (×2) of pre-polymer | 150 | R | | | |
| 3 | (1/2) of pre-polymer | 37.5 | R | | | |
| 4 | (×5) of pre-polymer | 375 | R | | | |
| 5 | (1/2) of surfactant | R | 1.625 | | | |
| 6 | (1/5) of surfactant | R | 0.65 | | | |

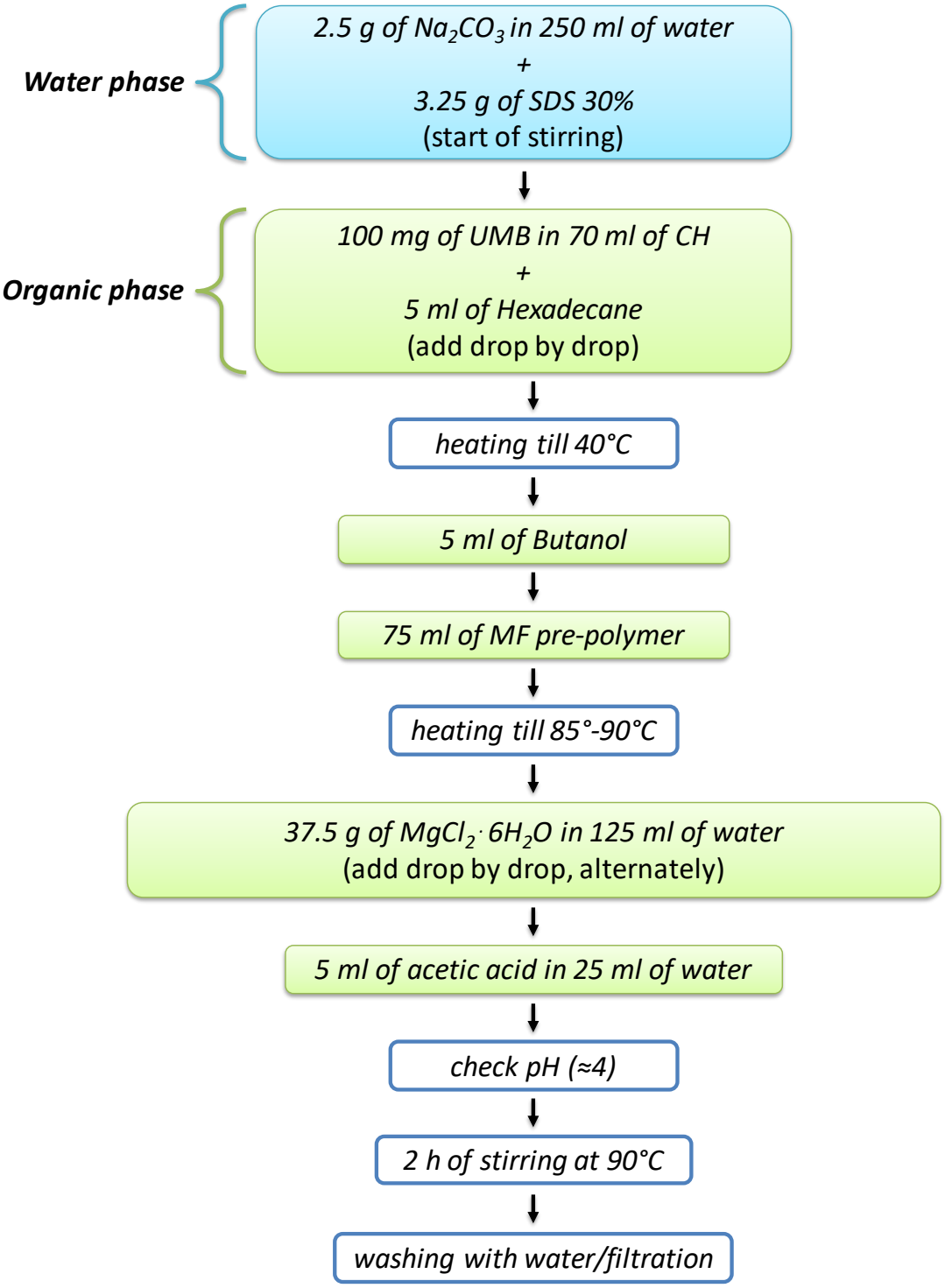


Figure 1.10. The protocol of the reference synthesis process of microcapsules with MF shell material.

Table 1.6. Summary of the SEM analysis of MF microcapsules.

| № | Modifications | Expected morphology | SEM Image | Comments |
|---|---|---|---|---|
| **Shell material - Melamine formaldehyde** | | | | |
| 1 | Reference – regular synthesis | Spheres with size diameter ~5μm | 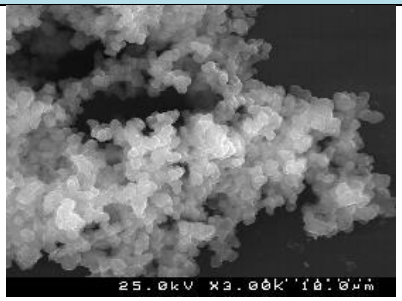 | Capsules/particles smaller than expected. Good size distribution. |
| 2 | (×2) of pre-polymer | Thicker microcapsule wall | 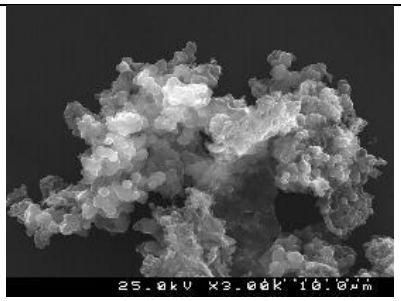 | Capsules/particles smaller than expected with a bit of polymer in the middle. |
| 3 | (1/2) of pre-polymer | Thinner microcapsule wall | Not observed on microscope | Brown “powder” in a minimal amount. |
| 4 | (×5) of pre-polymer | Even thicker microcapsule wall | 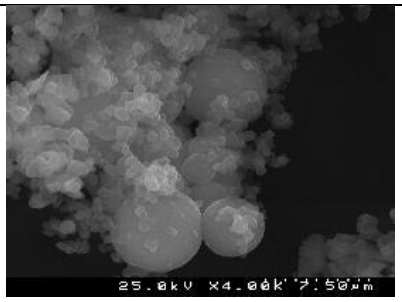 | Capsules with the expected size, covered with “particles” that needs to be identified. |
| 5 | (1/2) of surfactant | Bigger size diameter | 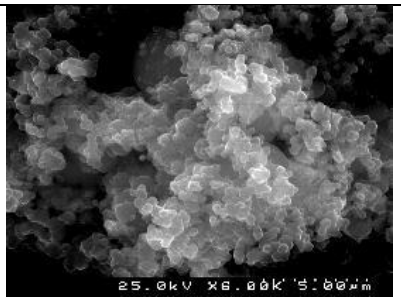 | Particles or capsules covering a matter that needs to be identified. Capsules should be bigger. |
| 6 | (1/5) of surfactant | Much bigger size diameter | 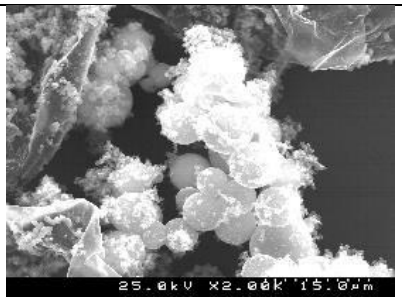 | Capsules with correct size, but with a matter on top (particles, capsules or just powder) of something. |

MF capsules from the Reference synthesis were also “washed”, like PU capsules, with the idea to get separate capsules. After “washing” or because of it, it was possible to see that there were not any separate capsules at all, see Figure 1.11.

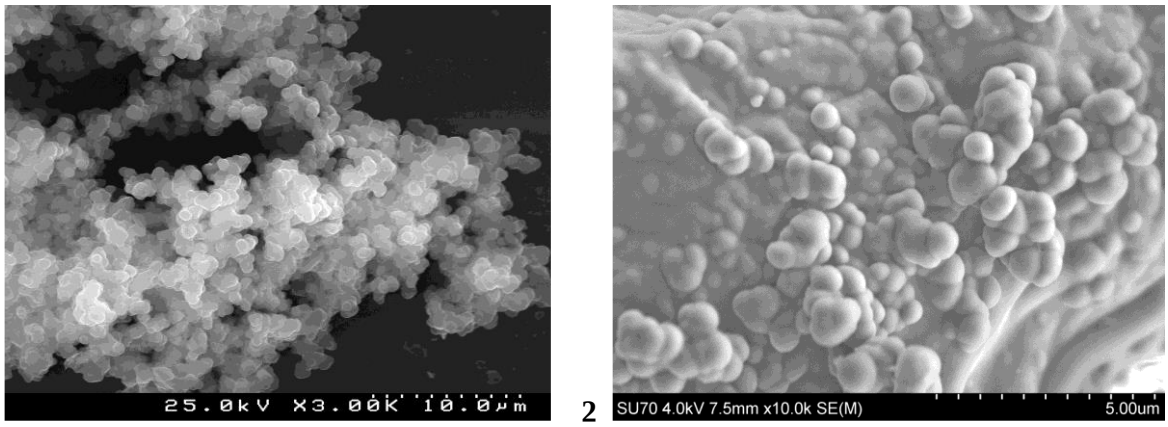


**1** **2**

Figure 1.11. MF capsules obtained by the synthesis № 1; before (1) and after (2) “washing”.

Conclusions of the synthesis of capsules with MF shell materials could be following. Synthesis with the reference amount of the main components did not allow obtaining separate capsules. With the modification of the amount of pre-polymer or surfactant, some not agglomerated, well-identified capsules were obtained, see № 4 and № 6 in Table 1.6. In other synthesis, capsules/particles were covered with a considerable amount of remaining material.

For the comparison, available commercial microcapsules [43], used for Carbonless copy paper manufacturing [65], were selected. Microcapsules with leuco dye and microcapsules with dye activator, as water-based dispersions were supplied by *Papierfabrik August Koehler Ag., Germany*. The shell of the microcapsule was made from melamine-formaldehyde resin. The nominal concentration of the microcapsules in the dispersion was ≈ 40 wt.% (data from the manufacturer). SEM photographs of commercial microcapsules are shown in Figure 1.12. On the photographs, the surface of the most microcapsules with leuco dye and microcapsules with dye activator is smooth, and the shape is very regular, some size distribution could be observed.

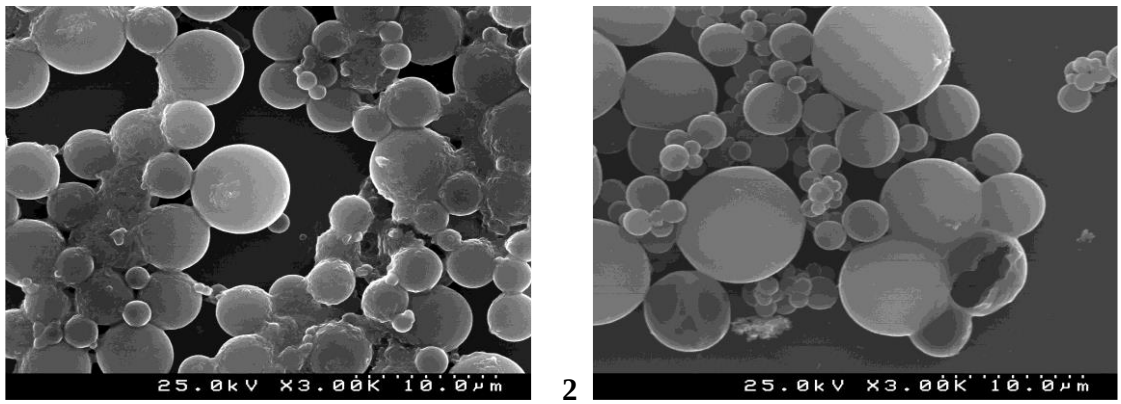


**1** **2**

Figure 1.12. Commercial microcapsules with leuco dye (1) and with dye activator (2).

After comparing three types of microcapsules by parameters like the smoothness of surface, spherical shape, a small variation in size, commercial microcapsules were selected for further work.

## 1.2 Physical properties of microcapsules

For the use of commercial microcapsules in further work, it was necessary to evaluate the physical properties of it. Two types of microcapsules were studied; microcapsules with leuco dye (MC-dye), and microcapsules with a colour activator (MC-activator). The microcapsules produced by *Koehler Ag.* are made from melamine-formaldehyde resin. The core of the capsules contains the solution of colourless leuco dyes. The oil was a mixture of diisopropylnaphthalene and dearomatized hydrocarbons, and their boiling points are higher than 200 °C. The most widespread colour former is Crystal violet lactone (CVL). When an acid substance cracks the lactone ring, the outcome is a brilliant blue. However, similar colour formers are also available (all of them lactones), which generate other colours (black, green, red, orange). The capsules for black-copy carbonless paper contain one dye black mixed with smaller amounts of the blue, red and green colour former. Colour activator could be encapsulated or presented as particles. Here colour activator was presented as a mixture of Zn-donated phenolic resins and Zn-salicylates (data from the manufacturer).

### 1.2.1 SEM analysis

Microcapsules with dye and activator were examined by the SEM (Hitachi SU-70). Single and agglomerated capsules images were obtained. To separate agglomerated capsules, at first, the suspension of microcapsules was diluted with water and after dispersed with an ultrasonic method. It was concluded that it was not possible to measure the wall thickness of microcapsules. Before repeated microscopy, MC were damaged with a scalpel. The microcapsules were examined by the SEM (Hitachi S - 4100). Using a micro photo of damaged microcapsules, a wall thickness was measured, see Figure 1.13. The average wall thickness of the microcapsules from 6 measurements of broken microcapsules was defined $h = 0.10 \pm 0.01$ μm.

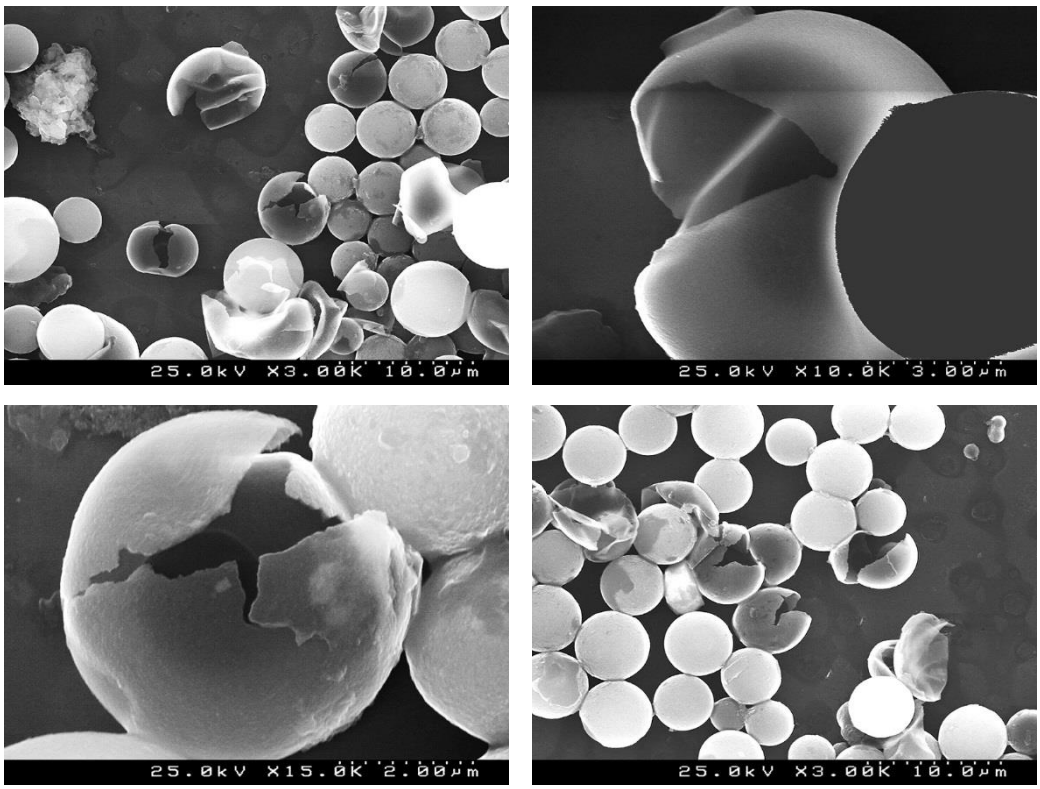


Figure 1.13. Micro photo of damaged microcapsules.

### 1.2.2 Size distribution analysis

The size distribution of MC-dye and MC-activator, see Figure 1.14, was measured by the particle size analyser (Coulter LS – 230), based on dynamic light scattering.

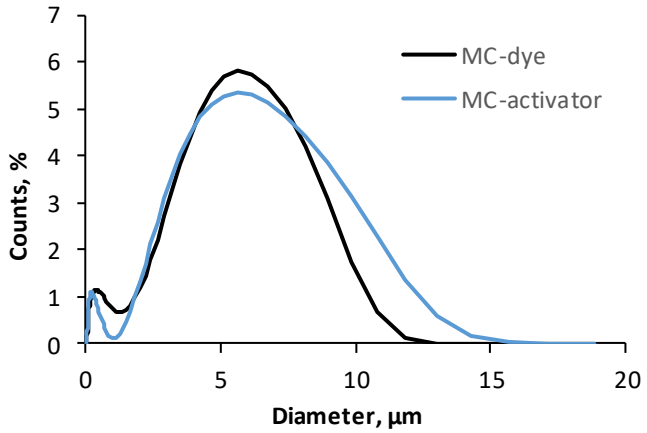


Figure 1.14. MC-dye and MC-activator size distribution obtained by the particle size analyser.

To verify the validity of the result, the measurement results of particle size analyser were compared with results obtained previously by an optical microscope. By image analysis, it was concluded, that the result obtained by particle size analyser was influenced mostly by agglomerations of microcapsules, and the result was not precise. Therefore, the size of the microcapsules was measured, and its size distribution was calculated from the images in automatic and manual modes using ImageJ software [66]. MC-activator sizes calculation in automatic mode

gave a significant mistake. A cause of this mistake was non-correct agglomerated particles image processing by ImageJ in automatic mode, Figure 1.15. The program divided the agglomerates into separate units along with a clear interface, which in most cases was not correct. Microcapsules did not lie side by side but rather were partly on top of each other. Besides, not all spherical objects were capsules; in some instances, they were bubbles. In the case of MC-activator, SEM image processing also could not give correct results. For MC-activator, the manual mode for the size distribution was applied. Measuring results and size distribution for MC-activator is shown in Figure 1.16.

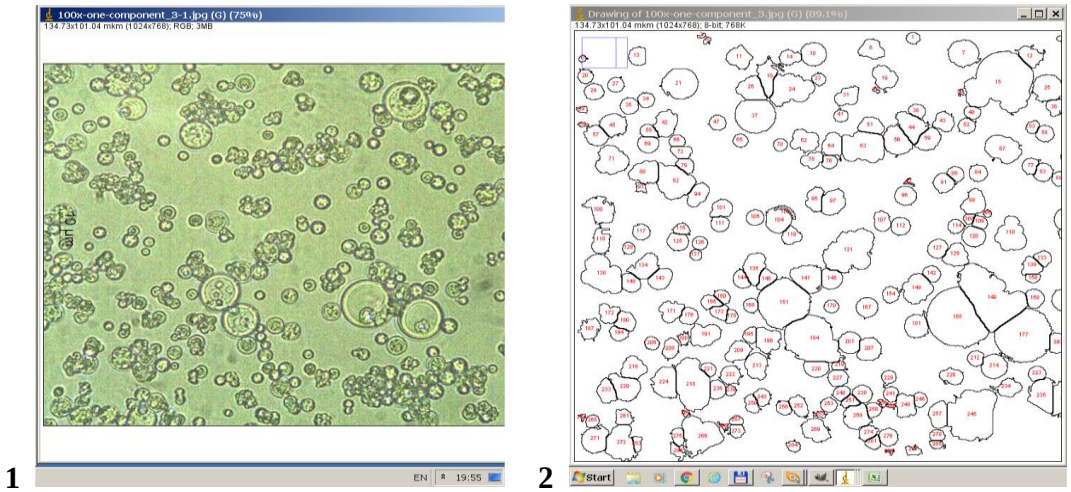

1 2

Figure 1.15. Image of MC-activator by optic microscope (1). The same image after processing in ImageJ (2).

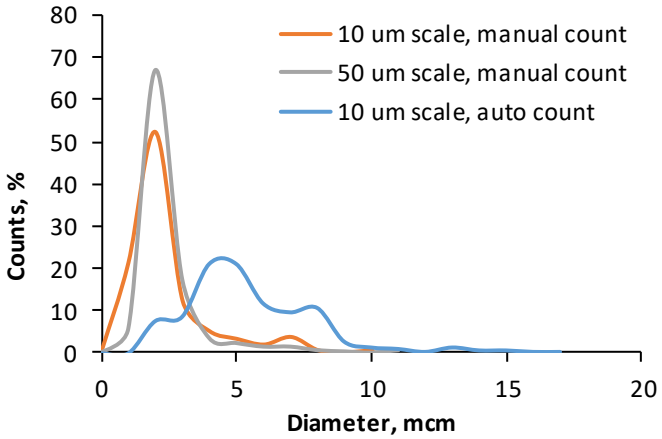


Figure 1.16. The size distribution of MC-activator performed in automatic and manual modes for photos in scales 10 and 50 µm.

ImageJ processing for MC-dye image in automatic mode gave a better result than one for MC-activator. Example of the SEM image processed in ImageJ is presented in Figure 1.17. Measuring results and size distribution for MC-dye is shown in Figure 1.18.

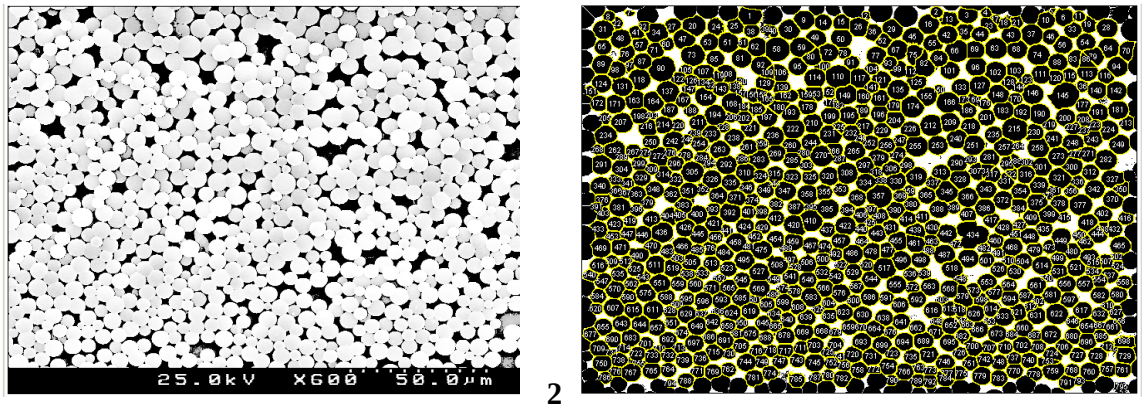


1 2

Figure 1.17. SEM image of MC-dye (1). The same image after processing in ImageJ (2).

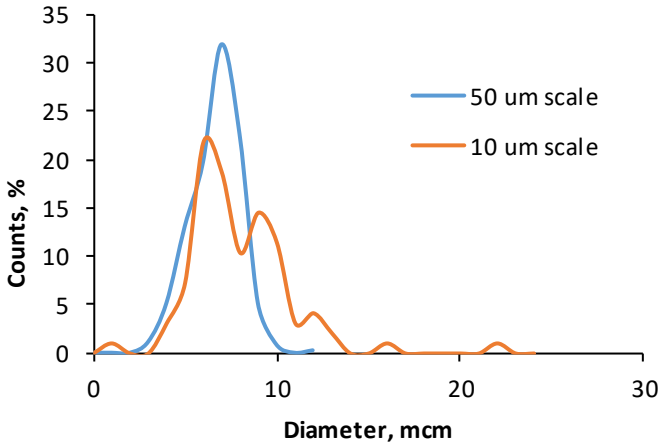


Figure 1.18. The size distribution of MC-dye performed in automatic mode for photos in scales 10 and 50 µm.

Summarizing, it could be concluded that capsules have some evident distribution by size. The average diameter of MC-dye was $D = 7 \pm 0.5$ µm while MC-activator was $D = 2 \pm 0.2$ µm (both results of SEM photo developed manually). Automatic counting and results of light scattering measurements gave essential errors in the case of not sufficient deagglomeration of microcapsules.

### 1.2.3 The ratio of colour agent – dye/activator

Historically, the manufacturer of microcapsules produces encapsulated only leuco dye, not the activator. Moreover, for this colour agent, the ratio of leuco dye and activator was known, and it was 2:1 by volume.

Since MC-activator was specially microencapsulated for this study, the manufacturer did not have any information about the optimal component ratio. For the colour response, this information is crucial, since, with the optimal ratio of components, more significant colour change will be observed [67]. For the evaluation of this, mixtures of MC-dye and MC-activator with different ratio (from 1:1 till 1:10) were prepared. Nylon and glass fabric were impregnated with ready

mixtures and subjected to load after the liquid evaporation. From Figure 1.19 and Figure 1.20 it is seen that increasing the MC-activator did not lead to a brighter colour response. Moreover, on the fabric, especially on the glass fabric, it was rather difficult to destroy microcapsules because of the fabric surface. To deal with this, and make experiment “purer”, flatter surface was necessary, so the paper was used. Here mixtures with an increased amount of MC-dye were also prepared. Mixtures with different ratio of MC-dye and MC-activator were applied to a paper, dried, and with a flat end of tweezers, microcapsules were crashed. The brightest spot was obtained in the centre of the mixture where the most microcapsules were located, thus for comparison, only the central part of the photo was used. Experiment results are presented in Figure 1.21. By increasing the amount of MC-activator, it was possible to see an intensive visual response. When comparing results for the ratio 1:1 and 1:2 the difference was noticeable but not critical. An amount of the mixture onto the paper might be different, the same as the applied force to break the capsules. Thus, for the future work ratio 1:1 was applied.

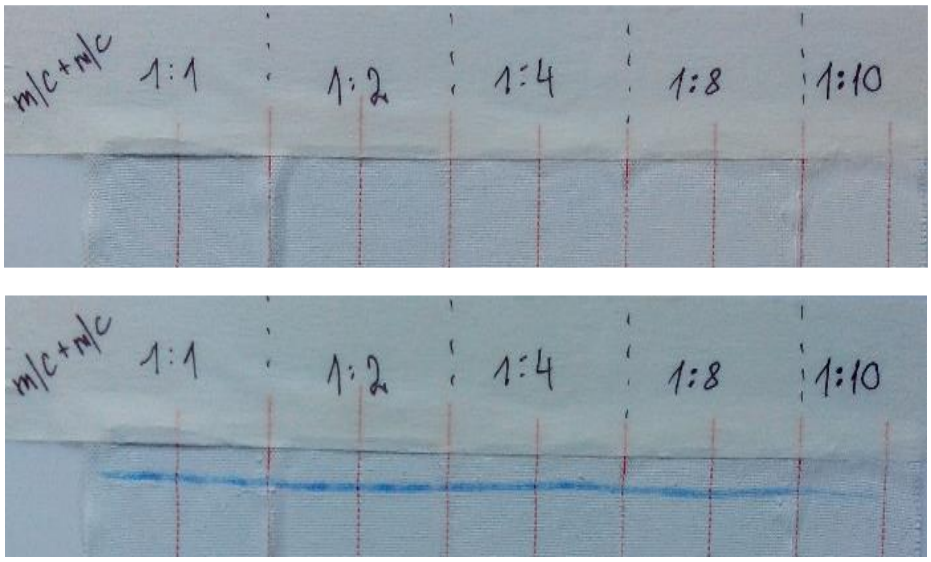


**1**

**2**

Figure 1.19. Nylon fabric impregnated with different ratio of MC-dye and MC-activator: before (1) and after (2) applied load.

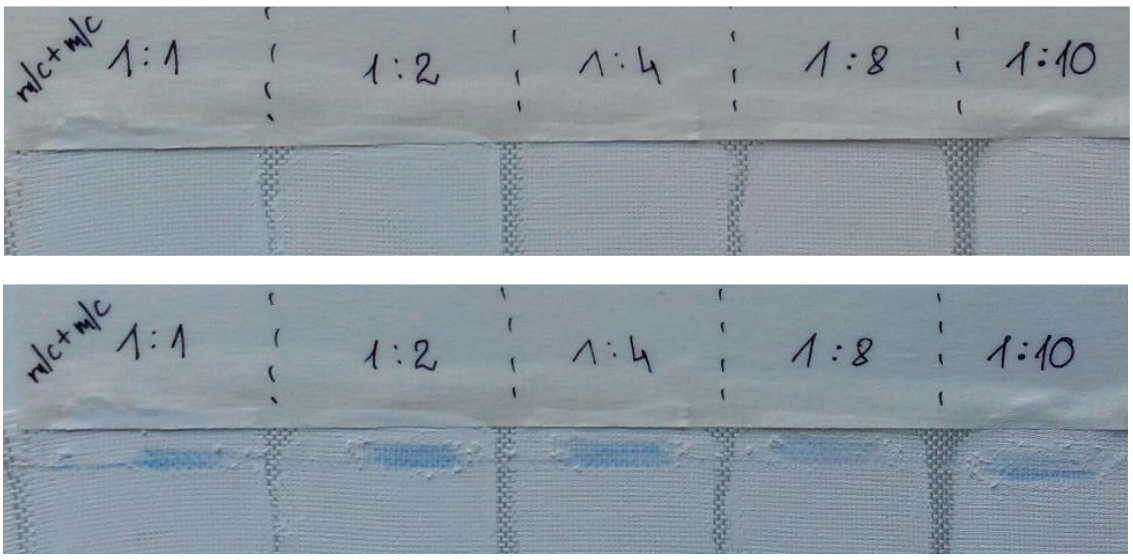


Figure 1.20. Glass fabric impregnated with different ratio of MC-dye and MC-activator: before (1) and after (2) applied load.

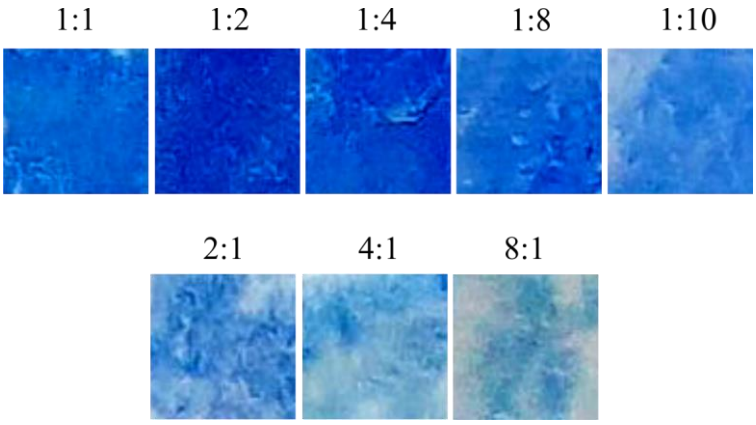


Figure 1.21. Paper impregnated with different ratio of MC-dye and MC-activator.

### 1.2.4 Thermogravimetric analysis

For the use of microcapsules in composite materials, it is necessary to know if they are stable after the rising of temperature because many composites are cured or used at elevated temperatures. Since the microcapsules are presented as dispersion, they can exhibit a weight change due to dehydration, or decomposition of shell material. The weight change of microcapsules as a function of increasing temperature was measured, using Thermogravimetric Analyzer Q500 (TA Instruments). Weight change of the MC-dye and MC-activator as a function of temperature is presented in Figure 1.22. A sharp change in weight around the temperature of 100 °C can be explained by the evaporation of water in which the microcapsules are dispersed. The next major weight loss step occurs above 350 °C when the methylene bridges start to breakdown. Above 400 °C, the three-dimensional polymer structure of MF resin continues to decompose slowly. From this temperature ammonia, formaldehyde and other volatile decomposition products are released [68]. However, microcapsules added to a material, may not

be exposed to such temperatures directly, and therefore, it can be assumed that the material with capsules can withstand higher temperatures.

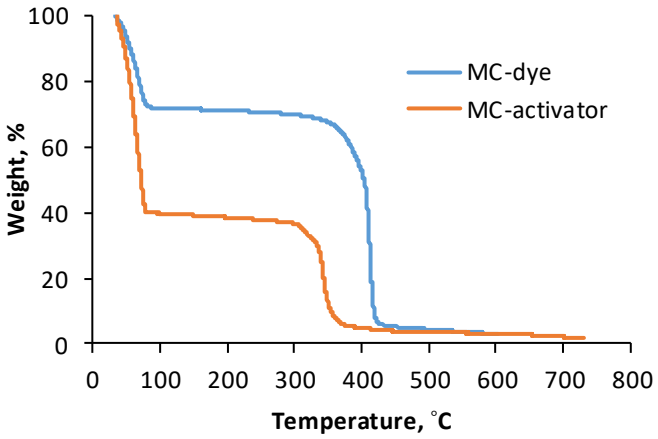


Figure 1.22. Weight change of MC-dye and MC-activator as a function of increasing temperature.

### 1.2.5 High-temperature limits for the colour change

Despite the Thermogravimetric analysis test results, where microcapsules showed thermal stability up to 350 °C, it was necessary to evaluate temperatures when the colour response is still observed. For this, a mixture of MC-dye and MC-activator with the ratio of 1:1 was prepared and placed into an oven. When heated, the liquid evaporated from the mixture and left the dry capsules in the powder form. As the temperature increased, part of the powder was selected from the oven and using paper as the substrate microcapsules were crashed with a flat end of tweezers. The first portion of the dried powder of microcapsules was selected from the oven at 50 °C and tested. Every hour small portion of microcapsules was taken off the oven and tested. After this, the temperature was increased by 25 °C for the next hour. In this manner, microcapsules were tested at 50, 75, 100, 125, 150 and 200 °C. Increasing temperature till 150 °C good stable visual response was still observed, Figure 1.23. The microcapsule filler – CVL is not stable at high temperatures and UV light, and temperatures above 200 °C lead to the full pigment degradation [69, 70]. In this case, more stable to high temperatures MF microcapsule shell did not protect CVL pigment.

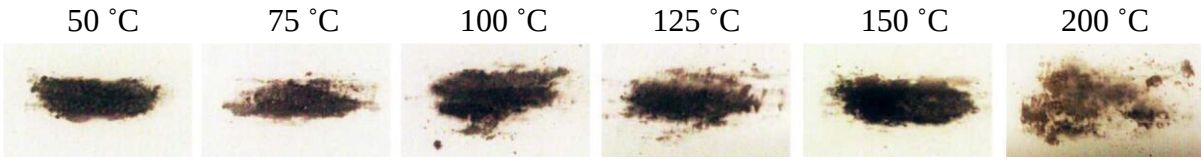


Figure 1.23. Colour response of destroyed microcapsules, stored at different temperatures.

## 1.3 Mechanical properties of microcapsules

### 1.3.1 Single microcapsule testing methods and analytical models

Applying microcapsules for specific tasks like damage indication requires understanding not only their physical but also mechanical properties. If the shell wall is too thick, the capsule will not rupture readily, preventing the release of the colour agent. On the other hand, if the shell wall is too thin, the capsules are not only fragile but also not suitable for storing colour agent inside the matrix. Microcapsules are located into materials to provide specific function - storage of colour agent until the defined critic stress. An optimal combination of microcapsule and matrix and properties of shell material is necessary to ensure mechanical triggering when the material is damaged. It is necessary to implement conditions for rupture of the microcapsule and to trigger of damage indication; thus the stiffness of the sphere relative to the matrix should be taken into account, meaning that crack should not be deflected away from the inclusion [71]. For these key parameters for efficient colour agent storage are the elastic modulus of the shell material and burst strength of the capsules [72]. Mechanical properties of capsules could be defined by various methods in general divided into two groups: methods for the measurement of an ensemble of capsules and methods for a single capsule.

Methods used for an ensemble measuring such as direct pressure mechanical strength test performed by placing different weight on the layer of microcapsules [73] and shear breakage microcapsules in a turbine reactor [74] allows to measure a batch of capsules simultaneously, but results are averaged. Such parameters like diameter or shell thickness are not considered. Due to the existing size distribution of microcapsules, in practice, estimated value corresponds to capsules that survive the smallest breaking force. Ensemble measurements are more suitable for microcapsules with monodisperse size, what is not our case, see section 2.2.2 Size distribution analysis. In the present work for the microcapsule ensemble, another approach was selected; effective properties of microcapsules were evaluated by indirect calculation. Microcapsules were placed in different matrices and systems were tested, see results in section 2.3.4 Effective properties of microcapsule ensemble.

For the characterisation of the mechanical properties of a single microcapsule different technique based on the measurement of deformation under well-defined stress are applied. Due to the small size and usually wide size-distribution, there are few instruments and methods available for the investigation of microcapsule's mechanical properties [75]. Micromechanical parameters (elastic modulus, strength, deformations, forces required to rupture the microcapsules, etc.) of microencapsulated particles are mostly determined by nanoindentation as atomic force microscopy (AFM) [76-80], and micromanipulation technique as single-capsule compression between two

parallel plates [72, 81-83], or combination of both methods [84]. Methods' main limitations are understandable from the titles - nanoindentation and micromanipulation, and they depend mostly on the size range of the tested object and applied loads, see Figure 1.24, as well resolution of the image of the tested sample, basically, micromanipulation technique uses optical microscopy. These methods are well studied and widely available to scientists. Some other methods mentioned in the literature, like optical tweezers, deformation of microspheres in a spinning drop apparatus, and micropipette aspiration are more suitable for the study of living cells, are usually lab-adapted and not widely available [85]. Thus in the present work, these methods will not be explored in details.

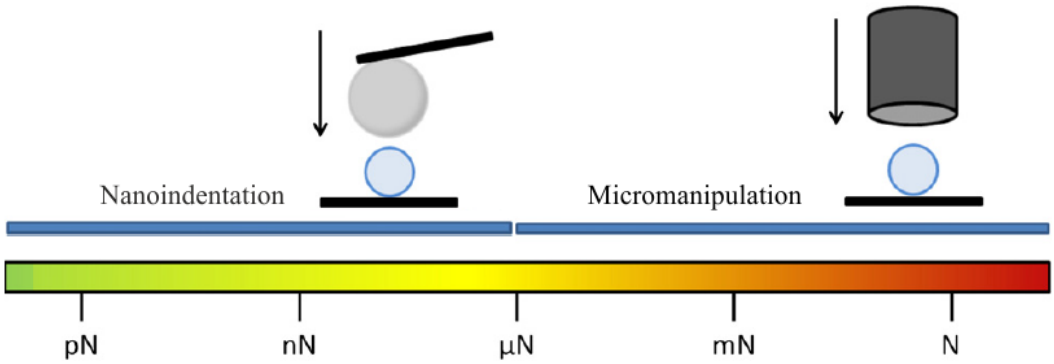


Figure 1.24. Schematic representation of single-capsule measurement techniques, each with typically available force range. Arrows indicate the directions in which forces are acting. Figure adapted from [75].

In general, nanoindentation and micromanipulation methods are based on recording the load and displacement; but acquired experimental data does not represent the intrinsic mechanical properties of a microcapsule. Several models for the calculation of elastic modulus from the experimental data are applied. Elastic moduli for the single microcapsules, defined by different techniques and applying various analytical models, are summarized in Table 1.7. For some microcapsules, tested with nanoindentation and micromanipulation methods, parameters that need additional data processing with analytical models were defined, but are not included in the summary table. Some examples of these parameters are; *rupture force* and *rupture deformation* obtained from the load-displacement curve [86-89], *nominal wall tension* [90] or *nominal rupture tension* [86] defined as $T_r = F_r / \pi D_m$, where, $F_r$ is rupture force of a single microcapsule and $D_m$ is a diameter of a single microcapsule before compression. The nominal wall tension, $T_r$, is interpreted as tension or stretch of wall at rupture. The nominal wall tension assumes that microcapsules have uniform wall thickness and allows to compare the mechanical strength of microcapsules in two samples with different mean size. The *nominal rupture stress* ($p$) is given by $p = F_r / \left(\pi R^2\right)$, where $F_r$ is rupture force, and R is the initial radius of the microcapsule [86]. The *contact stiffness* ($S$), which is defined as the slope at the beginning of the unloading curve, is given

by $S = dp / dh$ , where $p$ is the indentation load and $h$ is the indentation depth for the determination of the slope [91].

Table 1.7. Summary of the tested single microcapsules by different techniques.

| Microcapsule (core/ shell) | Diameter, *D* | Shell wall thickness, *h* | Elastic modulus, *E* | Method | Model | Ref. |
|---|---|---|---|---|---|---|
| dicyclopentadiene liquid monomer/ poly(ureaformaldehyde) | 213±12 μm<br>187±15 μm<br>65±7 μm | 175±33 nm | 3.7±0.2 GPa | compression between two parallel plates | analytical membrane theory | [72] |
| melamine–formaldehyde resin with core/shell ratio 1/3 and 1/1 | 22.5 μm | 4.50±0.50 μm<br>0.50±0.10 μm | 2.71–1.90 GPa<br>2.25–1.64 GPa | nanoindentation | - | [78] |
| dicyclopentadiene/ urea-formaldehyde | 100.25 μm | 0.15 μm<br>0.40 μm | 4.56 GPa<br>2.40 GPa | compression between two parallel plates | finite element modelling | [92] |
| tetradecane/chitosan | 5-25 μm | 134±10 nm<br>511±73 nm | 6.5±1.2 MPa<br>0.4±0.1 MPa | AFM | Reissner's theory | [80] |
| alginate-poly(L)lysine-alginate | 8.8 μm | 1.22 μm | 0.58 MPa | compression between two parallel plates | Reissner's theory | [81] |
| paraffin wax/ acrylic | 6 μm | - | 1.51±0.37 GPa<br>0.21±0.05 GPa | nanoindentation | - | [79] |
| dicyclopentadiene/ poly(phenol–formaldehyde) | 100-500 μm | 10-40 μm | 2.2±0.8 GPa | nanoindentation | - | [93] |
| dicyclopentadiene/ phenolic aldehyde | - | - | 2.46 GPa | nanoindentation | continuous stiffness model | [94] |
| poly(vinyl alcohol)/ silica | 140 μm<br>190 μm | 10-20 μm<br>10 μm | 1.57±0.02 GPa<br>1.61±0.04 GPa | compression between two parallel plates | finite element modelling | [95] |
| dicyclopentadiene/ poly(urea–formaldehyde) | 168 μm<br>95 μm<br>115 μm | - | 2.78 GPa<br>3.17 GPa<br>4.07 GPa | nanoindentation | Oliver and Pharr method | [91] |
| epoxy or mercaptan/ poly (melamine-formaldehyde) | 50 μm<br>100 μm | 0.2 μm | 4.66 GPa<br>2.83 GPa | nanoindentation | Oliver and Pharr method | [96] |
| hexyl salicylate/ melamine–formaldehyde | 5-35 μm | 0.20±0.05 μm | 1-2.5 GPa | compression between two parallel plates | finite element modelling | [97] |
| agarose | 15.4±0.3 μm<br>22±0.5 μm | - | 0.34–0.58 MPa<br>0.06–0.13 MPa | compression between two parallel plates | Hertz theory/ Tatara analysis | [98] |

| | | | | | | |
|---|---|---|---|---|---|---|
| protein/ alginate–chitosan | 15-25 μm | - | 12-43 kPa | nanoindentation | Hertzian half-space contact mechanics model | [99] |
| water-oil multiple emulsion/ poly-urethane elastomer | 50-100 μm | 1-2 μm | 2.7 MPa | compression between two parallel plates | Mooney-Rivlin law/ the neo-Hookean law | [82] |

For the calculation of the elastic modulus of the microcapsule shell materials, various models are applied. The selection of the proper model is defined by the method of the experiment. Testing of spherical capsules by nanoindentation and micromanipulation is mainly performed in three ways, see Figure 1.25, a capsule is placed on the flat substrate and 1) is indented by a sharp probe, 2) is compressed between sphere and substrate 3) is compressed between two parallel planes. Some explanation of the experimental data treatment by various models is presented below.

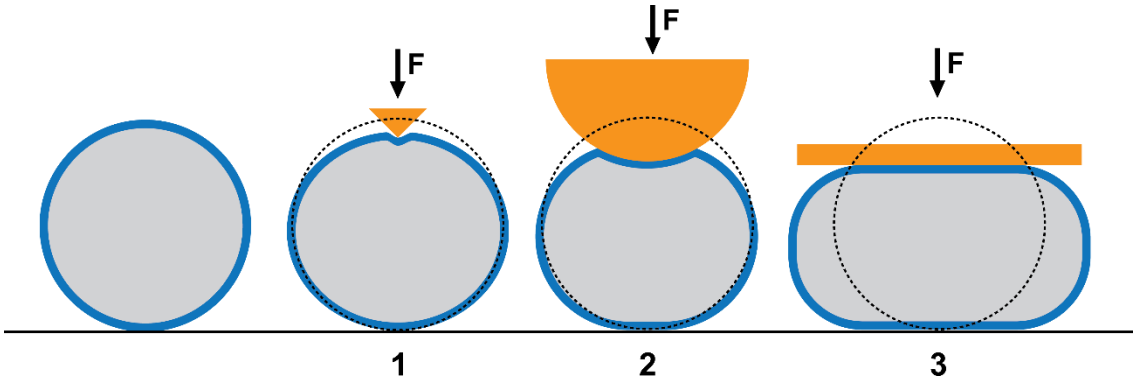


Figure 1.25. Capsule before testing (left) and indented by a sharp probe (1), compressed between sphere and substrate (2), and compressed between two parallel planes (3). With a dotted line, the initial shape of the capsule is shown.

**Reissner's theory**

Reissner's analytical result fits well if the deformation of a spherical shell under point loads on its poles. The value of the modulus was calculated according to the thin shell theory [76]. The normal displacement of the pole $d$ under point loading with force $F$ is given by

$$d = \frac{\sqrt{3\left(1-\nu^2\right)}}{4} \cdot \frac{FR}{Eh^2}, \qquad (1)$$

where $E$ is the elastic modulus of microcapsules, $h$ the shell thickness, $R$ the radius of the capsule, $\nu$ the Poisson ratio. From the Eq. (1), displacement $d$, or indentation of the microcapsule is related to the applied load

$$F = \left( \frac{4h^2}{R\sqrt{3\left(1-\nu^2\right)}} \cdot E \right) \cdot d \, . \tag{2}$$

For the utilization of thin shell theory, two assumptions are necessary to be fulfilled: the shell thickness needs to be less than 1/10 of microcapsule radius, and low forces (deformation) should be applied.

**Pogorelov's theory**

Under the assumption that the deformation energy is localized on the rim of the formed dimple, for the large deformation behaviour of spherical shells under a point load *F*, Pogorelov obtained the following result:

$$d = \frac{\left(1-\nu^2\right)^2}{3.56} \cdot \frac{F^2 R^2}{E^2 h^5} \, , \tag{3}$$

where *E* is the elastic modulus of microcapsules, *h* the shell thickness, *R* the radius of a capsule, *ν* the Poisson ratio. Hereafter buckling and formation of a dimple the deformation is no longer linear with force, but quadratic [76].

**Modified Reissner's theory**

This modification of the Reissner's theory is suitable for the case when a spherical microcapsule is compressed by a sphere which is highly rigid compared to microcapsules, and its deformation is neglected. Here indentation defined by AFM $d_{AFM}$ is proposed as a sum of the indentation on the top $d_T$ and bottom $d_B$, because of the capsule deformation from both sides during the loading process. Applying modification an indentation of the microcapsule is related to the applied load

$$F = \frac{4h^3}{R\sqrt{3\left(1-\nu^2\right)}} \cdot E \cdot \beta \cdot \left( C \frac{d_{AFM}}{h} \right)^{\alpha} \, , \tag{4}$$

where *E* is the elastic modulus of microcapsules, *h* the shell thickness, *R* the radius of the capsule, *ν* the Poisson ratio. The correction factor is $C = 0.5$, $\beta$ and $\alpha = 1$, for a very large radius probe $Rp/R >> 1$ and small shell thickness $h/R << 1$ [80].

**Hertz's theory**

For a linearly elastic spherical particle compressed between two flat rigid surfaces, the relationship between the force, *F*, and the relative displacement of the plates, *Δ*, could be described by

$$F = \frac{E\sqrt{2R}}{3\left(1-\nu^2\right)}\Delta^{3/2}, \tag{5}$$

where $R$, $E$, and $\nu$ are the radius, elastic modulus and Poisson's ratio of the capsule. The relative displacement $\Delta$ is equal to $2\delta$ where $\delta$ is the local compression at each contact point [98].

For the case, then the spherical particle is compressed by a spherical probe, the force on a particle as a function of (small) applied indentation defined by Hertz is described by

$$F = \frac{4E\bar{R}^{\frac{1}{2}}}{3\left(1-\nu^2\right)}\Delta^{3/2}. \tag{6}$$

Here the effective radius is $\bar{R} = R_1 \cdot R_2 / \left(R_1 + R_2\right)$, the probe radius $R_1$ and the particle radius $R_2$. Eq. (6) is valid for the elastic modulus of the indenter $E_1$ is much greater than $E_2$. Otherwise, the effective elastic modulus must be used [100].

**Tatara's analysis**

Tatara proposed the following relationship between the force and displacement for linear elastic deformation

$$\Delta = \frac{3\left(1-\nu^2\right)F}{2Ea} - \frac{2Ef\left(a\right)}{\pi E}, \tag{7}$$

where the contact radius is given by Hertz theory

$$a = \left[\frac{3\left(1-\nu^2\right)FR}{4E}\right]^{1/3}, \tag{8}$$

and the function $f(a)$ is given by

$$f\left(a\right) = \frac{2\left(1+\nu\right)R^2}{\left(a^2+4R^2\right)^{\frac{3}{2}}} + \frac{\left(1-\nu^2\right)}{\left(a^2+4R^2\right)^{1/2}}. \tag{9}$$

For a given force, the displacement determined by the Tatara model is always smaller than that from the Hertz theory since the value of $f(a)$ is always positive [98].

**The Hertzian contact model**

The Hertzian contact model gives an approximation for the relation between the acting force $F_c$ and the indentation $d_{12}$ appearing when two homogeneous elastic spherical half-spaces are pressed together. The Hertzian contact model assumes the adhesion between the two half-spaces to be negligible and the appearing strains to be linear. Therefore, $d_{12}$ should be small compared to the involved radii. The model is described by

$$d_{12} = \left( \frac{3F_c}{4E_{12}} \cdot \frac{1}{R_{12}^{1/2}} \right)^{2/3}, \tag{10}$$

with $\frac{1}{R_{12}} = \frac{1}{R_1} + \frac{1}{R_2}$ and $\frac{1}{E_{12}} = \frac{1-\nu_1^2}{E_1} + \frac{1-\nu_2^2}{E_2}$. Here $E_1$ and $E_2$ are the elastic moduli of the two spheres (indenter and tested particle), the Poisson's ratios of the spheres are given by $\nu_1$ and $\nu_2$, and their radii by $R_1$ and $R_2$ [101].

**Oliver's and Pharr's method**

In contrast to other models, Oliver and Pharr's method states that the elastic modulus can be measured by *analysing the unloading part of the load-displacement curve*. The elastic modulus can be calculated from the slope of the linear portion, *dp/dh* upon unloading, where *p* is the indentation load and *h* are the indentation depth for the determination of the slope. Here $E_r$ is the reduced modulus of the indentation contact:

$$E_r = \frac{\sqrt{\pi}}{2} \frac{dp}{dh} \frac{1}{A_c}. \tag{11}$$

$E_r$ is related to the elastic moduli of the sample $E$ and the indenter $E_i$ by

$$\frac{1}{E_r} = \frac{1-\nu^2}{E} + \frac{1-\nu_i^2}{E_i}, \tag{12}$$

where $\nu_i$ and $\nu$ are Poisson's ratio of the indenter and the sample [91, 96].

All microcapsules listed in Table 1.7 have different core/shell materials, are tested by various methods, and elastic modulus was calculated by applying different models. Listed models are based on the crucial assumption that the capsule deformations are elastic. In all cases, small deformation measurements were observed; thus deformations in the order of the shells' wall thickness should be applied [76]. For the testing of microcapsules in the present work, the nanoindentation with AFM was selected to obtain a load-displacement curve, and Reissner's theory was applied for further data treatment.

### 1.3.2 AFM and nanoindentation results

The topology of the dried microcapsules was monitored by AFM on the mica substrate. The separated microcapsules kept their original almost spherical character after drying with the height 1.6 μm and the width 1.8 μm, see Figure 1.26. AFM analysis was carried out on the device ICON (Bruker) with a probe SCANASYST-AIR, and resonance frequency 70 kHz, $k$ = 0.4 N/m. The measurements were carried out in the Peak Force QNM mode. The samples were prepared by spin coating on freshly stripped mica and dried on air [102].

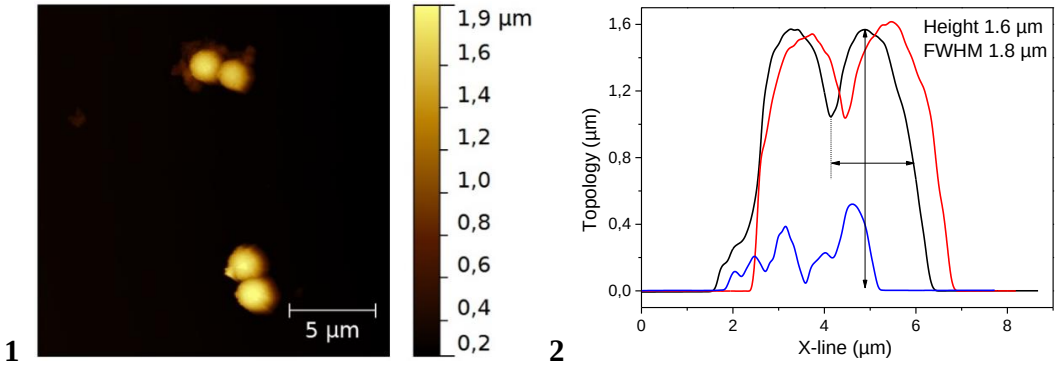


Figure 1.26. Topological image (1) and corresponding topological profile (2) of microcapsules.

Nanoindentation measurements were carried out at room temperature with the NEXT AFM (NT-MDT, Russia) equipped with a nanoindentation set-up and acoustic shelter. The indenter was a diamond Berkovich tip, the three-sided pyramid with a half angle of 30° with a nominal tip apex radius of curvature less than 30 nm, having a spring constant 10.2 ± 0.3 kN/m.

The nanoindentation measurement was used for both the maximal force loading necessary for rupture and the real quantification of the elastic modulus. The typical nanoindentation curve loaded until rupture of the microcapsule is illustrated in Figure 1.27. The force decreased quickly as the microcapsule was broken (ruptured) as it was observed on the microscope. The mean load necessary for rupture was determined as 107 ± 10 μN.

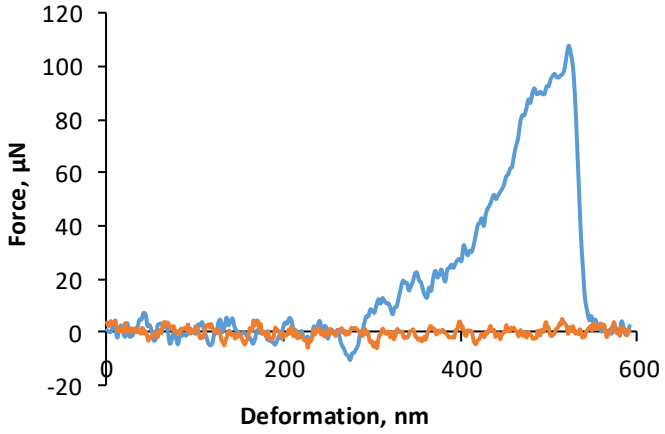


Figure 1.27. Applied force dependence on deformation until the rupture of the microcapsule.

Schematically deformation of a spherical shell under a point load is illustrated in Figure 1.28.

Experimental data, force versus indentation curves, obtained from AFM/nanoindentation tests are used. The calculation was done from the linear part of the nanoindentation curve obtained in a small deformation regime. Values of the force 2.1 μN and deformation 40 nm were obtained from Figure 1.29, and $h$ = 0.103 μm was defined from the SEM image of broken microcapsules. The Poisson ratio ν = 0.3 was applied [72].

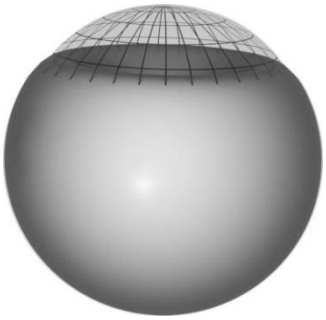

Figure 1.28. Deformation of a spherical shell under a point load: loading situation before deformation (grid) and curving after deformation (solid).

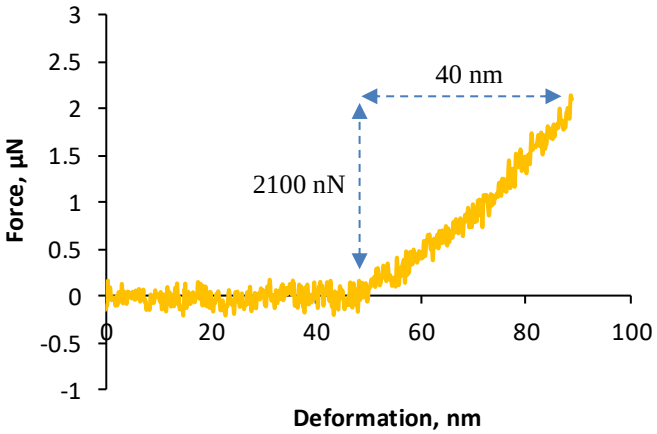


Figure 1.29. Nanoindentation curve in the small deformation regime.

Close to the pole, the modulus was calculated applying equation found for shallow spheres by *Reissner*, Eq. (1) [76], where the elastic modulus of microcapsules is (13):

$$E = 0.43 \cdot \frac{FR}{dh^2}, \tag{13}$$

where $d$ is half of the measured deformation, $h$ is a shell thickness, $R$ is a radius of a capsule, $F$ is a loading force.

Elastic modulus of shell material for the individual microcapsule with the diameter $D$ = 1.5 μm was estimated using Eq. (13) as $E$ = 1.6 GPa. The same procedure was carried out on the 10 individual particles. The mean elastic modulus was determined as $E$ = 1.7 ± 0.2 GPa [103].

### 1.3.3 Testing of the microcapsules' shell material

From the manufacturer of the microcapsules used in the present work, two types of shell material were supplied:

**A** - Only shell material resin (cross-linked);

**B** - Shell material and additives used for microencapsulation (cross-linked).

Shell materials A and B before testing are shown in Figure 1.30. According to the data from the manufacturer, the properties of original shell material might be somewhere between A and B. Samples of the material were not fully cured and become brittle and had an irregular form after the full drying.

**1**  **2** 

Figure 1.30. Microcapsules' shell material: cross-linked (1), cross-linked with additives (2).

Samples A and B were tested on compression test on universal testing machine *ZWICK 2.5* with test speed 0.5mm/min:

- with cylindrical indenter ( ∅ 6.115±0.136 mm);
- without indenter (only grips for compression tests).

Sample area, for the testing without indented, was calculated by image treatment in Adobe® Photoshop®. Example of the sample, tested on compression without indenter, is shown in Figure 1.31. Totally, 34 samples were tested: 5 samples of shell material A with indenter, 9 samples of shell material B with indenter, 10 samples of shell material A, and 10 samples of shell material B without indenter. Typical stress-strain curves for the shell material A and shell material B with and without indenter are presented in Figure 1.32. Summary of the compression tests, including Young's modulus - $E$, strength - $\sigma^*$, and corresponding deformation - $\varepsilon^*$, is presented in Table 1.8.

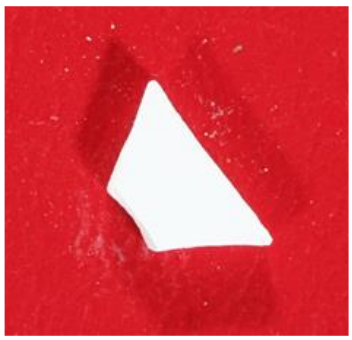

Figure 1.31. Example of the sample shell material A tested on compression without indenter.

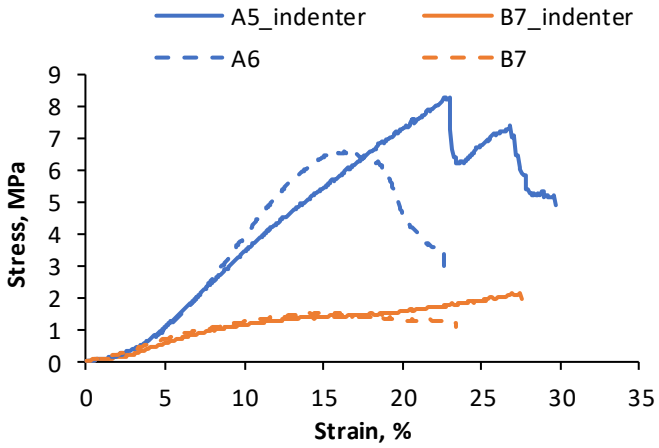


Figure 1.32. Typical stress-strain curves for the shell material A (blue), and shell material B (orange), where (–) is compression with and (– –) is compression without indenter.

Table 1.8. Summary of the compression tests of the shell material A and B.

| **Material** | **Test method** | **E, MPa** | **σ*, MPa** | **ε*, %** |
|---|---|---|---|---|
| **A** | with indenter | 53 ± 8 | 8.1 ± 0.7 | 20 ± 2 |
| | without indenter | 61 ± 16 | 6.2 ± 1.4 | 13 ± 2 |
| **B** | with indenter | 19 ± 3 | 2.6 ± 0.2 | 12 ± 4 |
| | without indenter | 17 ± 1 | 1.5 ± 0.1 | 15 ± 1 |

Comparing the results of the compression tests with and without indenter, there was no noticeable difference, and the values fell within the standard deviation, see Table 1.8. At the same time, there was a difference in the value for shell materials A and B. Thus, the true value of the elastic modulus of the shell material was expected to be in the interval from 17 ± 1 to 61 ± 16 MPa.

For the comparison of the results, in the laboratory of SMALLMATEK company, Aveiro, Portugal, melamine-formaldehyde samples were prepared and tested. The procedure like MF microcapsules synthesis was applied. To produce melamine-formaldehyde based rigid samples, it was decided to exclude the use of Sodium dodecyl sulphate and organic solvent to prevent the

formation of capsules. The high temperature over 70 °C and pH lowering (below pH 6) were used. Water was mixed with pre-polymer *Saduren 163* with adding the catalyst $MgCl_2$ for faster polymerisation. During the mixing, acetic acid was added, and the temperature was raised to 80 °C. The components were mixed for 40 min before polymerization occurred and in 10 min, almost all pre-polymer got viscous. Viscous material was removed from the water and placed on a flat surface in a dry room for 15 h. The final material was very hard and had a porous structure; however, it still could be tested to characterize the capsule shell material using mechanical testing, see Figure 1.33. Samples with the size - 4×4×3 mm were cut for the testing. Material quasi-static compression tests were performed on the universal testing machine *Zwick Roell 2.5kN* under the test speed of 0.5 mm/min.

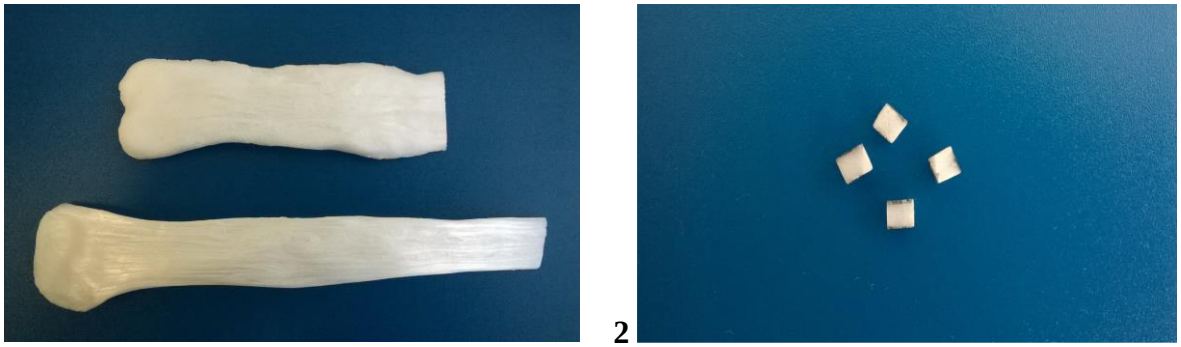

**1** **2**

Figure 1.33. MF resin after drying (1) and samples for compression tests (2).

Sample between ZWICK testing machine grips and some representative melamine-formaldehyde samples after compression tests are shown in Figure 1.34. Tests were done for two groups of 3 replicate samples. Compression force was applied to each group in mutually perpendicular directions. Quasi-static compression test graphs are represented in Figure 1.35. Summary of the compression tests, including the elastic modulus $E$, strength $\sigma^*$, and corresponding deformation $\varepsilon^*$, is presented in Table 1.9. The difference in the elastic modulus values along and transverse directions of the whole sample could be explained by the manufacturing process; before the final polymerization, the sample was pulled from the mixer. Thus some polymerizations chains along the pulling direction could appear. The value of the elastic modulus of melamine-formaldehyde samples should be in the interval from 490 ± 77 to 635 ± 56 MPa. It is quite different from the values obtained from the samples of the shell material received from the microcapsule manufacturer, as well from the value of the shell material obtained from AFM testing and calculated by the analytical model.

In literature, there is not a significant amount of experimental data about the mechanical properties of the MF material, because it is not exactly a material, but rather a chemical component used in a synthesis and polymerization process to obtain other materials. The value of $E$ = 6-7 GPa [104] for the MF material is even more different from the values obtained in this research. Value

for the MF microcapsule shell material, $E$ = 1-2.5 GPa, defined from the testing of the single capsule and calculated by FEM [97] is close to the value obtained in this study. A similar difference between tested material and value obtained from the capsule testing is described in [93], where poly(phenol-formaldehyde) were tested. Applying the analytical model for the capsule, the modulus was two times lower than obtained experimentally for the pure shell materials (2.2 ± 0.8 and 5.5 ± 0.8 GPa, respectively).

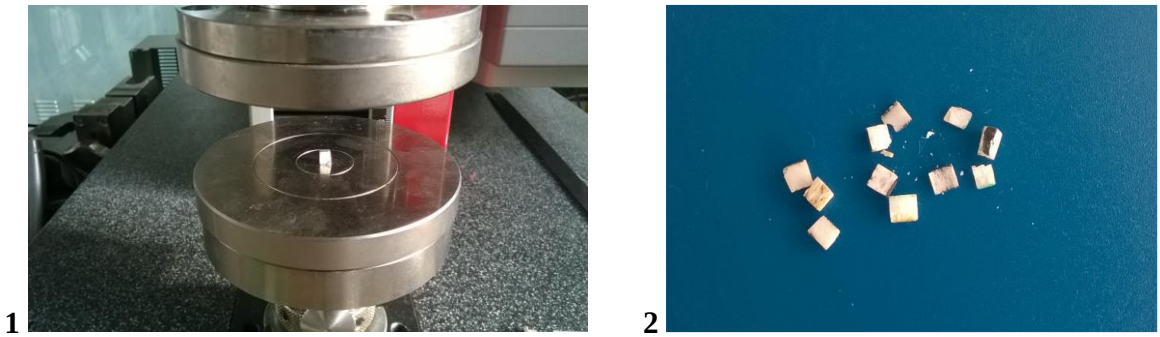


Figure 1.34. Melamine formaldehyde samples before (1) and after (2) compression tests.

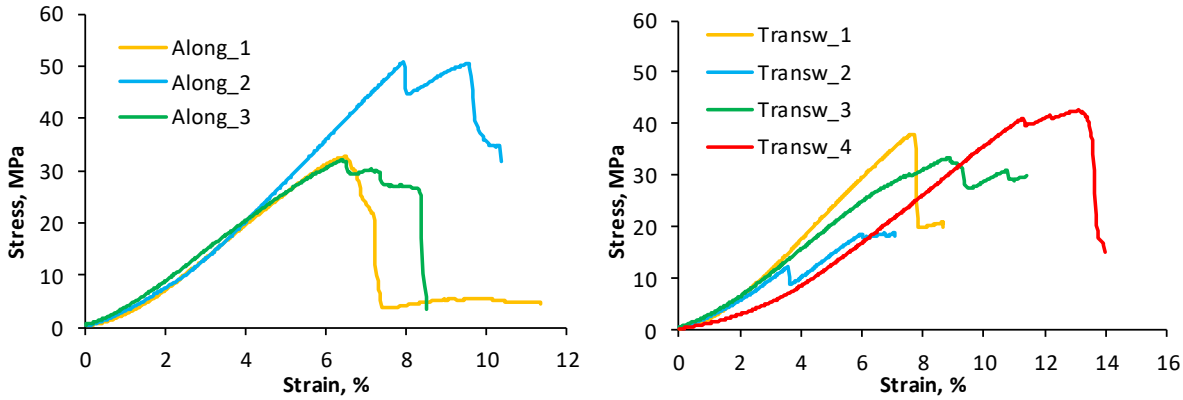


Figure 1.35. Typical stress-strain curves for the melamine-formaldehyde material samples.

Table 1.9. Summary of the compression tests of the melamine-formaldehyde material samples.

| **Direction** | **E, MPa** | **σ*, MPa** | **ε*, %** |
|---|---|---|---|
| **Along** | 635 ± 56 | 39 ± 9 | 8 ± 2 |
| **Transverse** | 490 ± 77 | 37 ± 9 | 11 ± 3 |

After testing three types of pure melamine-formaldehyde material samples, three different results were obtained. It could be assumed that the mechanical properties of the material directly depend on the method of manufacture. Thus, the results cannot be correlated with the results obtained by calculation from the AFM experimental data of the single microcapsule.

### 1.3.4 Simulation of shell-core systems

Proceeding from the assumption that the hollow system and the system filled with fluid under the load behave differently, it was necessary to choose a model system for further investigation. Since the model system must simulate a filled microcapsule, some requirements have been put forward regarding the model system. In the ideal case, it must be sphere, shell – core, with a brittle shell. As a result, a partially compliant with the requirements available option was selected - a Table Tennis ball (TT ball). Empty and filled with the water TT balls were tested on compression, see Figure 1.36 and Figure 1.37.

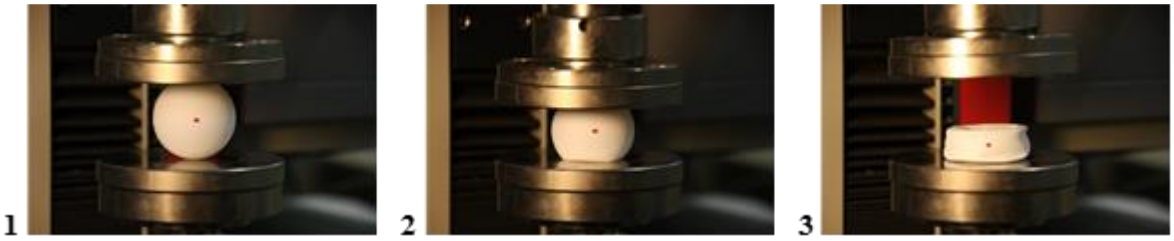


Figure 1.36.Empty TT ball before (1), during (2), and after (3) the compression experiment.

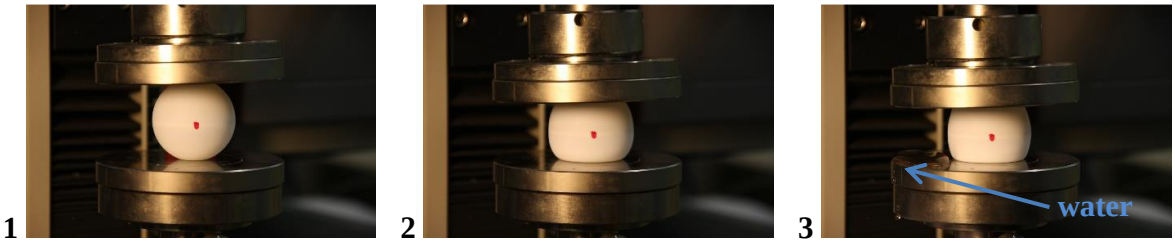


Figure 1.37. Water filled TT ball before (1) and during (2) the compression experiment. The shell cracked after the compression (3).

From Figure 1.38, obtained during the experiments, it is possible to see, that on the initial stage of loading, the deformation depends only on the properties of the shell material. Further, with increasing load, the deformation depends on the filler.

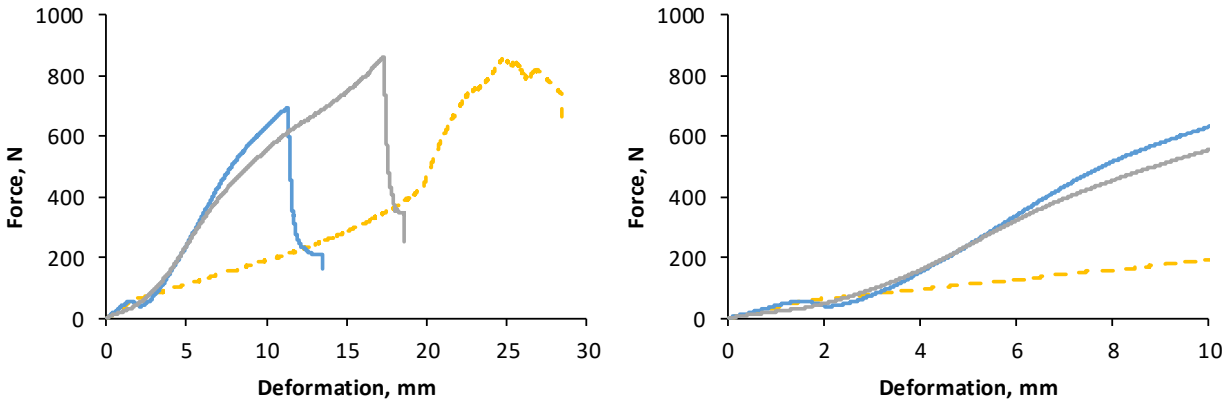


Figure 1.38. Force-displacement curves for the empty model system (– –) and filled with the water (–); the full load cycle to failure (left) and the initial stage (right).

A similar experiment was repeated with the closed cylindrical shell (CC shell), which in the cross-section has the form of a circle (before load) and the form of the ellipse (after applied load). In the course of the experiment, it was necessary to evaluate how the volume of the object changes during compression, considering the change in volume is in proportion to the change in the cross-sectional area and the circumference is constant. For the calculated curve, the *Ramanujan* approximation was used

$$l \approx \pi\left(3(a+b)-\sqrt{(3a+b)(a+3b)}\right), \tag{14}$$

where $l$ is a circumference of an ellipse with semi-major axis $a$ and a semi-minor axis $b$ [105]. The area of the cross-section was calculated from

$$S = \pi \cdot a \cdot b, \tag{15}$$

where $a = \frac{3l - 4\pi b + \sqrt{-20\pi^2 b^2 + 12\pi b l + 3l^2}}{6\pi}$, with the further determination of the change in the cross-sectional area – *ds.*

Empty and filled with the water CC shells were tested on compression. The results of the experiment were compared with the calculated curve, see Figure 1.39.

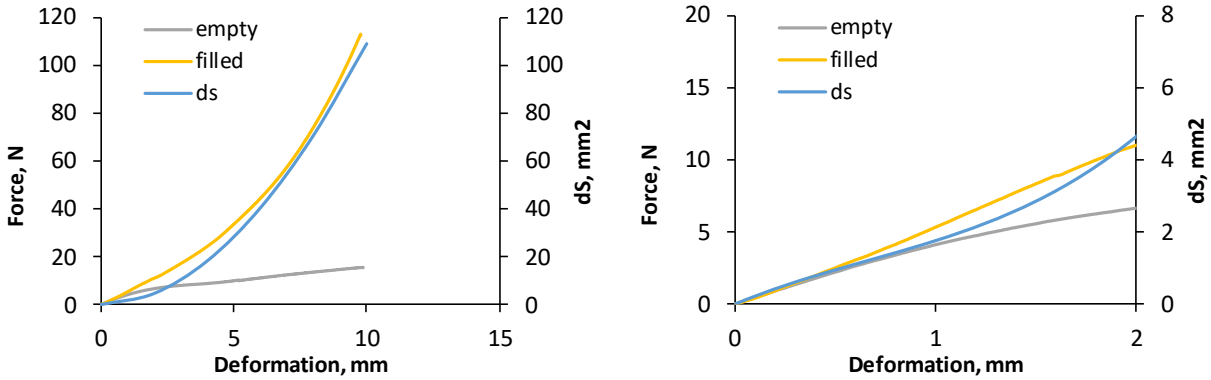


Figure 1.39. Force-displacement curves for the empty and filled model system compared with the calculated curve of the change in the cross-sectional area; the full load cycle (left) and the initial stage (right).

At the initial stage of loading, the deformation depends only on the properties of the shell material. Further, with increasing load, the deformation depends on the filler properties. For further calculation, it is necessary to consider the change in the volume of the microcapsule.

### 1.3.5 Effective properties of microcapsule ensemble

Mechanical properties of a single microcapsule obtained during AFM tests could be used in further calculation and modelling. While, this does not represent real behaviour of microcapsules in the DVIS, where MC are used in large quantities and have some variation in size. The

mechanical properties of the heterogeneous polymer blends depend on many parameters. Properties are determined by the ratio of the elastic moduli of the phases, adhesion between the phases, the particle diameter of the dispersed phase, and others. The existing approach to analyse such composite structures is to use the effective (homogenized) material properties rather than to consider all the details of the individual constituent properties and geometrical arrangement [92]. To date, few studies have investigated mechanical properties of incorporated polymeric shell-core microcapsules as fillers in matrices since these fillers usually decrease the strength and stiffness of matrix, on the contrary to solid particles. Results of such experiments are predominantly described not as a focus of the research, but rather as a part of the study of shell-core microcapsules devoted to obtaining extra functionality of the system, like self-healing or similar. Here, for the evaluation of the effective mechanical properties of microcapsules, the indirect method was applied. By tensile tests [106] or dynamic mechanical analysis [92, 107], properties of composite (films with integrated microcapsules) with the known concentration of microcapsules were measured. Further, experimental results were applied for the modelling.

**Materials**

Theoretical models describe cases then particles are soft or hard in comparison with the matrix material. In this work, only one type of aggregate was used, thus, to observe both situations, matrices with different mechanical properties for the evaluation of the effective properties of microcapsules were selected.

For the preparation of samples and testing the following materials were used as matrices in this work:

1. PVAc glue – *Klebstoff 811/2504.* One-component adhesive based on poly (vinyl acetate) and additives, bought in the market (further referred as **PVAc_1**).
2. PVAc glue - *TDS WOODMAX SW 12.47*. One-component adhesive based on poly (vinyl acetate) and additives, provided by company Synthos S.A (further referred as **PVAc_2**).
3. Water-based epoxy resin and hardener *Verniz Epoxi 2K*, used in ratio 2:1, provided by University of Aveiro (further referred as **E_1**).
4. Water-based epoxy resin *CHS 200 V 55* epoxy and *Telalit 180* hardener, in ratio 100:27, provided by company SYNPO (further referred as **E_2**).
5. Water-based epoxy coating *Sikafloor - 2540 W***.** It is grey, two-part, water dispersed, epoxy resin-based coating, used in ratio 7:3, provided by company SYNPO (further referred as **E_3**).

**Preparation of films with microcapsules**

Since microcapsules were in the water-based liquid, for the preparation of films, it was necessary to use a matrix with a water base. In order to manufacture qualitative thin films of water-

based polymer specific conditions of the manufacturing method were experimentally checked. During the work, several matrices were tested: different types of water-based epoxy resins and different types of polyvinyl acetate (PVAc) commonly referred to as 'wood glue'.

Firstly, the substrate was chosen to obtain a smooth and flat surface of the sample and from which the sample could be easily removed without the use of additional release agents. Secondly, the applicator's thickness was selected; and lastly, the mixing method to obtain maximally well-mixed solution without bubbles was chosen. All factors were checked, and, at the end, the final manufacturing conditions were chosen:

- The substrate – it was placed on the horizontal table with an adjustable level. For the water-based epoxy mixtures, glass substrate covered with PE film was used. For samples with PVAc matrix Teflon substrate was selected.
- Mixing – matrix material was mixed with microcapsules in the necessary proportion. In the case of two-component epoxy resin, microcapsules were pre-mixed before with epoxy resin and hardener was added later. Here two options are possible; by hand-mixing and by a magnetic stirrer, both methods allow to get the homogenous mixture, and there are no obvious benefits of one. After the mixing process for an epoxy mixture, some presence of bubbles was noticed - this can be fixed by the vacuuming process. To reduce air bubbles that emerge after mixing for epoxy resin CHS 200 V 55, except vacuuming method the other one was applied. For this, the defoamer BYK 1710 was used. Defoamer BYK 17100 should be added into an epoxy component in the maximal weight content 0.3 wt.%, mixed and left for 24 h. Then, the epoxy component can be mixed with hardener and filler by a magnetic stirrer, and after 10 min mixture could be applied to the substrate.
- Applicator – a form with a cubic profile and with slits of a given height at the base, see Figure 1.40 (left). On each side of the applicator, there are slits of different depths (0.2 – 0.6 and 0.8 – 1 mm, in 0.1 mm increments). Depending on the viscosity of the mixture, it is possible to select a suitable thickness for samples. For the sample preparation, sides with the slot depth 0.5 and 0.8 mm were selected. The mixture of matrix material and microcapsules were placed in the middle of the applicator, see Figure 1.40 (middle). Slowly moving the applicator over the surface of the substrate, a certain amount of the mixture passes through the slit, creating a film of a given thickness. After the curing of the film, samples with the size 7×1 cm were cut, see Figure 1.40 (right).

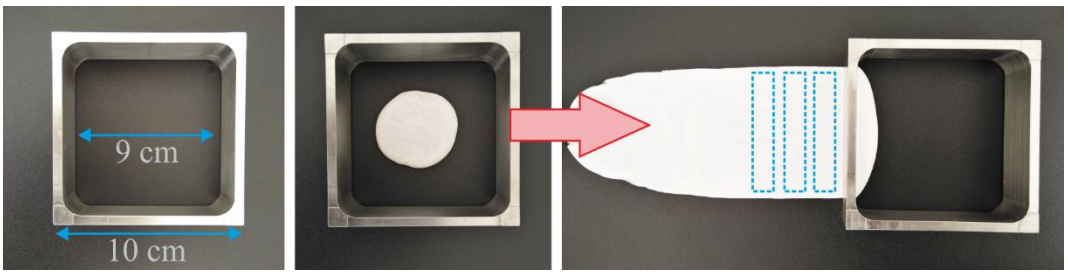


Figure 1.40. The applicator to produce thin films with a given thickness (left). Used material is placed in the middle (middle), and by slowly moving the applicator, the material with a constant thickness is applied to the surface. Samples cut from the film are shown with a dashed line (right).

- Curing time – for PVAc samples, it was 4-5 h at the lab temperature (22-24 °C). For epoxy samples, it was 24 h at the lab temperature. Samples with epoxy matrix were additionally checked by DSC if the polymer was fully cured. Post curing temperatures were checked (at 60 °C for 3 h and 80 °C for 2 h) as well, but the results did not show that the material would be fully cured even after the post-curing. Probably due to water content into samples.
- The maximal filler content – it was determined experimentally. Cured films showed that after increasing microcapsules' content over 50 wt.%, the films become brittle and with non-homogeneous thickness due to low viscosity caused by higher water content.
- The concentration of microcapsules in sample was recalculated, considering that microcapsules are presented by weight as 40% suspension in water. The non-volatile substance of water-based epoxy resin was 55% and of PVAc was 50%. The concentration of MC in PVAc and in water-based epoxy resin by weight was calculated by Eq. (16) and Eq. (17), respectively.

$$\frac{MC \cdot 0.4}{(PVAc \cdot 0.5) + (MC \cdot 0.4)} \cdot 100\% \tag{16}$$

$$\frac{MC \cdot 0.4}{(Epoxy \cdot 0.55) + (MC \cdot 0.4)} \cdot 100\% \tag{17}$$

In the results, a sample with a constant thickness was obtained, which was cut later in the form of strips for tensile tests. Several samples before and during the tensile test are shown in Figure 1.41.

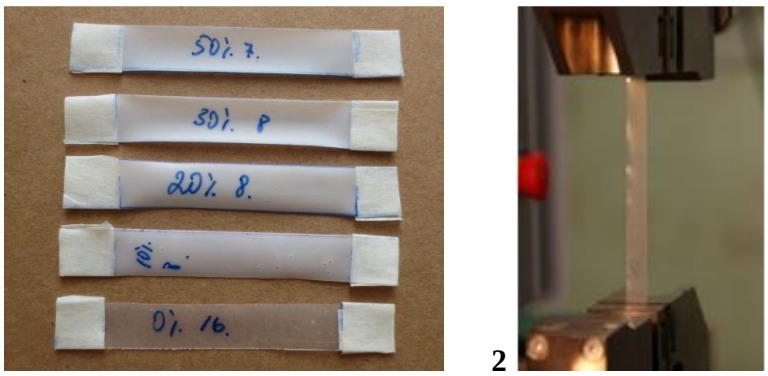


1 2

Figure 1.41. Samples for tensile tests made from PVAc as a matrix with different concentration of microcapsules (1). On the samples are indicated the mass fraction of the solution with microcapsules and not the concentration of them. Sample fixed into machine grips before testing (2).

**Testing and results**

Let's consider the behaviour of filler in a polymer matrix under tensile load. Depending on the ratio of the elastic modulus of filler and matrix, two limit cases are possible.

The first case is when the elastic modulus of the matrix is much lower than that of the filler $E_m \ll E_f$. As an example of such system PVAc glue matrix and MC could be considered. Behavoiur of such system under tension is illustrated in Figure 1.42.

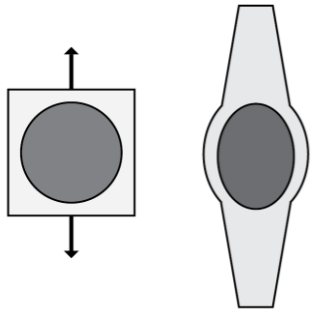

1 2

Figure 1.42. Matrix and microcapsule before (1) and after (2) applied load.

Using PVAc_1 as a matrix, 7 samples for each concentration were prepared and tested. Typical stress-strain curves obtained for the PVAc_1 sample with different concentration of microcapsules is presented in Figure 1.43. As was expected by adding microcapsules in the PVAc_1 matrix, the strength of the composite increased, see Figure 1.44 (left). From the experimental data, the elastic modulus of composite for different concentrations of microcapsules was calculated, see Figure 1.44 (right). The composite modulus consistently increases with increasing microcapsule loading.

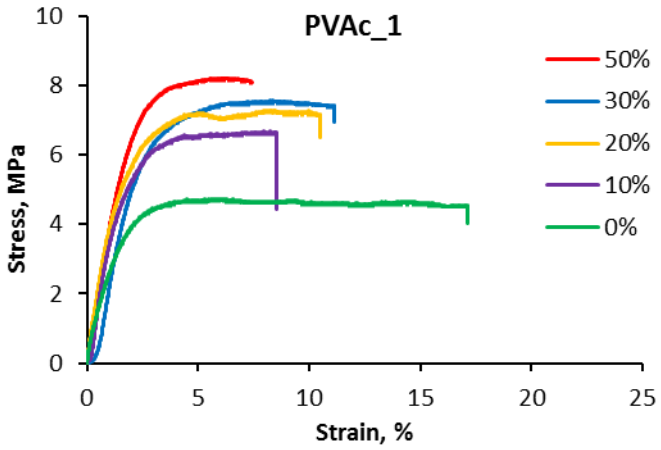


Figure 1.43. Typical stress-strain curves obtained for the PVAc_1 sample with different concentration of microcapsules.

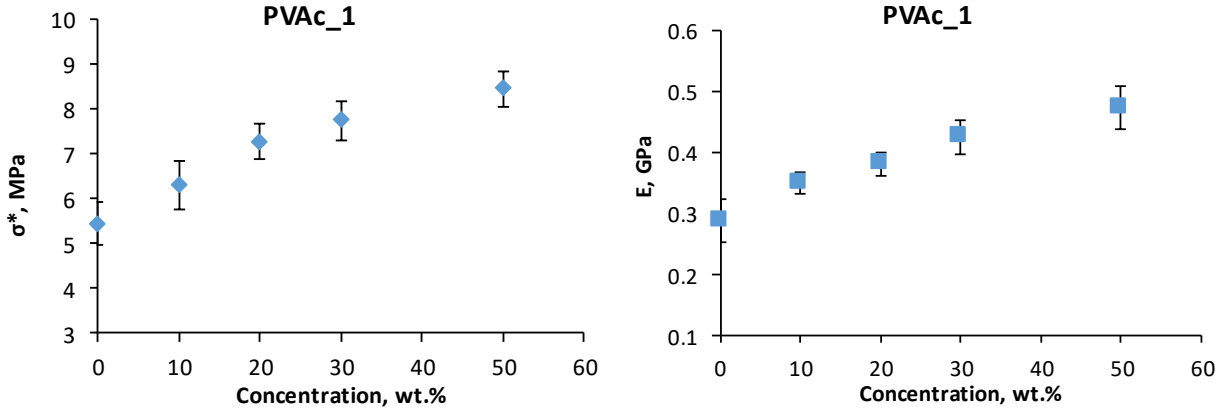


Figure 1.44. The correlation between the strength (left) and elastic modulus (right) of the composite with matrix PVAc_1 vs the microcapsule's concentration.

Using PVAc_2 as a matrix, 5 samples for each concentration were prepared. During the mixing process, increased blistering was observed. Since samples are undergoing drying, meaning that water or solvent evaporates, there is a risk for warm and cold creep in physically drying adhesives and limited thermal stability. Prepared samples were inhomogeneous in the thickness; thus, these samples weren't tested.

The second case is when the elastic modulus of the matrix is much higher than that of the filler $E_m \gg E_f$. As an example of such system water-based epoxy resin matrix and MC could be considered. The behaviour of such a system under tension is illustrated in Figure 1.45.

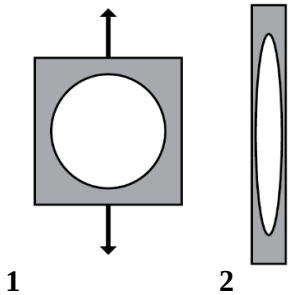


Figure 1.45. Matrix and microcapsule before (1) and after (2) applied load.

In composite MC-dye and MC-activator were used as a mixture, in the same ratio. Therefore, by preparation of two series of matrices with different concentration of MC-dye and MC-activator is possible to evaluate whether microcapsules have similar mechanical properties or not and apply this data in modelling. Using E_1 as a matrix, at least 5 samples for each concentration and type of microcapsules were prepared and tested. Typical stress-strain curves obtained for samples with epoxy matrix and with different concentrations of microcapsules are presented in the left part of Figure 1.46. As it was expected by adding microcapsules in the epoxy matrix, the strength of the composite decreased, see the right part of Figure 1.46. From the experimental data, the elastic modulus of composite for different concentrations of microcapsules was calculated, Figure 1.47. The composite modulus consistently decreased with increasing microcapsule loading. For E_1 obtained result demonstrated that composite filled with MC-dye and MC-activator has different effective elastic modulus for different concentrations of microcapsules.

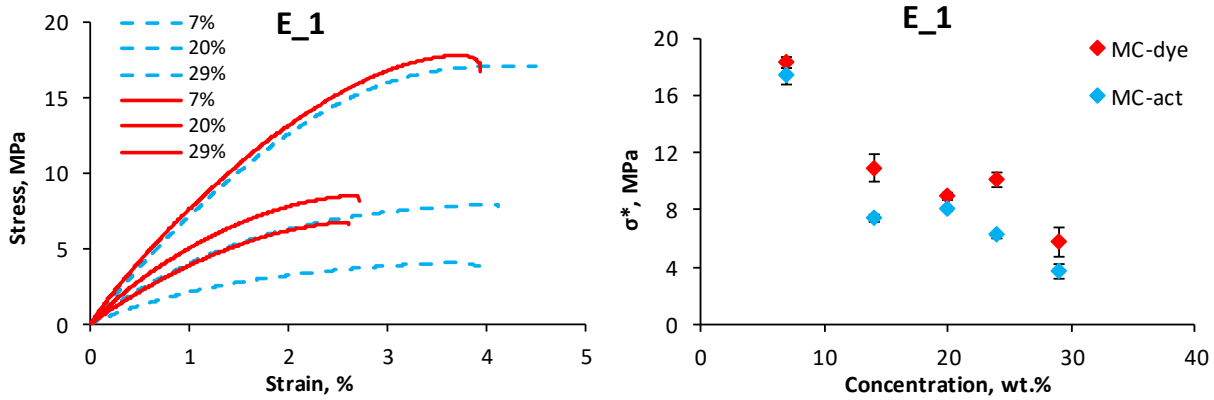


Figure 1.46. Typical stress-strain curves obtained for the E_1 sample with different concentration of MC-dye (–) and MC-activator (- -). The concentration of microcapsules increased in matrix going from the top curve to bottom (left). The correlation between the strength of the composite and the microcapsule's concentration (right).

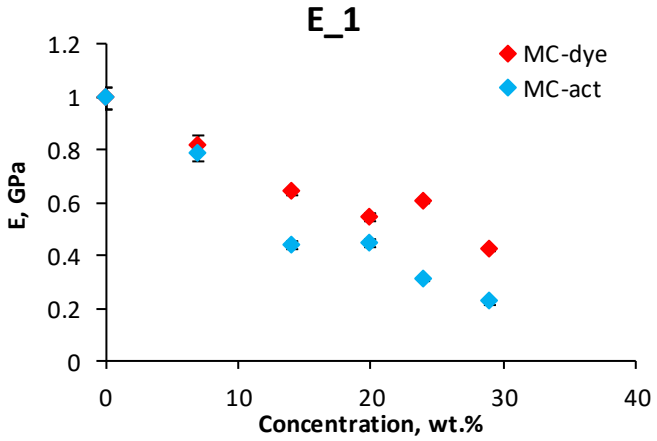


Figure 1.47. Elastic modulus of the composite with matrix E_1 vs the concentration of two types of microcapsules.

Using matrix E_2, at least 5 samples for each concentration filled with MC-dye, MC-activator, and the mixture of both were prepared and tested. By increasing the concentration of microcapsules in the epoxy matrix, the strength of the composite decreased. The composite modulus as well consistently decreased with increasing microcapsule loading, see Figure 1.48. The title E_2.1 was given to the first series of samples made with E_2 matrix. Comparing the values of the effective elastic modulus for the E_2.1 matrix filled with different microcapsules and the mixture of both, it is not possible to unequivocally ascertain which capsules influenced the properties of the composite more. At low concentration (5 wt.%), the moduli values coincide. At 20 wt.% the module of the composite with MC-activator coincides with the module of the composite with a mixture of capsules. In contrast, at 30 wt.% the module of the composite with MC-dye coincides with the module of a composite with a mixture of capsules. For E_2.1 samples, these changes probably could be related to unfixed changes in moisture or temperature during curing time or unfinished curing process affected on sample properties. Here defoamer BYK 17100 was not used. Also, the size of errors indicates poor repeatability.

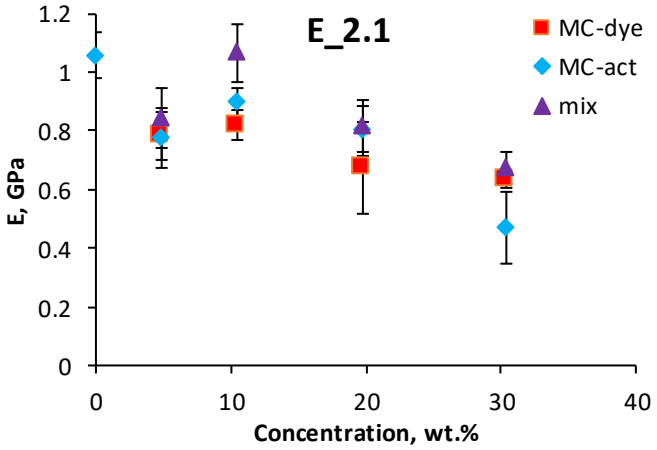


Figure 1.48. Elastic modulus of the composite with matrix E_2 vs the concentration of two types of microcapsules and a mixture of both.

For the second series, E_2.2 samples were prepared using defoamer BYK 17100. At least 5 samples for each concentration filled with MC-dye were tested. Typical stress-strain curves obtained for samples with epoxy matrix and with different concentration of microcapsules are presented in the left part of Figure 1.49. As it was expected by adding microcapsules to the epoxy matrix, the strength of the composite decreased, see the right part of Figure 1.49. With E_2.2 samples with good repeatability were obtained, except samples with MC-dye 42 wt.%. To obtain samples with such high concentrations of microcapsules, a high amount of water is also added. The resulting samples are heterogeneous in thickness. The reference sample E_2.2 (without microcapsules) has elastic modulus higher compared to reference E_2.1, see Figure 1.50. It can be

assumed that the samples preparation process was performed more accurately, and curing process in samples has finished.

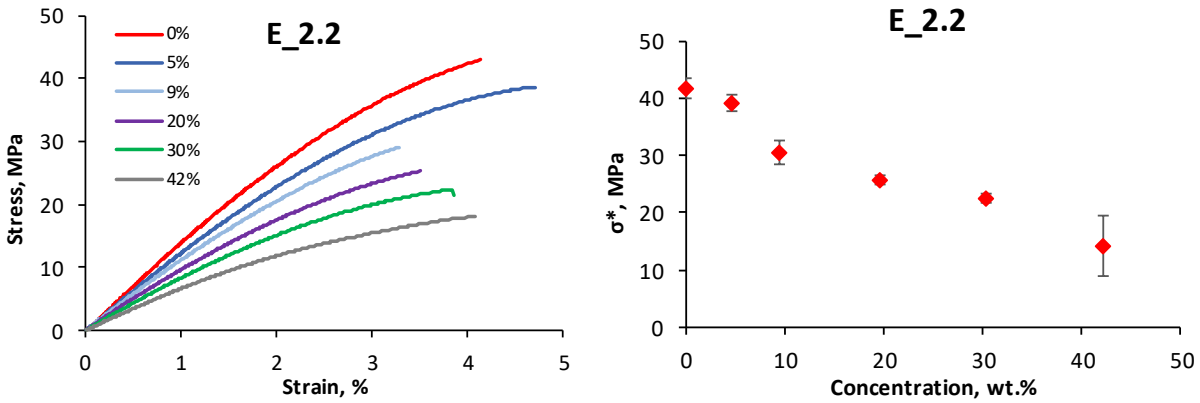


Figure 1.49. Typical stress-strain curves obtained for the E_2.2 sample with different concentration of MC-dye (left). The correlation between the strength of the composite vs the microcapsule's concentration (right).

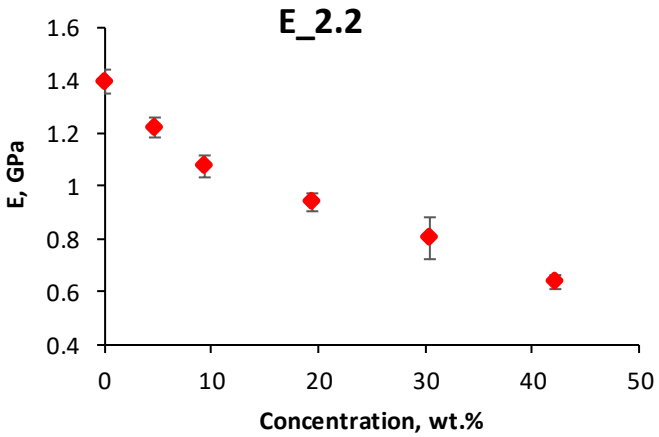


Figure 1.50. Elastic modulus of the composite with matrix E_2 vs the concentration of MC-dye microcapsules.

Using matrix E_3, at least 5 samples for each concentration filled with MC-dye were prepared and tested. Typical stress-strain curves obtained for samples with epoxy coating and with different concentration of microcapsules are presented in the left part of Figure 1.51. As it was expected by adding microcapsules in the epoxy coating, the strength of the composite decreased, see right part of Figure 1.51. Samples with good repeatability were obtained using E_3 matrix. Elastic modulus of the composite with matrix E_3 vs the concentration of MC-dye microcapsules is presented in Figure 1.52.

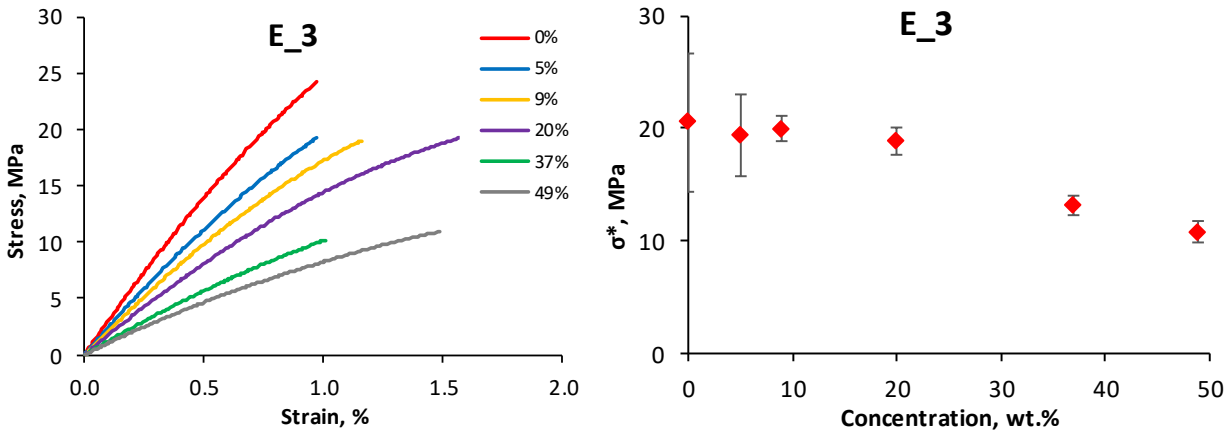


Figure 1.51. Typical stress-strain curves obtained for the E_3 sample with different concentration of MC-dye (left). The correlation between the strength of the composite vs the microcapsule's concentration (right).

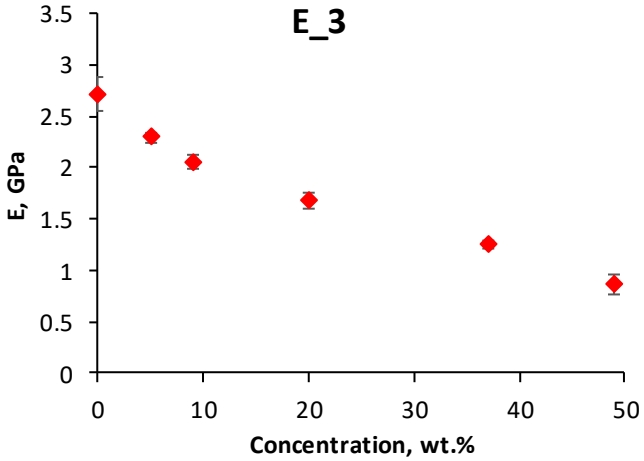


Figure 1.52. Elastic modulus of the composite with matrix E_3 vs the concentration of MC-dye microcapsules.

The value of the average elastic moduli obtained for different concentrations of microcapsules in PVAc and epoxy matrices were used for the calculation of effective elastic modulus of microcapsules applying different analytical models.

### 1.3.6 Effective elastic modulus of microcapsules by different models

The elastic modulus of polymer composite filled with capsules is generally determined by the elastic properties of its components - capsules and matrix, and its volume fraction. The effective elastic modulus of microcapsules applying empirical or semi-empirical equations could be recalculated using data obtained experimentally; mechanical properties of the matrix and matrix with the filler and the volume fraction of the latter [108].

Some empirical or semi-empirical equations for the experimental data treatment are presented below using the notations listed in Table 1.10.

Table 1.10. Notations used in equations.

| | Composite | Matrix | Filler |
|---|---|---|---|
| Elastic modulus | $E_c$ | $E_m$ | $E_f$ |
| Volume | $V$ | $V_m$ | $V_f$ |
| Volume fraction | 1 | $\phi_m$ | $\phi_f$ |

The volume fractions $\phi_f$ and $\phi_m$ are expressed by $\phi_f = \frac{V_f}{V}$, $\phi_m = \frac{V_m}{V}$, and $\phi_f + \phi_m = 1$.

**Einstein's equation**

Einstein's equation (18) was originally derived for the effective shear viscosity for dilute suspensions of rigid spheres and was extended to study the effective viscosity of concentrated suspensions of mono-sized spheres. The simple Einstein's equation based on the rigid particle assumption [109] is valid only at low concentrations of fillers. For high concentrations, the interaction between fillers takes place and this effect is not considered [110]. The equation assumes perfect adhesion between filler and matrix, and perfect dispersion of individual filler particles

$$E_c / E_m = 1 + 2.5\phi_f . \tag{18}$$

This equation implies that the composite modulus is independent of particle size and predicts a linear relationship between $E_c$ and $\phi_f$ [111].

**Guth's equation (Einstein-Guth-Gold equation)**

Here a particle interaction term was added in the Einstein equation (18) which becomes

$$E_c / E_m = 1 + 2.5\phi_f + 14.1\phi_f^2 . \tag{19}$$

The linear term is the stiffening effect of individual particles and the second power term is the contribution of particle interaction [111]. This equation is applicable only to matrix reinforced with spherical inclusions [110].

Another Guth's equation has been developed for other shapes and is not restricted to spherical particles. It was developed for rod-like shapes characterized by the ratio of the length to the width of the particles or the filler aggregate structures [112]

$$\frac{E_c}{E_m} = 1 + 0.67 g_f \phi_f + 1.62 \left( g_f \phi_f \right)^2 , \tag{20}$$

where $g_f$ is a shape factor related to the length/diameter ratio of the particles [113]. This model attempts to account for the fact that particle aggregation has a significant impact on stiffness at higher volume fractions (i.e. $\phi_f \geq 0.15$) [112].

**Mooney's equation**

This modified equation (21) is reduced to Einstein's equation (18) at low volume fractions of spherical particles and represents test data at high volume fractions

$$\frac{E_c}{E_m} = e^{\left(\frac{2.5\phi_f}{1-s\phi_f}\right)}, \tag{21}$$

where $s$ is a crowding factor for the ratio of the apparent volume occupied by the particle to its own true volume, $1.0 \leq s \leq 2.0$ [114]. For close sphere packing $s = 1.35$ [108].

**Voight and Reuss equations**

The composite scheme by Voigt (uniform strain) and Reuss (uniform stress) models is the simplest arrangements of fibres in a two-phase material containing continuous fibres and matrix. Such laminates are anisotropic since they represent an identical structure subjected to a different orientation of stress, see Figure 1.53. It is a simple model for elastic two-phase composite. There is no restriction on the shape of the two phases. Adhesion and particle diameter are not considered and could be used for an approximate result also for the system with spherical inclusions. Applying Voight and Reuss equations, also known as "Rule of mixture" and "Inverse rule of mixture" – ROM, it is possible to define the theoretical upper limit - Voight model, Eq. (22), which fits better to soft particles embedded in a hard matrix, i.e. low-density aggregate polymer and lower limit - Reuss model, Eq. (23), which fits better to hard particles embedded in a soft matrix, i.e. normal-density aggregate polymer, and where the real values are located between the limits [115]

$$E_c = E_f \cdot \phi_f + E_m \cdot \phi_m, \tag{22}$$

$$E_c = \left[\frac{\phi_f}{E_f} + \frac{\phi_m}{E_m}\right]^{-1}. \tag{23}$$

In practice, at the microscopic level, see Figure 1.54, the microcapsules are not separated from each other and consideration of uniform stress/strain is a simplification [110]. Despite the fact, that ROM provides an only rough estimation of the effective elastic properties of composite materials, these are the most widely used models in engineering calculations due to their simplicity.

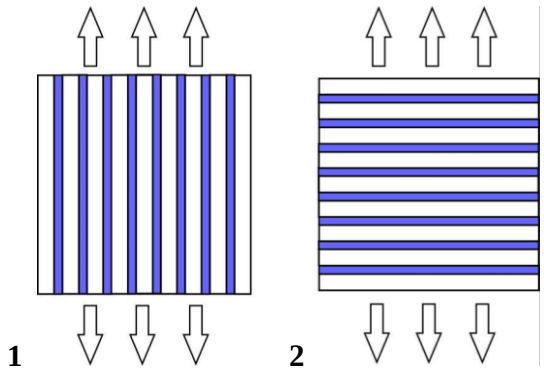


Figure 1.53. A composite scheme by Voigt (1) and Reuss (2) models.

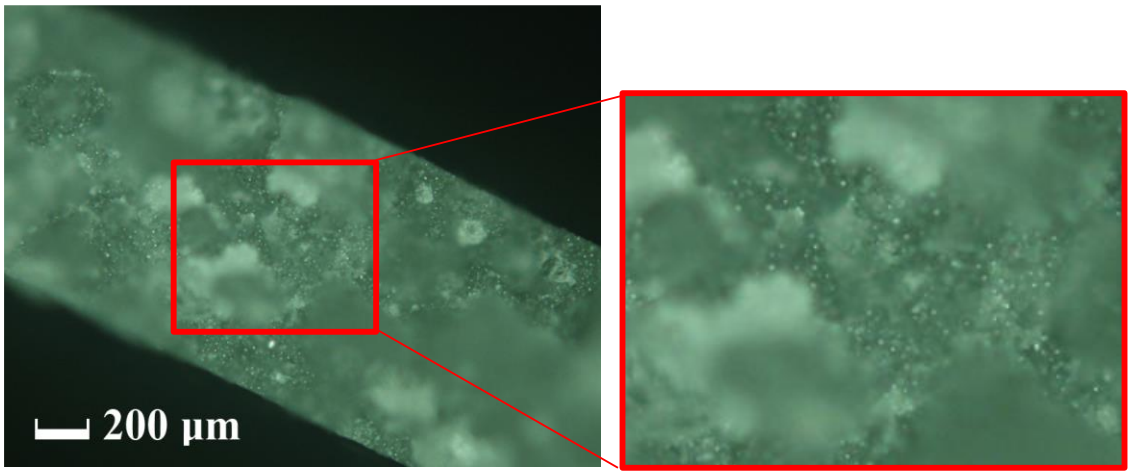


Figure 1.54. The fracture surface of the epoxy matrix filled with microcapsules.

**Voigt-Reuss-Hill model**

The arithmetical mean of the Reuss and Voigt equations can be used as an approximation within these bounds, often referred to as the Reuss-Voigt-Hill average

$$E_c = \frac{E_c^R + E_c^V}{2}, \tag{24}$$

where *R* and *V* superscripts refer to Reuss and Voigt equations.

The stress and strain are generally unknown in the composite and are expected to be nonuniform. The Voigt and Reuss averages are interpreted as the ratio of average stress and average strain within the composite [116].

**Hirsch model**

This is a combination of Voight and Reuss models, where bound is expected to be somewhere in the middle of upper and lower limits [117]

$$\frac{1}{E_c} = 0.5\left(\frac{1}{(1-\phi_f)E_m + \phi_f E_f}\right) + 0.5\left(\frac{1-\phi_f}{E_m} + \frac{\phi_f}{E_f}\right). \tag{25}$$

**Hashin-Hobbs model**

This model assumes equal Poisson's ratio for two phases, and no particle interaction [117]

$$E_c = E_m \left[ \frac{\left(1-\phi_f\right)E_m + \left(1+\phi_f\right)E_f}{\left(1+\phi_f\right)E_m + \left(1-\phi_f\right)E_f} \right]. \tag{26}$$

**Hashin-Shtrikman equations**

In contrast to ROM, where the bounds do not typically give a close prediction of the effective elastic moduli of composites with spherical geometry [118], closer bounds for the elastic moduli have been developed for multi-component composites by Hashin and Shtrikman (H-S) [108]. Moduli given by the H-S formulae are exactly attainable by several hierarchical structures. One is the coated sphere morphology. In this composite the full volume is filled with spheres of different sizes of one phase; each sphere has a coating of a given fraction of the sphere radius, made of a material of the second phase, see Figure 1.55 [119]. For the H-S model, the shape of the filler is not a limiting factor and estimated the upper and lower bounds of the composite based on variational principles of elasticity. The upper $K^+$ and lower $K^-$ bounds of the bulk moduli and shear moduli $G^+$ and $G^-$ of the composite are given as Eq. (27)-(30) [120]:

$$K^+ = K_f + \left(1-\phi_f\right)\cdot\left[ \frac{1}{K_m - K_f} + \frac{3\phi_f}{3K_f + 4G_f} \right]^{-1}, \tag{27}$$

$$K^- = K_m + \phi_f \cdot \left[ \frac{1}{K_f - K_m} + \frac{3\left(1-\phi_f\right)}{3K_m + 4G_m} \right]^{-1}, \tag{28}$$

$$G^+ = G_f + \left(1-\phi_f\right)\cdot\left[ \frac{1}{G_m - G_f} + \frac{6\phi_f\left(K_f + 2G_f\right)}{5G_f\left(3K_f + 4G_f\right)} \right]^{-1}, \tag{29}$$

$$G^- = G_m + \phi_f \cdot \left[ \frac{1}{G_f - G_m} + \frac{6\left(1-\phi_f\right)\left(K_m + 2G_m\right)}{5G_m\left(3K_m + 4G_m\right)} \right]^{-1}. \tag{30}$$

The upper and lower bounds of the elastic modulus are simplified to the following relationships

$$E_c = \frac{9K}{1+3K/G}. \tag{31}$$

For the case when the filler particles are almost incompressible, and the load is transferred to the filler through deformation of the matrix, H-S upper bound equation can be written as

$$E_c^+ = E_f \frac{5E_m + 3\phi_f\left(E_f - E_m\right)}{5E_f - 2\phi_f\left(E_f - E_m\right)} \tag{32}$$

and the H-S lower bound is [112]

$$E_c^- = E_m \frac{3E_m + 2E_f + 3\phi_f\left(E_f - E_m\right)}{3E_m + 2E_f - 2\phi_f\left(E_f - E_m\right)}. \tag{33}$$

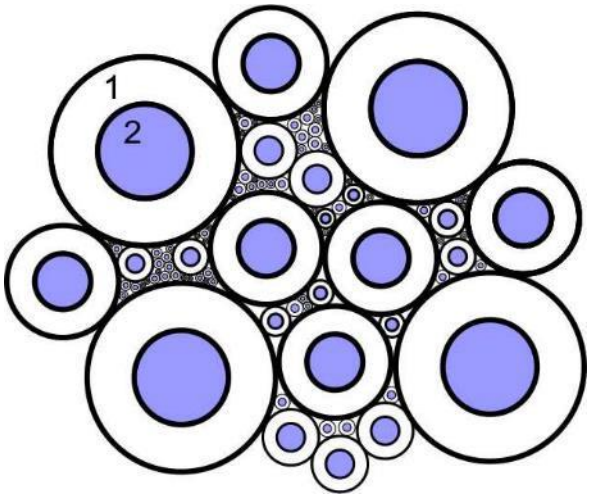


Figure 1.55. Composite by H-S model; the full volume is filled with spheres of different size of one phase (2); each sphere has a coating of a given fraction of the sphere radius, made of a material of the second phase (1).

**Counto equations**

Counto proposed a simple model for a two-phase particulate composite by assuming perfect bonding between filler and matrix [108, 111, 121]. The composite modulus is given by

$$\frac{1}{E_c} = \frac{1-\phi_f^{1/2}}{E_m} + \frac{1}{\left(1-\phi_f^{1/2}\right)/\phi_f^{1/2}\cdot E_m + E_f} \tag{34}$$

and is generally applied for a full range of aggregate stiffness [117].

**Kerner's equation**

Composite scheme by Kerner's model is presented in Figure 1.56. Key considerations in this model are that the composite inclusions are perfectly bonded to the matrix, and they are isolated from each other. In Kerner's equation assumes that the spherical particle 2 is embedded in a spherical shell of matrix 1 surrounded by an "infinite" body with the average composite properties

$$\frac{E_c}{E_m} = \frac{\dfrac{\phi_f G_f}{(7-5\nu_m)G_m + (8-10\nu_m)G_f} + \dfrac{\phi_f}{15(1-\nu_m)}}{\dfrac{\phi_f G_m}{(7-5\nu_m)G_m + (8-10\nu_m)G_f} + \dfrac{\phi_m}{15(1-\nu_m)}}, \tag{35}$$

where ν is the Poisson's ratio, and $G$ is the shear modulus.

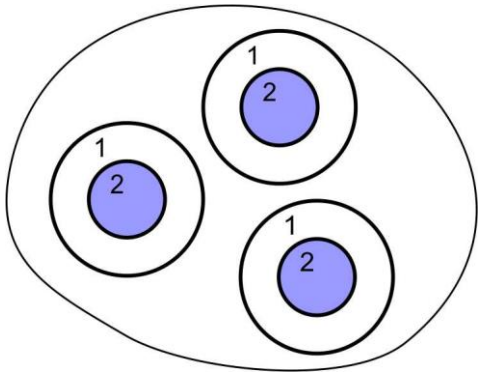


Figure 1.56. The composite scheme by Kerner's model; the spherical particle 2 is embedded in a spherical shell of matrix 1 surrounded by an "infinite" body with the average composite properties.

Kerner's model for estimating the modulus of a composite filled with spherical particles for the case $E_f >> E_m$ is simplified to [108]

$$\frac{E_c}{E_m} = 1 + \frac{\phi_f \cdot 15(1-\nu_m)}{\phi_m (8-10\nu_m)}. \tag{36}$$

For the experimental data treatment by models listed before the correlation between the weight fraction $\phi_{wt}$ and the volume fraction $\phi$ should be defined as

$$\phi_f = \frac{V_f}{V_f + V_m} \tag{37}$$

$$\phi_f = \frac{\dfrac{M_f}{\rho_f}}{\dfrac{M_f}{\rho_f} + \dfrac{M_m}{\rho_m}}$$

$$\phi_f = \frac{\dfrac{\phi_{wt} \cdot M}{\rho_f}}{\dfrac{\phi_{wt} \cdot M}{\rho_f} + \dfrac{(1-\phi_{wt}) \cdot M}{\rho_m}}$$

$$\phi_f = \frac{\phi_{wt}}{\phi_{wt} + (1-\phi_{wt})\frac{\rho_f}{\rho_m}}$$

Here $\rho_f$ and $\rho_{fm}$ are densities of filler and matrix. In the case, when densities of the filler and matrix are similar $\rho_f \approx \rho_m$, i.e. $\phi_f \approx \phi_{wt}$, values of a fraction by weight and volume fraction could be equated. For the epoxy resin, PVAc and microcapsules values of densities were 1.1-1.2, 1.1, and 1, respectively. Thus, experimental data could be used in analytical models without recalculation to the volume fraction.

In the result of the experiment for all tested epoxy matrices filled with two types of microcapsules, a significant decrease of the elastic modulus was observed. Comparing elastic modulus of the neat epoxy-based matrix to the matrix filled with 20 wt.% of MC-dye microcapsules, the average decrease in the value of elastic modulus of about 40% was observed, see Figure 1.57

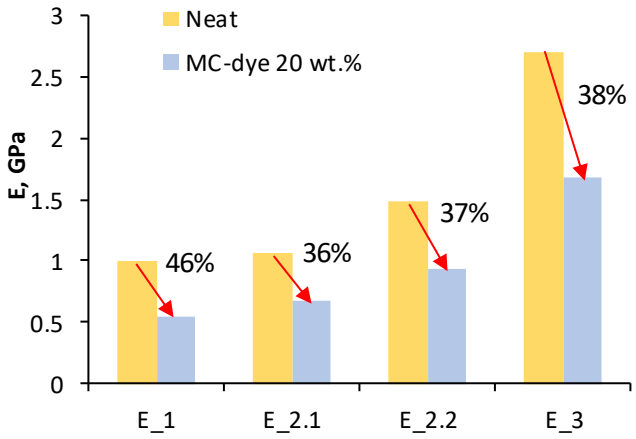


Figure 1.57. Values of elastic modulus for neat epoxy-based matrices comparing with the same matrices filled on 20 wt.% with microcapsules.

The decrease in the value of elastic modulus could be related to the weak bonding between filler and matrix. In that case, the conditions for using analytical models are not fulfilled, and an effective elastic modulus of microcapsules could not be defined correctly.

In the result of the experiment for the PVAc_1 matrix filled with two types of microcapsules following average elastic moduli for different concentrations were obtained, see Table 1.11. These data were used for the prediction of the effective elastic modulus of microcapsules applying some analytical models described before, see Figure 1.58.

Table 1.11. Summary of the experimental results: elastic moduli of PVAc_1 films filled with different concentration of microcapsules.

| Concentration, wt. % | 0 | 10 | 20 | 30 | 50 |
|---|---|---|---|---|---|
| ***E* average, GPa** | 0.29 | 0.35 | 0.38 | 0.43 | 0.47 |
| **Standard deviation** | 0.04 | 0.02 | 0.02 | 0.03 | 0.04 |

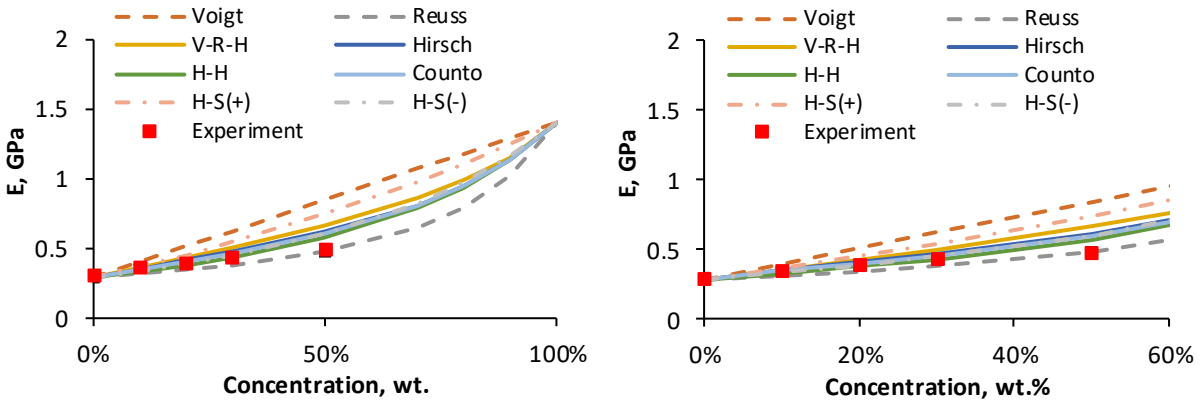


Figure 1.58. Experimental results of elastic modulus of PVAc films filled with different concentration of microcapsules and curves obtained for different analytic models.

By fitting experimental results between the upper and lower interval obtained by Reuss and Voigt models, the effective elastic modulus of microcapsules was defined as $E = 1.4 \pm 0.2$ GPa.

## 1.4 Main results of Chapter 1

- As a part of damage visual indication system, the mononuclear microcapsules with a spherical shape were selected.
- The comparative SEM analysis of laboratory synthesized, and commercially available microcapsules was performed. Commercial MC were selected as a more suitable for the DVIS based on shape regularity, smoothness of the surface and absence of the remaining material.
- An average diameter of MC-dye $D = 7 \pm 0.5$ μm and MC-activator $D = 2 \pm 0.2$ μm, and the average wall thickness of broken microcapsules $h = 0.10 \pm 0.01$ μm was defined by SEM images analysis.
- The optimal ratio of MC-dye and MC-activator was defined as 1:1. With this ratio, the visual response after the damage of microcapsules and the chemical reaction of components was the brightest.
- Thermogravimetric analysis revealed that microcapsules are stable till 350 °C, but the stable visual response after the damage of microcapsules was observed till 150 °C.
- Mechanical properties of the microcapsules shell material were defined by testing samples of pure melamine-formaldehyde material. The experiment demonstrated that mechanical properties depend on the way of synthesis of the samples; the values of the elastic modulus $E$ =

17 - 61 MPa for samples obtained from microcapsule manufacturer and $E$ = 490 - 635 MPa for laboratory-made samples were defined.

- For the single microcapsule tested by nanoindentation on AFM, the average load necessary for rupture of a microcapsule was determined as 107 ± 10 μN.
- The average elastic modulus for similar size microcapsules was determined as $E$ = 1.7 ± 0.2 GPa through the application of Reissner's analytical model.
- Mechanical properties of an ensemble of microcapsules in polymer films with different concentrations were evaluated by tensile tests. As a result, the dependence of the elastic properties of the film on the concentration of MC were defined.
- The effective elastic modulus of microcapsules was defined as $E$ = 1.4 ± 0.2 GPa by applying analytical models like Reuss and Voigt models, Hashin-Shtrikman, Counto, Hirsch, etc.

# 2 THE DAMAGE VISUAL INDICATION SYSTEM

For the development of the DVIS, the colour agent was supplied in two variations: A) MC with dye and MC with an activator, B) MC with dye and particles of activator. In both cases, all components were supplied as water-based dispersion. In work, both approaches were applied, because each of them has its advantages and specificity of application. The concept of colour change after the mechanical damage of capsules both for cases with encapsulated activator and in particles is schematically illustrated in Table 2.1. Additionally, the same table presents some cons and pros of each variation. The use of a fabric base is also critical since impregnation of fabric with a mixture of colour former and activator ensures the contact between them.

Table 2.1. Encapsulated activator and activator as particles; pros and cons of application.

| | **A** | **B** |
|---|---|---|
| | 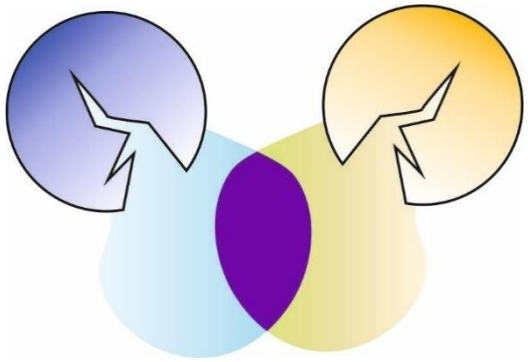 |  |
| **Pros** | • Microcapsule protects colour activator from the influence of the surrounding environment. | • System B is cheaper compared to A because there is no need to encapsulate activator additionally. |
| **Cons** | • For A to ensure visual response with a similar colour intensity as B, there is a need to use more activator (for A ratio of components is 1:1, for B 2:1).<br>• By using A, the total amount of microcapsules in a composite increase, this could negatively affect mechanical properties of it. | • Activator is sensitive to the pH level of the environment; thus, applications of B are limited. |

When the colour former and colour activator for the DVIS were selected, for the manufacture of the DVIS, it was necessary to solve the following tasks:

- select a base for the DVIS (fabric to be coated with the two-component colour agent);
- select a substance / or a method that holds the colour agent on the surface of the base;
- develop a technology for the DVIS manufacture following the chosen base and a method to hold the colour agent on the surface.

The choice of the base depended on the DVIS further application. For this reason, two directions of applications were defined: the DVIS for external use and the DVIS for internal use.

## 2.1 Visual response measuring procedure

In the present work, the main reason for utilising of colour agents was to visualize a place of damage. Thus, it was necessary to develop a procedure for the quantitative evaluation of the visual response during the development, testing, and optimization of the DVIS. Visual response on the applied load was observed immediately; however, a two-hour pause was afforded to ensure that all released dye gets into the contact with activator and colour reached saturation. In the current study two methods were used for the quantitative evaluation of the visual response: image data analysis in Adobe® *Photoshop*® software and in *Mathcad*® software written algorithm (further in text *Photoshop* and *Mathcad* respectively). In *Mathcad* algorithm was developed first and adapted for the visual response evaluation of the presented DVIS. In *Photoshop* procedure was developed later as faster and user friendly. Both procedures showed a good correlation between results.

### 2.1.1 Image data analysis in *Photoshop*

The *RGB* (red, blue, green) colour mode was selected for data treatment. These are basic colours; thus, any colour is a combination of *RGB* in different ratios. Colours are defined in an interval from 0 to 255. When the value of each colour is 255, the white colour is observed. When colour equals 0, the resulting colour is black [122]. For the data treatment in *Photoshop*, it was necessary to scan samples before and after applied load. The scan of the samples before the applied load was used as a background and the scan after applied load – as an object under study. For a quantitative estimation, the parameter *Mean*, characterizing the average brightness value of the image, was selected. The difference between the reference image (before compression) and experimental image (with visual response) was measured Figure 2.1. The value of *Mean* from *Histogram* was used for further data analysis. Here *Mean* – the average level of image brightness, which is obtained by multiplying each level of brightness by several levels, and then divided by the total number of brightness levels. The higher the average value is, the higher the lightness of the image [123].

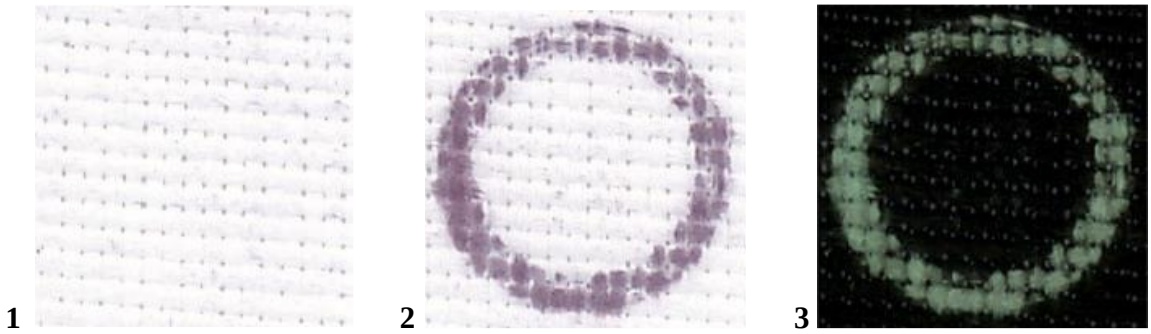

Figure 2.1. Data treatment procedure; scan before compression (1), scan after compression (2), the difference between (2) and (1) is a scan (3).

In our case, the bigger light area is in the image after *Difference* procedure; the more capsules are destroyed – the bigger load was applied. In the case where two layers are completely identical, the value of *Mean* is equal to 0.

Data treatment procedure consists of the following steps:

- lay on of 2 images (images of the sample before and after the load);
- subtraction of one layer from another by *Difference* option, Figure 2.2;
- collection of *Mean* data from the histogram, Figure 2.3.

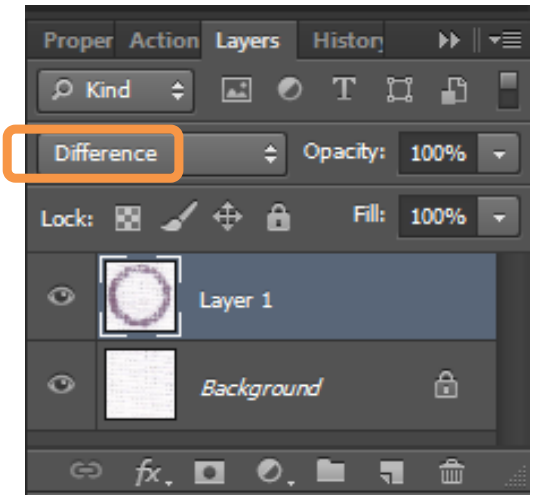


Figure 2.2. Print screen from the *Photoshop* Layers menu; *Difference* option is selected for two layers.

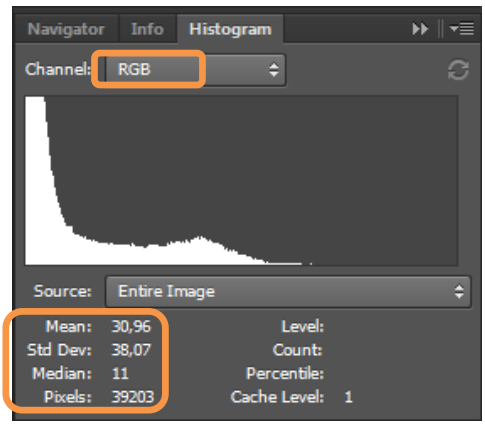


Figure 2.3. Print screen from the *Photoshop* Histogram menu; *Mean* value for the difference of two layers could be defined.

### 2.1.2 Image data analysis in *Mathcad*

In the programme, an image is presented as a matrix, where each element of the matrix refers to 1 pixel, namely, for each pixel (px) the value is defined. From these, the time of a data treatment directly depends on an image size; when the size of the image increases – the processing time increases [124]. The image size 400 on 400 pixels was defined as optimal for further work.

Applying in *Mathcad* written algorithm, developed in the Institute of Polymer Mechanics, University of Latvia [125], for data treatment it is not necessary to scan sample before a load (image for the background). At the same time, for the data treatment using in *Mathcad* written algorithm, there are following requirements for the image:

- it is necessary to crop each place of applied load;
- size of the image in pixels must be an even number;
- a shape of the cropped image must be square, and positioning of the colour change must be in the middle;
- the area of the colour change must be surrounded by some free space with no colour change.

All requirements listed above are possible to complete using any image editing software. Sample after applied load with the selected area for data treatment is shown in Figure 2.4.

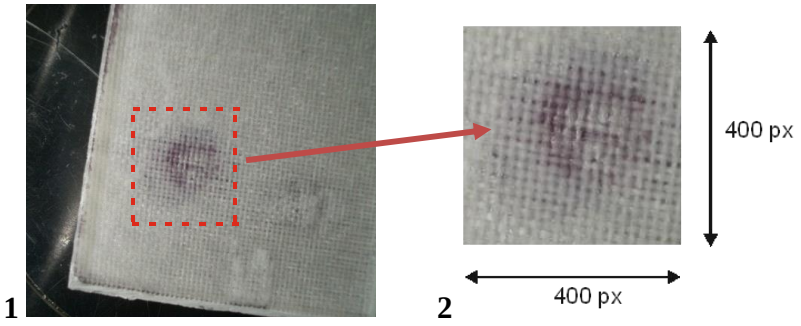


Figure 2.4. Sample after applied load; selection of the area for data treatment (1), cropped area 400 on 400 pixels for further calculations (2).

In details, image data treatment applying in *Mathcad* written algorithm is following. The first step in the algorithm is to define which colour is dominating in each pixel – R (red), G (green), or B (blue). An example of the colour distribution where the red colour is dominating is shown in Figure 2.5.

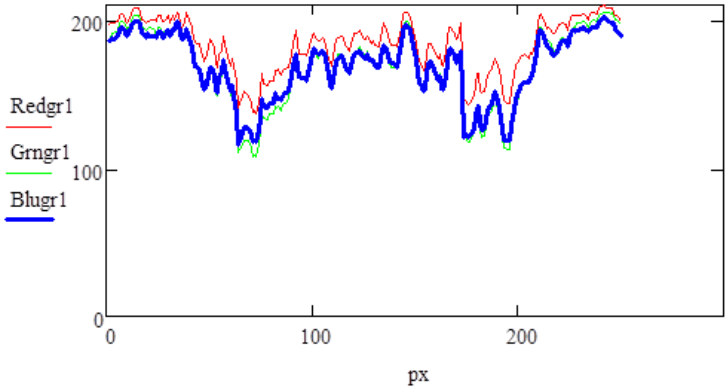


Figure 2.5. Print screen from the Mathcad calculation results; an example of the colour distribution in the selected area of the sample.

The next step is to calculate the difference between red colour and grey colour in each pixel, where grey colour is defined from R, G, B minimal value – min (R; G; B). The difference is in the range from 0 till 255 and is calculated by

$$BC_{i,j} = R_{i,j} - \min\left(R_{i,j},\ G_{i,j},\ B_{i,j}\right), \tag{38}$$

here *BC* is the coloured place ("bruise" colour), in pixel with coordinates *i* and *j*. $R_{i,j}$ , $G_{i,j}$, $B_{i,j}$ are red, green, and blue colours numerical values in the range from 0 till 255, in pixel with coordinate *i* and *j*.

To reduce the influence of light fluctuations in each pixel of the image the transition to relative values is applied

$$BCR_{i,j} = \frac{\left(R_{i,j} - \min\left(R_{i,j},\ G_{i,j},\ B_{i,j}\right)\right)}{\min\left(R_{i,j}+1,\ G_{i,j}+1,\ B_{i,j}+1\right)}. \tag{39}$$

Here *BCR* is *a* coloured place in relative values ("bruise" colour relative).

The next step in the algorithm is to define the background for further calculations. As it was mentioned before, the place of the colour change must be in the middle, since the algorithm by itself cannot define where the background is and where is the coloured place. For simplicity was decided that coloured place has to be in a circle inscribed in a square of the image, space outside the circle (blue squares in corners) is defined as background, see Figure 2.6.

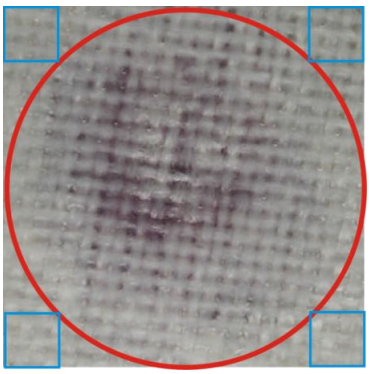

Figure 2.6. Selection of a coloured place and background for calculations.

When the background location is defined, the average value for the background relative colour (mean BCRbg) and a standard deviation (stdevBRCbg) are calculated.

According to the probability theory, for the normal distribution, 99.7% of the data are within 3 standard deviations of the mean and is in the range $\{\bar{x}-3\sigma;\bar{x}+3\sigma\}$, where $\sigma$ is the mean of the squared deviation [126]. For the signal separation, the parameter $3\sigma$ was used. For all matrix (for each pixel) the difference between coloured place and background in relative values is calculated – BCR- BCRbg.

If the difference value is larger than $3\sigma$, the signal is real: BCR- BCRbg > $3\sigma$ – real signal and the numerical value of the signal is determined.

If the difference value is smaller than $3\sigma$, the signal is noise: BCR- BCRbg < $3\sigma$ – signal is not real, is defined as noise with the value – 0.

After the separation of the noise, the clear signal - colour response (CR) total value above zero is calculated. Schematically, BRC value distribution and the "clear" signal after the separation of the noise is shown in Figure 2.7.

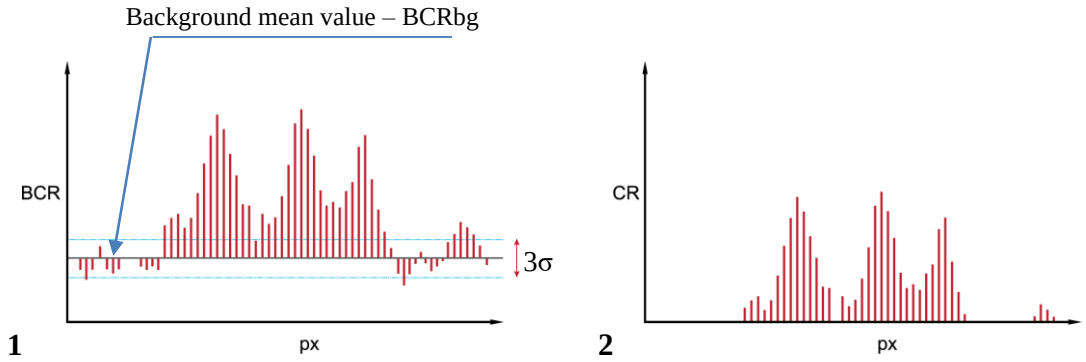


Figure 2.7. Schematically, BRC value distribution of an image (1), and "clear" signal CR after the separation of the noise (2).

After data treatment, the resulting signal distribution - CR image represents a "clear" signal and signal distribution of all image area in two dimensions. Images before the data treatment and "clear" signal distribution are shown in Figure 2.8.

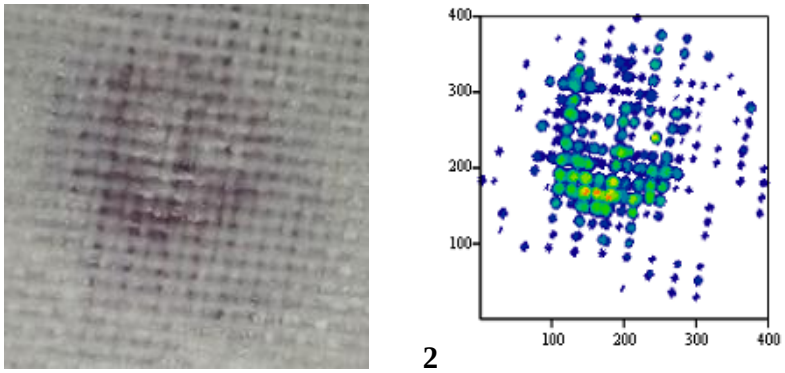


Figure 2.8. Image before the data treatment (1) and signal distribution of all image area in two dimensions after data treatment (2).

The next step in the algorithm is to calculate the total signal value above zero - Integral colour response (ICR),

$$ICR = \sum_{i=1}^{rows} \left( \sum_{j=1}^{cols} CR_{i,j} \right). \tag{40}$$

This value is shown as the result of image processing and can be further used for quantification of damage visual indication.

## 2.2 Technology for the DVIS as an external layer

Since the DVIS for external applications is not a structural element, a nylon fabric was selected as a base for the DVIS. Nylon fabric using rubber roller was impregnated on the Teflon substrate with a mixture of two components (MC-dye and P-activator) in the volume ratio 2:1. After impregnation, the nylon fabric was dried for at least 5 h at room temperature to remove the excess liquid. Nylon fabric samples before and after impregnation with microcapsules are shown in Figure 2.9.

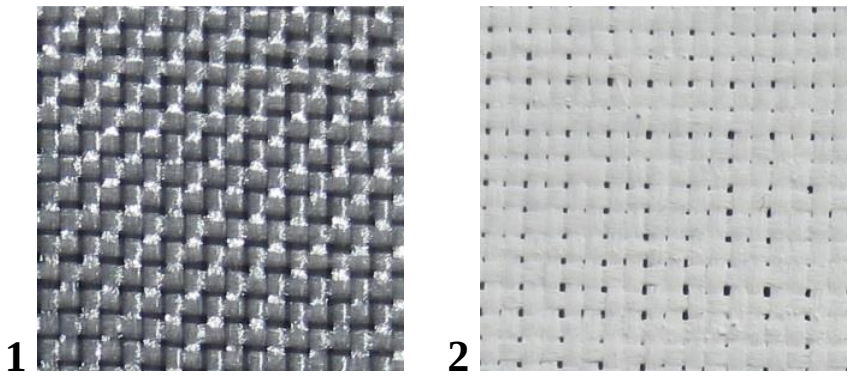


Figure 2.9. Nylon fabric samples before (1) and after (2) impregnation with colour formers.

To ensure repeatability of the DVIS manufacturing method, this procedure was repeated five times. Before and after drying of the fabric it was weighed, the density values of the microcapsules on the fabric were compared. In the result, 40 g/m$^2$ ± 3 % of colour agents was observed on the nylon fabric [127].

The laminating process was selected as a method that holds the colour agent on the surface of the base. Thus, the appearance and barrier properties of the DVIS were improved. It was more "friendly" to manipulations, such as transportation and fixating. Here in Figure 2.10, an example of the laminated DVIS is presented. The piece of paper was covered with microcapsules and dried. It is noticeable that the surface of the paper is not perfectly clean. Dark stains are detectable in many places that appeared as a result of contact between the fingers and the sample. Therefore, the lamination of such samples immediately after manufacture avoids the unnecessary visual response to touching the sample. It is possible to compare the visual response to applied load 400 N with the ring indenter. The first line of rings in Figure 2.10 was obtained as a visual response before the lamination of the sample. The second line was obtained after lamination and with the same load. Thus, it is possible to conclude that the lamination increased the visual response sensitivity threshold of the sample on the applied load.

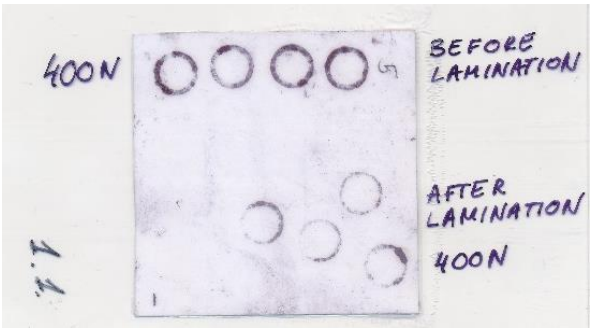


Figure 2.10. Example of the laminated DVIS; the sensitivity of the sample to external load before and after lamination was compared.

Comparing film laminated DVIS of different thicknesses, it is notable that by increasing the thickness of the film, the load needed to gain visual response increase as well. In Figure 2.11, at the top example of the DVIS laminated with 80 µm thick film, in the middle – 125 µm, below – 175 µm. Comparing, for example, the visual responses in all samples after 200 N applied load it was observed that in the first sample the stable, bright ring was seen, in the middle, the ring did not appear completely. On the last, only a weak outline could be seen. Thus, by using cover sheets with different thicknesses, it was possible to vary the threshold of the DVIS sensitivity to external loads.

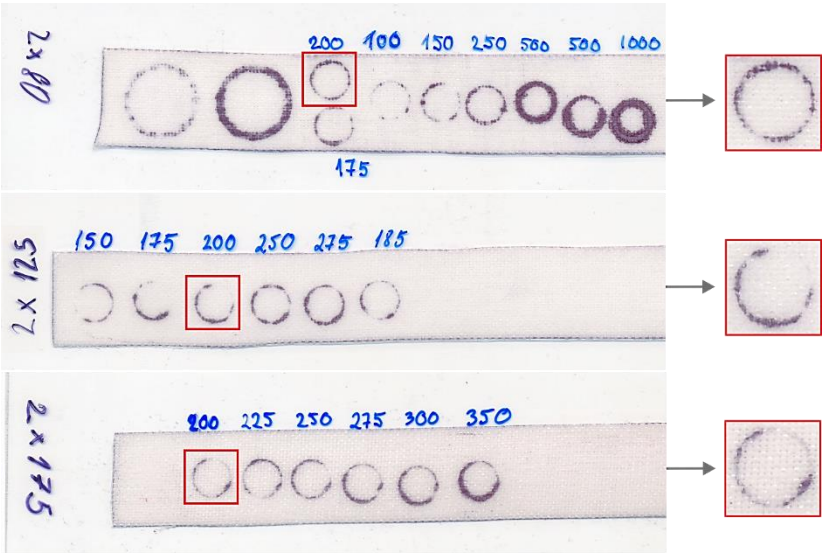


Figure 2.11. Samples of the DVIS laminated with films with different thicknesses (left). The visual response obtained after ring indenter applied with 200 N load (right).

### 2.2.1 Selection of the load for testing

Samples were tested on compression with the ring indenter to obtain controlled visual response. Zwick 2.5 universal testing machine with a rate of 2 mm/min at a temperature of 22 ± 2 °C was used for this purpose. The applied load was ranging from 0 to 400 N to find a necessary load for the good visible indication. The DVIS tested with different loads is shown in Figure 2.12. For subsequent measurements, the load of 400 N was selected as minimal to ensure good visible indication.

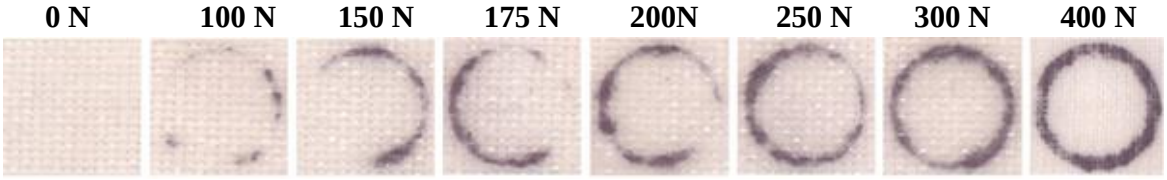


Figure 2.12. The DVIS tested on compression with the ring indenter ranging from 0 to 400 N.

### 2.2.2 Selection of colour

For the selection of the dye colour to ensure a better perception of visual response after the applied load, the following steps were done. The DVIS samples with red, green, blue, and black dye colours in microcapsules were manufactured and tested. For the compression test, 400, 500, and 600 N loads were selected. Samples with different dye colours in microcapsules after compression tests are shown in Figure 2.13.

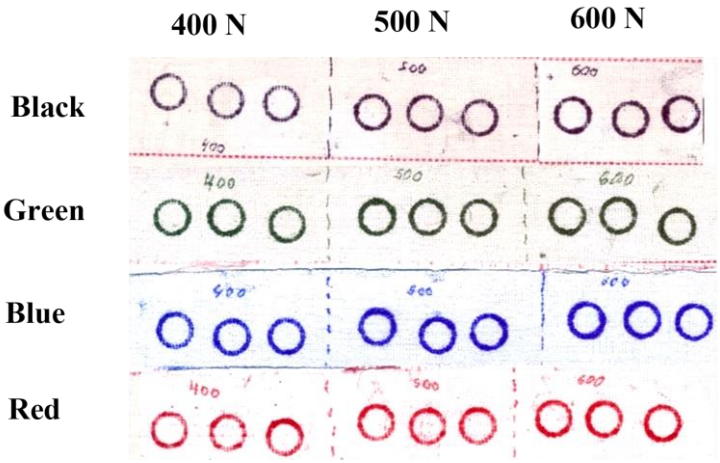


Figure 2.13. Samples with different dye colour in microcapsules after compression tests.

It was identified that the treatment of the data with the same applied load leads to different colour responses for different colours. Samples with blue and green dye colour in microcapsules showed a more bright visual response after applied load, Figure 2.14, comparing to other colours [127].

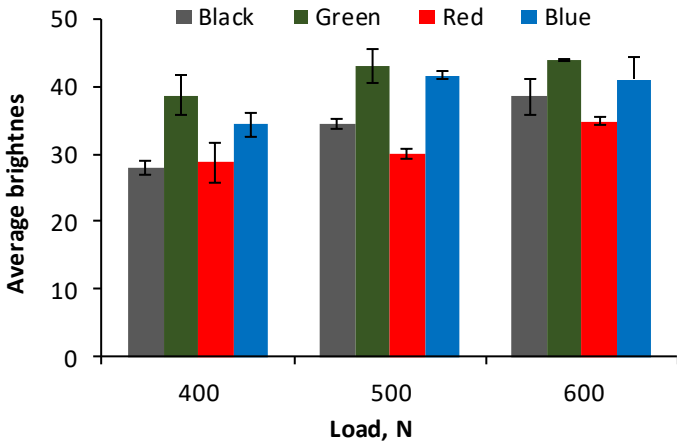


Figure 2.14. Samples with different dye colour in microcapsules; colour response vs applied load.

### 2.2.3 Selection of concentration of microcapsules for maximal visual response

Due to the fact, that colour agents are used initially in paper production with the density approximately 2 g/m², but after impregnation of the nylon fabric were obtained a density of colour agents 40 g/m², it could be suggested that amount of the colour agent on the nylon was with a surplus. The nominal concentration of the microcapsules in the dispersion was 40% (data from the manufacturer). The DVIS samples with microcapsule concentrations from 2.7% to 40% were prepared and tested on compression with 400 N load to determine the minimal quantity of microcapsules for the DVIS on nylon base which ensures maximal visual response after applied

load. Four samples of the DVIS with different concentration of microcapsules after compression test are shown in Figure 2.15.

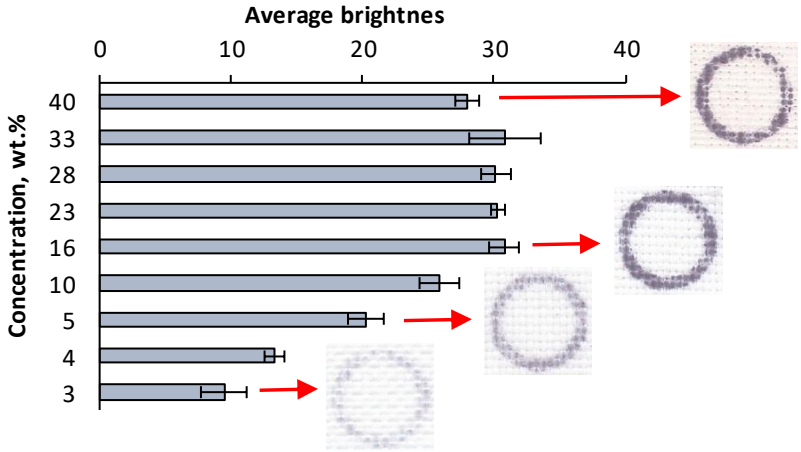


Figure 2.15. The DVIS samples on nylon base after compression tests; colour response vs different concentration of microcapsules.

The result of this experiment showed that the decrease of the concentration of microcapsules down to 16% in the DVIS samples on a nylon base, by adding water to the dispersion before nylon fabric impregnation, did not affect the brightness of the visual response, Figure 2.15. Thus, it is more reasonable to use ~ 20 % microcapsule concentration in the manufacture of the DVIS on nylon base; the layer is lighter and the manufacturing costs are lower [127].

### 2.2.4 Kinetics of colour change at different temperatures

The DVIS samples were tested to estimate colour change (visual response) vs time after loading at different temperatures. Before this, the test samples were laminated. Samples were subjected to a load, destroying the capsules. Immediately after applied load series of photos were taken, starting from 5 photos/sec and to 1 photo/min. The same procedures were implemented for temperatures -20, +11, +21, +38 °C. Typical visual response curve vs time after the applied load is shown in Figure 2.16.

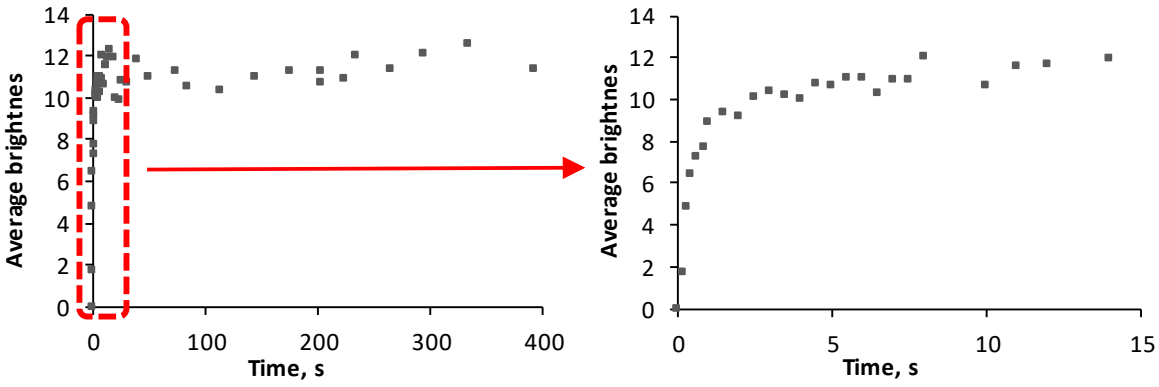


Figure 2.16. Typical visual response curve vs time after applied load.

It was defined that temperature in the range from -20 till +38 °C does not affect the kinetics of colour change (visual response) after applied load. For all samples, the maximal visual response was reached in 10-15 s, and the brightness practically remained unchanged [127].

## 2.3 Technology for the DVIS as an internal layer

Since the DVIS for internal applications is a structural element, as a base of the DVIS, the glass fabric was selected. The glass fabric *Aeroglass plain*, 130 g/m$^2$ (Havel Composites CZ s.r.o., Czech Republic) was impregnated on the Teflon substrate using rubber roller with a mixture of three components: dispersion of MC-dye, P-activator, and *HALWEDROL UV 20/40 W* an epoxy modified polyurethane-acrylic emulsion (Koninklijke DSM N.V, The Netherlands) in the volume ratio 6:3:2. After impregnation, the glass fabric was dried for at least 5 h at room temperature in a vertical position to remove the excess liquid and then irradiated with ultraviolet light for 30 min on each side to complete polymerization of the third component. The resulting DVIS was a dry glass fabric containing microcapsules with colour former and particles of colour activator on its surface and was ready for further use as the structural element of a composite.

### 2.3.1 Epoxy modified polyurethane-acrylic polymer

In the present work, epoxy modified polyurethane-acrylic polymer (further an adhesive) was selected for two reasons:

- to be used as a substance that holds the colour agent on the surface of the base,
- to isolate encapsulated colour former and particles of activator from the alkaline environment of hardener in the case of manufacture composite with epoxy matrix [128].

Since the ratio of the colour agent was 2:1, and it was known before, to define the ratio of adhesive mixtures with the colour agent and a different ratio of adhesive were prepared and tested. Glass fabric pieces were homogeneously impregnated with a mixture of MC-dye, P-activator, and epoxy-modified polyurethane acrylic polymer, using components ratios ratios 6:3:0.2, 6:3:0.5, 6:3:1, 6:3:1.5, 6:3:2, 6:3:2.5, 6:3:3, and 6:3:4 respectively. Summary of the components combinations and indenters used for the testing is presented in Table 2.2. After impregnation, the fabrics were dried until full removal of the water basis. Dried fabrics were exposed to the ultra-violet irradiation for 30 min from each side to provide polymerization of the adhesive. The DVIS samples with different adhesive concentrations were tested by quasi-static compression tests. For each component combinations, 5 measurements were performed with two types of indenters – ring and lens. An example of the tested sample is presented in Figure 2.17. Using digital image analysis for data processing, an average brightness of the coloured response depending on the concentration of adhesive was estimated, see in Figure 2.18.

Figure 2.17. Sample after compression test with two types of indenters.

Table 2.2. Summary of components combinations.

| Component | Amount, ml | | | | | | | | Indenter |
|---|---|---|---|---|---|---|---|---|---|
| MC-dye | 6 | | | | | | | | - |
| P-activator | 3 | | | | | | | | - |
| adhesive | 0.2 | 0.5 | 1 | 1.5 | 2 | 2.5 | 3 | 4 | lens |
| adhesive | 0.2 | 0.5 | 1 | - | 2 | - | - | 4 | ring |
| adhesive, % vol. | 2.2 | 5.3 | 10 | 14.3 | 18.2 | 21.7 | 25 | 30.8 | - |

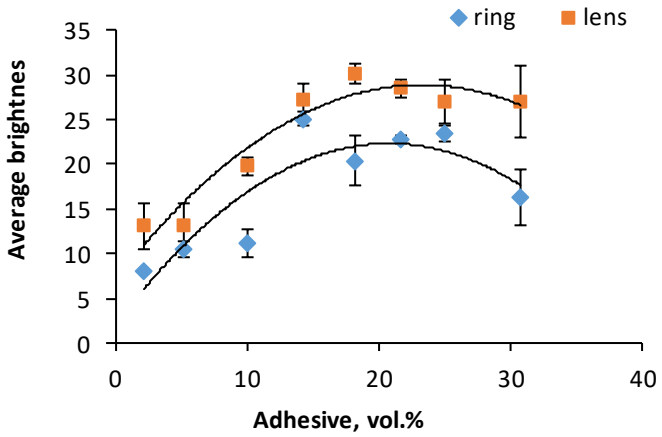


Figure 2.18. Average brightness vs adhesive concentration after compression with ring (♦) and lens (■) indenters.

In the result, it was experimentally determined that the most intensive coloured response under load was obtained using the ratio of the components 6:3:2.

### 2.3.2 Polymerization of the adhesive by ultra-violet irradiation

After the ratio of the adhesive in the mixture was defined, it was necessary to define the time of adhesive polymerization process. For this, impregnated with the mixture and dried samples were subjected to ultraviolet irradiation by the SVD-120A mercury-quartz lamp for the times from 5 to 45 min with an interval of 5 min. The exposure rate, measured in the range of wavelength 280-320 nm, was 10.5 W/m$^2$. UV irradiation provided polymerization of the adhesive and isolation of particles of colour activator from the alkaline environment of hardener simultaneously. DVIS

samples with different time of irradiation were tested by quasi-static compression tests. For each irradiation time, 5 measurements were performed with lens indenters with the load of 250 N. Using digital image analysis for data processing, an average brightness of the coloured response depending on irradiation time was estimated. From the data, see in Figure 2.19, it is difficult to define after what duration of UV irradiation the visual response to the applied load was maximal. On the other hand, it was defined that the ability to change colour after the applied load even after UV irradiation has been preserved, see Figure 2.20. Analysing other data from the images, it was noted that the colour of the DVIS after irradiation changed from the white to light orange, see Figure 2.21. After data treatment, it was defined that colour change is dependent on the duration of irradiation, see Figure 2.22. Image analysis revealed that when using a UV lamp, minimal irradiation time is 15 minutes. Thus, when the irradiation time is reduced by 50% relative to the time was used at the beginning, DVIS is obtained with a similar visual response to the applied load. The irradiation time reduction could save on electricity consumption and extend the lamp lifetime.

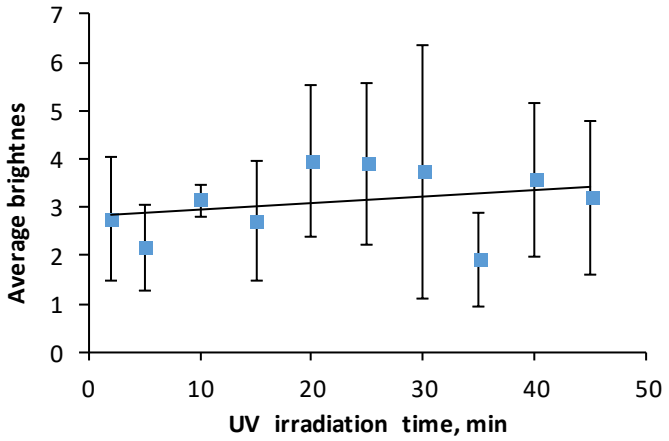


Figure 2.19. Average brightness vs UV irradiation time after compression.


Figure 2.20. Sample of the DVIS after 45 min UV irradiation and compression test.

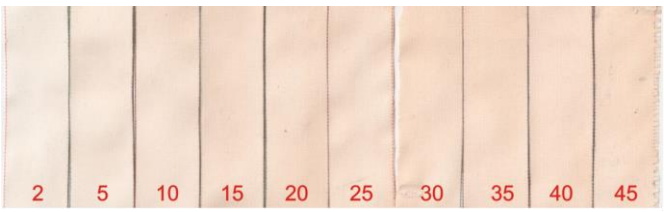


Figure 2.21. Samples of the DVIS after UV irradiation from 2 till 45 min.

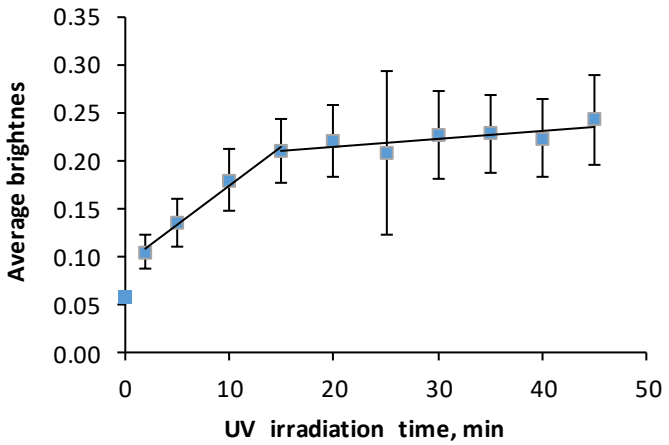


Figure 2.22. Colour change of the DVIS vs UV irradiation time.

## 2.4 Main results of Chapter 2

- The damage visual indication system (DVIS) was developed for applications as an external and an internal layers.
- It was defined that for the manufacture of the DVIS, it is possible to use two combinations of colour agent: (1) mixture of microcapsules with leuco dye and microcapsules with dye activator, (2) mixture of microcapsules with leuco dye and particles of dye activator.
- The procedure of the quantitative estimation of the visual response on the damage was developed. It includes two algorithms of digital image analysis in the software *Adobe*® *Photoshop*® and *Mathcad*®. These algorithms allow evaluating relative changes of the visual response obtained under applied loads.
- The technologies for the manufacturing of the DVIS in laboratory conditions were developed for both applications. Those included selection of the base, impregnation and drying methods, and method of fixation the colour agent on the base. The minimal concentration of microcapsules, which ensures maximal visual response after the applied load was defined.
- Operational characteristics of the DVIS were evaluated. DVIS kept the ability to change colour in the temperature interval from -20 to +38 °C.
- Kinetics of colour change for DVIS samples was evaluated. It was defined that the maximal visual response was reached in 10-15 s and after the brightness practically remained unchanged. The temperature in the tested interval does not affect the kinetics of colour change after the applied load.
- The brightest visual response after applied load was obtained for microcapsules containing blue and green dyes, comparing to the DVIS samples with red and black ones.

# 3 MODEL COMPOSITES WITH INTEGRATED DVIS

Prepared in advance, the DVIS could be placed as one of the top layers during the assembling of composite or on the already existing one. In the present work model composites with the integrated DVIS are presented as two demonstrators: a) the DVIS integrated into a composite by vacuum bagging method, b) the DVIS as a separate layer, which was placed on a surface of existing construction or element. The concept of demonstrators is presented in Figure 3.1. Manufacture technologies and testing of the mechanical and physical properties are described below for both types of model composites.

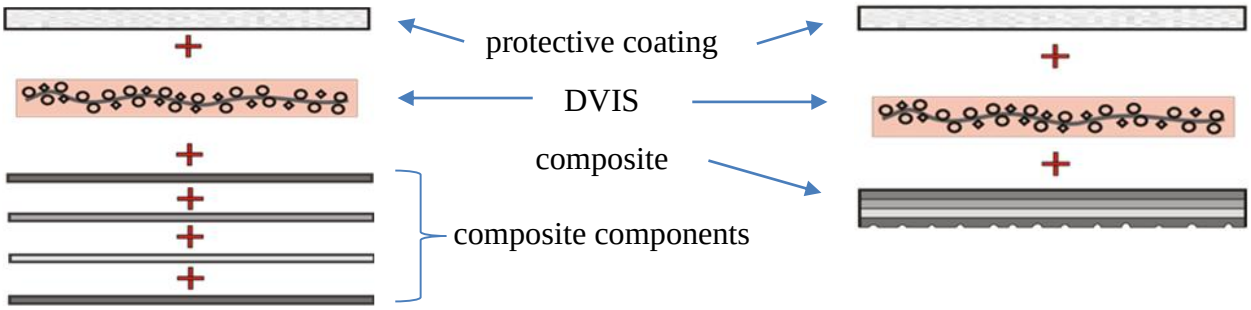


Figure 3.1. The concept of the model composite with the integrated DVIS; the DVIS is integrated into the composite during it assembling (left), the DVIS is placed on a surface of an existing composite element (right).

## 3.1 Model composite with the DVIS as an external layer

The DVIS as an external layer could be prepared by the technology described in 3.2 Technology for the DVIS as an external layer and could be stored unused for a long time, observing the minimum requirements for the storage of material (deposited on a flat surface and the absence of an external load on the surface). In this case, the DVIS "waiting time" before usage could be months or even years. The option to make the DVIS ready for the immediate usage upon requirement is available; it is to make the DVIS as a prepreg.

### 3.1.1 Technology for the DVIS as a prepreg

Here, the technology for the preparation of the DVIS for the immediate usage upon requirement is presented. "Prepreg" is the common term for a reinforcing fabric which has been pre-impregnated with a resin system. This resin system (e.g. epoxy) already includes the proper curing agent. As a result, the prepreg is ready to lay into the mould without the addition of any more resin. For the laminate curing, it is necessary to use a combination of pressure and heat [129]. A laboratory method of the prepreg manufacture included several steps:

1. The selected fabric was impregnated with a mixture of components (dye, activator, adhesive) and polymerized. This step was entirely identical to the manufacture of the DVIS for internal applications.
2. Epoxy and hardener were mixed in the appropriate ratio. In addition to this mixture, acetone in the amount of 5 and 20 wt.% was added.

Acetone added to a mixture of epoxy and hardener, to thin the mixture, to reduce the viscosity, thus to provide deeper penetration into the fabric [130]. Here acetone was used mostly to delay the start of the curing process. The presence of acetone in the mixture influenced the physical and mechanical properties of epoxy after curing [131], but for the prepreg, epoxy was used only as a binder.

Two types of epoxy resin based on bisphenol A and corresponding hardeners based on cycloaliphatic polyamines suited to the production by hand layup were used to make DVIS prepregs Table 3.1.

Table 3.1. Epoxy binders for prepregs.

| Sample series Designation | Binder composition |
|---|---|
| DVIS I | A room-temperature cured LH 289 epoxy resin and H 289 hardener in the ratio of 100:33 (Havel Composites CZ s.r.o.). |
| DVIS II | A high-temperature performance epoxy resin EL160 and EL160 hardener (use at service temperatures up to 170 °C) in the ratio of 100:35 (Easy Composites Ltd.). |

3. The DVIS was saturated with an epoxy binder using a brush. After even distribution of the binder, its excess was forced out by the Teflon roller on the Teflon board, Figure 3.2.

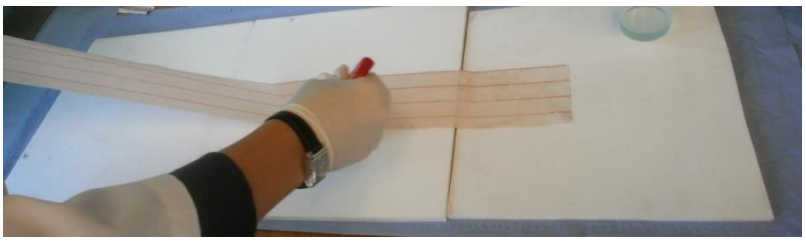

Figure 3.2. Saturation of the DVIS with an epoxy binder.

4. Saturated DVIS was placed on a polyethylene terephthalate (PET) film, which has the properties necessary for the storage of the prepreg, such as the anti-sticking effect, resistant to moisture, high tensile strength, resistance to punctures and other mechanical stress. The width of the prepared film must be several times the width of the sample. It was necessary to wrap the sample in the film several times.

5. After placing the sample inside the film, it is necessary to align the sample and remove possible bubbles. The most suitable way to do this is by using a soft rubber roller, Figure 3.3.
6. Then the ends of the strips tightly wrapped and packed in the film were sealed by adhesive tape. The packages were tightly wound on cardboard reels and fixed with adhesive tape, Figure 3.4.

Figure 3.3. Sample aligning and bubble removal.

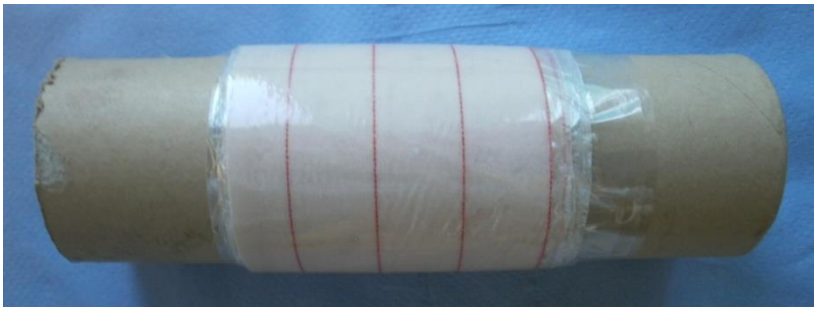

Figure 3.4. The ready DVIS as a prepreg.

For the ready DVIS as a prepreg, see Figure 3.4, the time of storage in different conditions was defined. Part of the DVIS was used for the peel resistance evaluation. The other part was glued on the top of the composite object, as a demonstrator. The DVIS as a prepreg was glued on the top of the composite wind turbine blade and after it was tested on the ability to change colour in the place of the applied load, see Figure 3.5.

**1** 

**2**

**3**

**4**

5

Figure 3.5. Composite wind turbine blade with the DVIS as an external layer; the DVIS as a prepreg is located on the top of the blade (1), using rubber roller it is pressed to the surface (2), blade with a glued DVIS was covered by PET film and left for the curing of the resin (3), wind turbine blades with and without the DVIS (4), place of the applied load is identified with a colour change (5).

Another part of the DVIS as a prepreg was glued on the top of the safety helmet. Safety helmet before and after the impact is presented in Figure 3.6.

1

2

Figure 3.6. Safety helmet with the DVIS as an external layer before (1) and after the impact (2).

For these demonstrators, wind turbine blade and safety helmet were defined that the DVIS saved function of damage visualization for at least 7 years of storage at laboratory conditions.

### 3.1.2 Determination of the DVIS prepreg time of storage

The shelf life of the prepreg is an important exploitation property and storage conditions strongly affect it [132]. During the research, the storing conditions efficiency was determined by the possibility of prepregs to be sticky to an electro-technical textile laminate used as a substrate material and storing the impact-indication ability (colour changing).

For the experiment, 5 DVIS prepreg samples in a shape of the strip with approximately one-meter length and with 2 types of the epoxy binder with or without acetone were prepared. Samples were placed into the refrigerator temperature (+2 °C) and freezer (-18 °C). Summary of samples and storage conditions is presented in Table 3.2.

Table 3.2. List of samples for shelf-life testing.

| Binder composition notations | Storage T, °C | Acetone, % wt. |
|---|---|---|
| DVIS I, 20% | +2 | 20 |
| DVIS I | -18 | - |
| DVIS I, 5% | | 5 |
| DVIS I, 20% | | 20 |
| DVIS II | | - |

Starting from the first day, samples of the prepregs were cut off with scissors from the samples. The remainders of the samples, after sealing in the film, were returned to continue the storage at the reduced temperature. The cut pieces were glued to the substrate using a soft rubber roller. If the glued piece stayed fastened on the substrate on the next day, it was thought that the prepreg could continue to be successfully stored. The above check of prepregs was conducted every day for the first 10 days, then for the following 10 days – every 3-4 days and then once a week. The expiration of the storage period was noted when the prepreg ceased to adhere to the substrate. Results of the storage experiment for the DVIS prepregs made from different binders and stored at +2 and -18 °C with an addition of acetone and without it are shown in Figure 3.7.

Experimentally it was defined that prepregs with the addition of acetone or without it, as well as both types of binders' compositions, kept the ability to be glued to the substrate, for around 20 days regardless of the storage temperature. By adding acetone, the ability to be glued to the substrate was prolongated to 43 days when stored at -18 °C. At the same time, the amount of added acetone 5 or 20 wt.% does not make any difference.

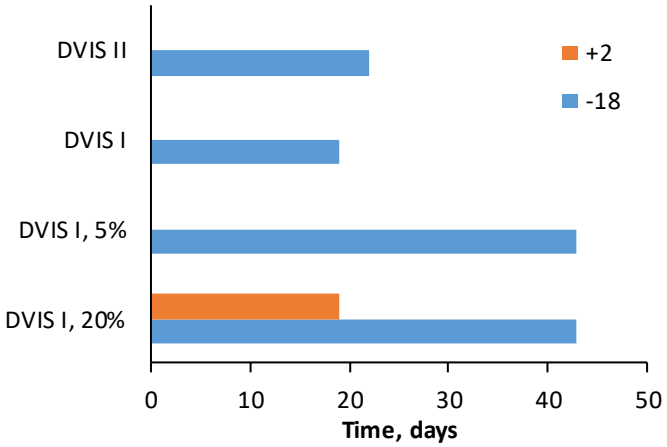


Figure 3.7. Comparison of the storage times for different types of DVIS prepreg samples (notations see in Table 3.2).

### 3.1.3 The DVIS prepreg peel resistance

Since the DVIS is a single-use product, it is important not only to quantify how long the prepreg keeps the ability to be glued on the surface but also it is essential to establish whether it is possible to remove it from the surface after usage without causing damage to the object's integrity. To quantify the performance of adhesion or peel ability of the DVIS prepregs test analogous to ASTM D 6862 was used [133]. A peel angle 90° was chosen for tests because peel force usually reaches the highest value at this angle [134], besides, it is easy to set an angle of 90° on the testing machine.

Considering the previous results that the presence of 5% or 20% acetone does not affect the number of days when the layer's ability to glue is retained, samples of the DVIS I with 5% acetone were made and tested. To check the influence of the type of fabric as a prepreg, three types of fabric were used:

- Stitch Ply A (AIRTECH Europe Sarl.) nylon with density 88 g/m$^2$. It is traditionally used in preforms as a peel ply because it could be easily stripped off of cured laminate, it has red tracers with high visibility to reduce the risk of peel ply being left on the part [135].
- E-glass fiber fabric (Valmiera SSR), density 125 g/m$^2$.
- E-glass fiber fabric (Valmiera SSR), density 160 g/m$^2$.

Samples of three types of fabrics with the size 15.5 mm width and at least 20 cm length were prepared by applying DVIS prepreg technology, see Figure 3.8 and placed in the freezer at temperature -18 °C. At certain time intervals, samples were taken from the freezer and adhered to the substrate, see Figure 3.9. Samples were stored 24 h at + 45 °C to cure the binder, see Figure 3.10. After the samples were conditioned at room temperature, they were subjected to peel test.

Figure 3.8. The DVIS prepreg sample.

Figure 3.9. The DVIS prepreg sample on the substrate.

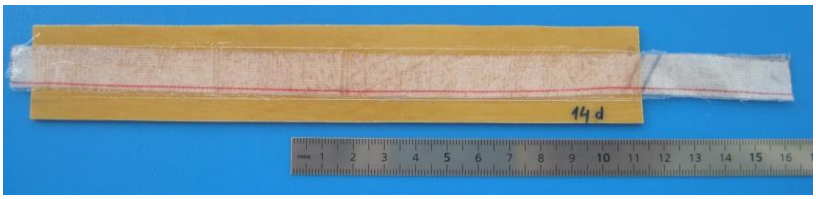


Figure 3.10. The DVIS prepreg sample glued on the substrate after 14 days at -18 °C and ready for the peel test.

The universal electromechanical testing machine Zwick 2.5 was equipped with specifically designed grip to fix the substrate and to ensure the removal of the DVIS at an angle of 90°, see Figure 3.11. Speed displacement of grips was 2 mm/s. The typical force-displacement curve is shown in Figure 3.12. During the peel tests, the relation between peel force and time of sample storage in the freezer was studied. The results for the DVIS prepregs on a base of nylon and glass fibre are presented in Figure 3.13.

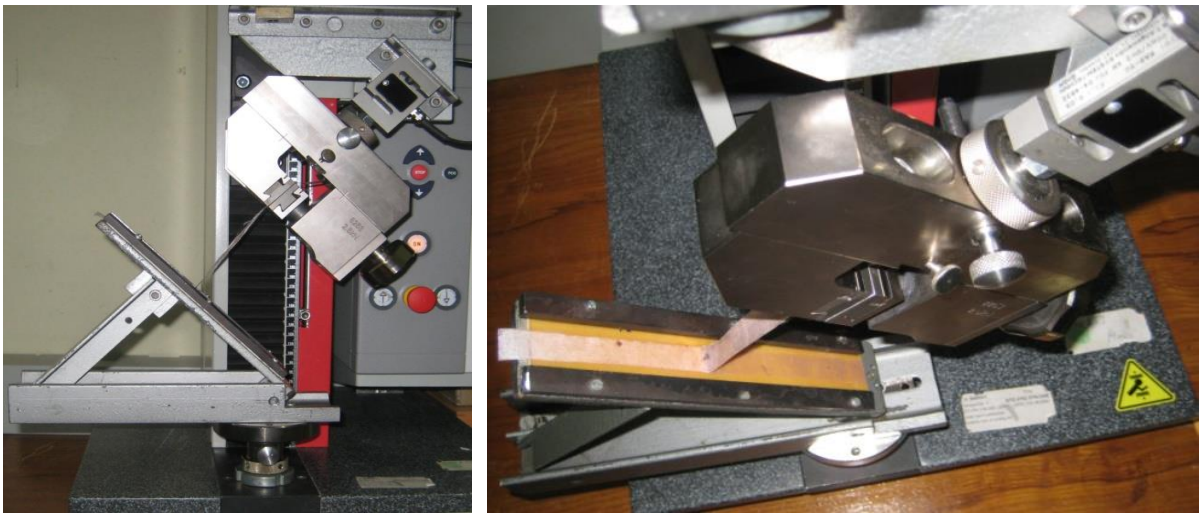

Figure 3.11. Peel test of the DVIS prepreg, the side and top views.

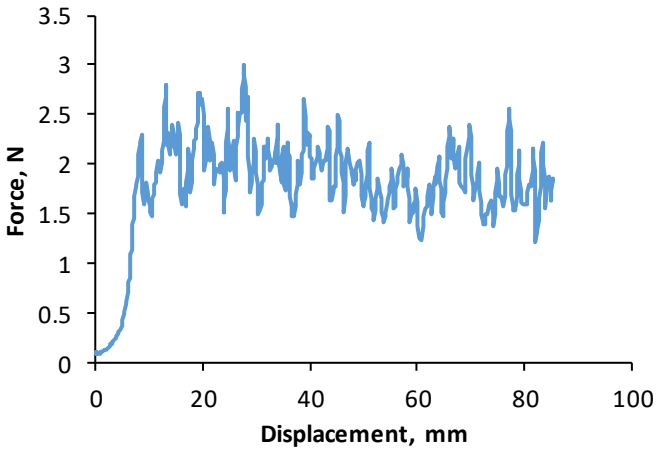


Figure 3.12. The typical load-displacement curve obtained during peel tests for the DVIS prepreg samples.

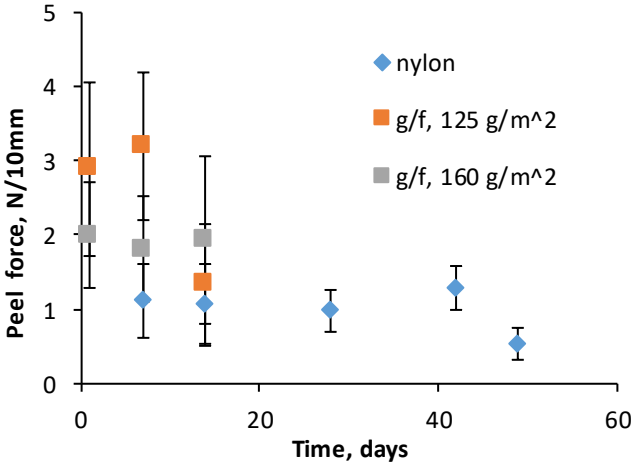


Figure 3.13. Peel force vs time of storage in freezer for the DVIS prepreg nylon and glass fabric (g/f) samples.

The peel tests confirmed results of the previous experiments dealing with the time of storage of the DVIS I prepregs with a nylon fabric base. In particular, the peel force decrease started after 45 days. The prepregs with glass fabric base, especially glass fabric 125 g/m$^2$ had a lower shelf life, comparing to nylon-based prepreg, but had higher peel strength. At yarns crossing points, existing cavities could be more filled with epoxy binder comparing to nylon. These points can work as mechanical interlocking sites with a surface of the substrate [136]. Peel forces obtained for the DVIS prepreg with a glass fabric base are in 2-3 times higher (200-300 N/m), compared to the DVIS prepreg with a nylon base (100 N/m). But these values are still lower than peel forces obtained for different types of peel plies on the base of polyester fibres 740 N/m, where a large number of tendrils left on the surface of material [134]. Such relatively low peel forces allow removing the DVIS prepreg (after an indication of the damage) from the inspected area without any consequences; the integrity of the upper layer of the material was not broken, the surface of the material remains smooth, without the residue of tendrils and adhesives.

### 3.1.4 Effect of substrates on the DVIS visual response

Series of tests were performed to evaluate how the substrate effects on visual response of the DVIS after applied load. For the tests, the DVIS was prepared according to the 3.2 Technology for the DVIS as an external layer and laminated with a protective layer with a thickness of 100 µm. The impact was imitated by free drop test of the steel balls. For a quantitative estimation of the visual response after an impact and comparison of results, image treatment in *Photoshop*, and the parameter Mean was used.

**Test №1**

During the test №1 the visual response on different substrates was evaluated. Substrates used: a) linoleum b) polyurethane foam c) polytetrafluoroethylene - Teflon. Three steel balls with masses 5, 8 and 130 g were dropped from a controlled height. The brightness of the visual response is affected by choice of the substrate, see

Figure 3.14. Using a substrate of lower stiffness, the energy of the ball is absorbed upon falling while the area of damaged microcapsules is more significant compared with the stiffer substrates.

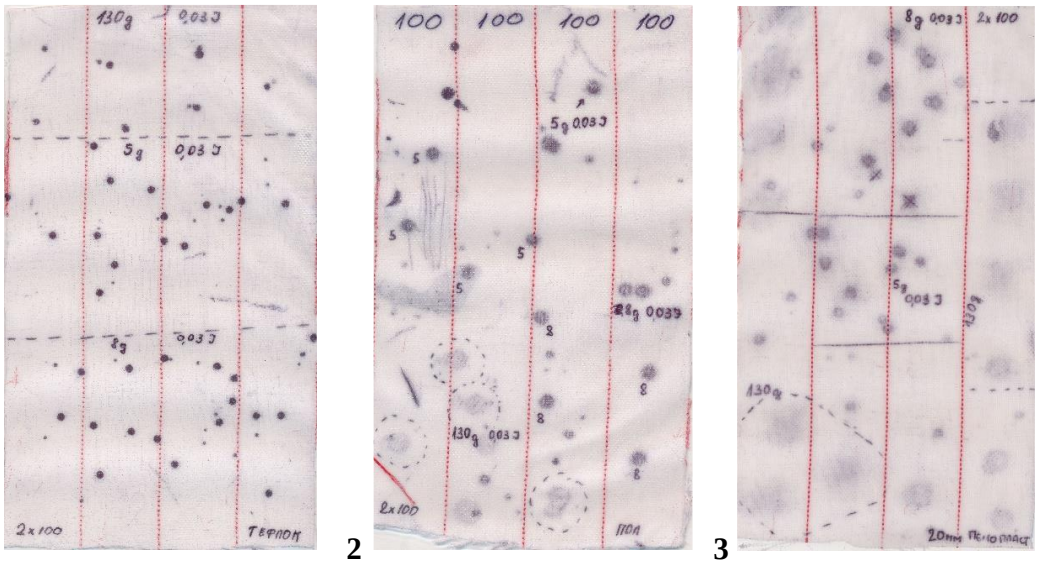


**1** **2** **3**

Figure 3.14. The DVIS on Teflon (1), on linoleum (2), and polyurethane foam (3).

**Test №2**

During the test №2 visual response caused by different size of the balls was evaluated. For the Teflon substrate steel balls with the mass 5, 8, and 130 g were used. For all balls, the constant energy *Ep* = 0.03 J was selected. Photos after drop tests with different mass balls are presented in Figure 3.15. The average level of image brightness after free ball drop with different size balls, see Table 3.3. By data treatment, it was defined that for the DVIS placed on a rigid substrate like Teflon, the size of the ball did not affect the brightness of the visual response.

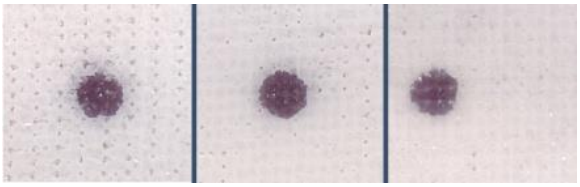

Figure 3.15. Visual response after impact with an energy *Ep* = 0,03 J with 5 g (left), 8 g (middle), and 130 g (right) balls.

Table 3.3. Mean value of the visual response after free ball drop tests with different size balls for the DVIS on the Teflon substrate.

| **Selected *Ep* 0,03 J** | | | |
|---|---|---|---|
| Height, m | 0.5651 | 0.3651 | 0.0235 |
| Teflon | 5 g ball | 8 g ball | 130 g ball |
| Mean | 18.16 | 16 | 14.4 |
| | 14.94 | 18.42 | 16.66 |
| | 18.02 | 17.64 | 16.19 |
| | 19.11 | 16.72 | 16.04 |
| **Average** | **17.36** | **17.59** | **16.30** |
| St. dev | 2.16 | 0.85 | 0.32 |

**Test №3**

During the test №3 the influence of the impact energy on the visual response was evaluated. On the selected Teflon substrate tests were performed with a steel ball of mass 1 g. In the result, the effect of the energy of the impact on the average image brightness and on the diameter of the indentation was defined, Figure 3.16. The increase of the applied energy led to an increase in the diameter and average brightness of visual response.

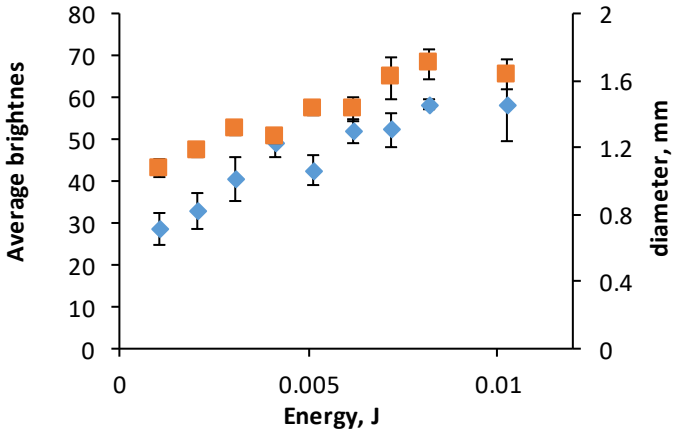


Figure 3.16. The average image brightness value vs energy of the impact (♦) and diameter of the indentation vs energy of the impact (■) for DVIS tested with the 1g steel ball on Teflon substrate.

## 3.2 Model composite with the DVIS as an internal layer

For the manufacture of a model composite, the DVIS was prepared in advance, applying the approach described before in Sec. 3.3 Technology for the DVIS as an internal layer. The fabric for the base was selected depending fabric that was used to make the composite. For the model composite, with the DVIS as an internal layer, a method for regulating the sensitivity threshold of the composite was proposed and validated. In this case, the DVIS was placed as a top layer to get the visual response, after applied load, more distinct. To evaluate the effect of integrated DVIS on the mechanical properties of the composite, the sample with the DVIS integrated into a composite, and similar reference samples were prepared and tested.

### 3.2.1 The threshold of damage visualization for composite with an integrated DVIS

Protective epoxy coatings with different thicknesses were proposed as a method for regulating the sensitivity threshold of composite with an integrated DVIS.

As a base of the DVIS, a polyamide (nylon) fabric, Stitch Ply A (AIRTECH Europe Sarl) without a coating with a surface density of 88 g/m$^2$ was selected. The model composite with integrated DVIS was assembled by vacuum bagging with the subsequent applying of layers: a colourless nylon distributive mesh for the formation of a protective coating, the DVIS, and two load-carrying unidirectional glass yarns connected by a network with the surface density of 500 g/m$^2$ (Havel Composites). The DVIS and both yarns were preliminarily impregnated with an epoxy binder using a roller. As an epoxy binder, an LH 289 epoxy resin based on bisphenol A with the viscosity 500-900 MPa·s at 25 °C and an H 289 hardener based on cycloaliphatic polyamines (both Havel Composites CZ s.r.o.) in the ratio of 100:33 were used. The pressing and subsequent curing of plane composite samples were performed in a vacuum under 0.4 bars at a temperature of 40-60 °C for 20 h. Such technology was applied to manufacture composites with a protective layer of thickness $z$ less than 0.5 mm.

For the composite with a protective layer thicker than 1 mm, the same package of layers was stacked on a preliminary moulded and cured plate of an epoxy binder of thickness varied from 1 to 4.5 mm. The thickness of the protective epoxy coating was determined by measuring the cross-section of the sample under a microscope near the place of indentation.

For the determination of the dependence of the threshold of visual response on the thickness of the protective coating, a series of quasi-static compressions tests with spherical indenter were performed. Using Zwick 2.5 universal electromechanical testing machine with a constant indenter speed of 0.4 mm/min, samples with define thickness were tested with increasing load from 50 to 2000 N. For each protective coating thickness, the minimal load causing visual response was

defined. The visual response was estimated by image data treatment applying digital image analysis. As a result, the correlations between integral colour response ICR and indentation load $P$ for the defined protective epoxy coating thickness was established. As an example, the correlation between Integral colour response and indentation load $P$ for the protective epoxy coating thickness $d$ =1.26 ± 0.05 mm is shown in Figure 3.17. The intersection of the linear trend of the second section and the abscissa axis was defined as a threshold $P^*$ of visualization of the load for the given thickness of the protective epoxy coating.

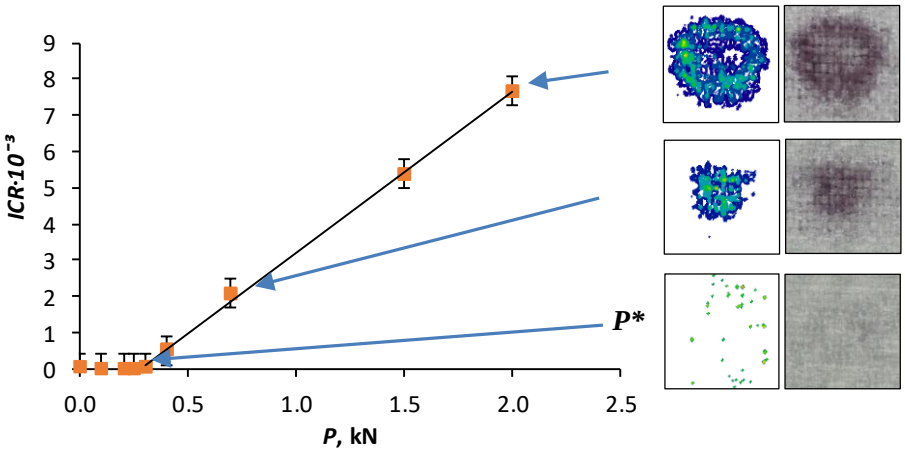


Figure 3.17. The correlation between integral colour response ICR and indentation load $P$ for the protective epoxy coating thickness $d$ =1.26 ± 0.05 mm. $P^*$ is the threshold of visualization of the load and images of samples after visual response on the applied load.

Analysis of data collected from tested samples with different thicknesses of the protective epoxy coating allowed to determine, the correlation between the threshold $P^*$ of visualization of the load and protective epoxy coating thickness $d$, see Figure 3.18. During the experiments, the irreversible deformation of protective epoxy coatings $3 < d < 4.5$ mm was detected. Besides the visual response, an indentation on the surface of the protective epoxy coatings was visible.

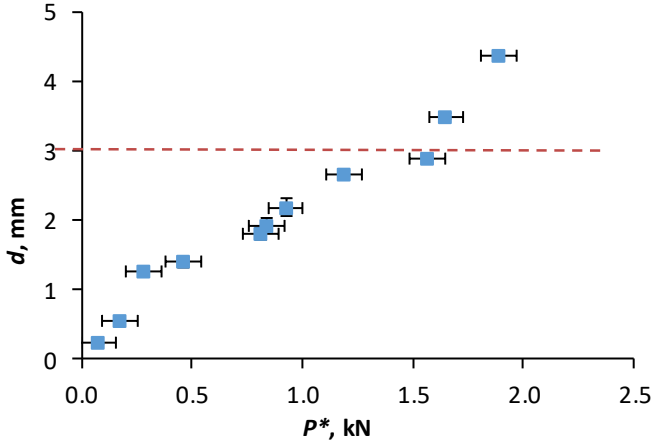


Figure 3.18. The correlation between the threshold $P^*$ of visualization of the load and protective epoxy coating thickness $d$. For $d$ > 3mm, an irreversible deformation was detected.

### 3.2.2 The effect of integrated DVIS on mechanical properties of composite

Evidently, embedding foreign objects (here the DVIS), presumably with lower mechanical characteristics in comparison to the neat glass fabric layer, leads to the degradation of the mechanical properties of the composite. In this part of the work, the effect of the integrated DVIS on mechanical properties of the composite was evaluated.

As a base of the DVIS, the glass fabric *Aeroglass plain*, 130 g/m$^2$ was used. To manufacture the composite, *UD*, 511 g/m$^2$ unidirectional glass fabric, *LH 288* epoxy resin, and *H 284* hardener in the ratio 100:23 (all components supplied by Havel Composites CZ s.r.o., Czech Republic), and the DVIS prepared previously were used. By vacuum bagging method, two series of composite panels 20×30 cm were made: with the integrated DVIS and reference ones without the DVIS. The thickness of the panels was $h$ = 2.3 and 1.9 mm, respectively. In the reference samples, the DVIS was replaced with the same layer of glass fabric, but not impregnated with colour agents. The composite was cured for 20 h at 40 °C in a vacuum oven and then for 72 h at 50 °C in an oven. Unidirectional reinforced 6-layer composite samples of length $L$ = 120 mm and width $x$ = 25 mm were cut from the panels. Two notches were made in the samples to test them for the interlaminar shear strength. According to the ASTM D3846 – 02 standard [137], notches are centred perpendicular to the length of the sample, reach half of the thickness, and are in a distance $l$ from each other on opposite planes. The sample geometry is shown in Figure 3.19. In the case of the samples with the integrated DVIS, the notches were cut at a depth reaching the DVIS, which was confirmed by a change in colour. Samples with distances between the notches $l$ from 5 to 21 mm were tested.

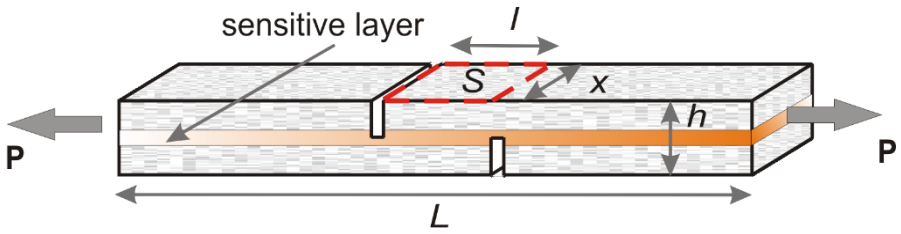


Figure 3.19. General view of double-notch samples with the DVIS used in tests for the interlaminar shear strength.

The interlaminar shear strength of the composite was determined in quasi-static tensile tests performed on the universal testing machine Zwick 2.5 with a rate of 2 mm/min at a temperature of 22 ± 2 °C. The shear strength in the plane was calculated as the ratio of the maximum load applied to the damaged area, $\tau^* = P/(lx)$. The fracture was observed between the notches. The typical force-displacement curves obtained during the quasi-static tensile tests of reference samples and samples with the DVIS, with distances between notches $l$ = 10 and 20 mm, are shown in Figure 3.20.

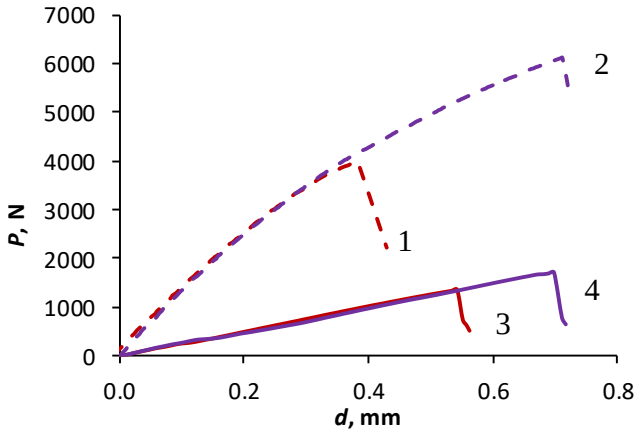


Figure 3.20. Typical force-displacement curves for the reference samples (– –) and samples with the DVIS (–), for $l$ = 10 (*1*, *3*) and 20 mm (*2*, *4*).

The interlaminar shear strength $\tau^*$ of given a sample with certain distance $l$ is a maximal value of shear stress $\tau$ obtained in tensile tests and depends on stress concentrations near notches. The interlaminar shear strength of the composite $\tau_{\max}$ is considered as extrapolation for $l$ = 0 and was defined as

$$\tau_{\max} = \tau^* \theta \operatorname{cotan}\theta\,, \tag{41}$$

where $\tau^* = P/(lx)$ is the shear strength, $P$ is the tensile load, $\theta = \left(\frac{2l}{h}\right)k$, $k = \sqrt{G_{xz}/(2E_x)}$, $G_{xz}$ is the shear modulus, and $E_x$ is the elastic modulus [138, 139].

The experimental and calculated values of strength of samples as functions of distance between the notches and the $\tau^* = f(l)$ curve obtained by approximation according to Eq. (41), are shown in Figure 3.21.

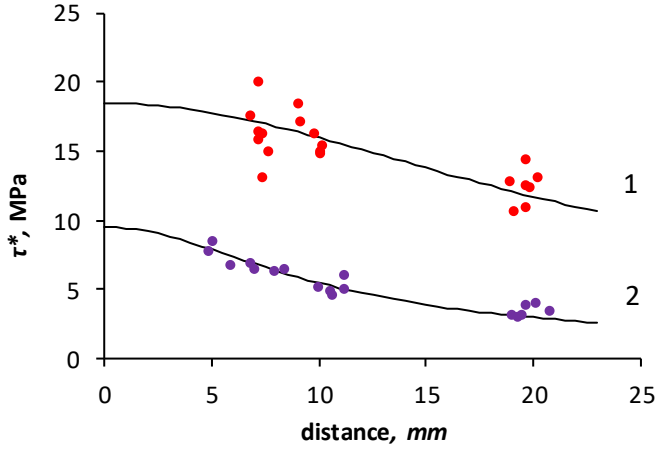


Figure 3.21. Sample strength τ* vs the distance $l$ between notches for the reference samples (1) and samples with a DVIS (2): (●) – experiment and (—) – calculation.

By the extrapolation of the $\tau^* = f(l)$ curve to $l = 0$, the value of $\tau_{max}$ was determined. As a result, the values of $\tau_{max}$ = 9.5 and 18.5 MPa were found samples with the DVIS and for the reference samples, respectively. As seen, the DVIS reduced the interlaminar shear strength roughly twofold, which is quite reasonable for non-crucial structures [140]. Such a significant reduction in the strength of load-carrying structures must be compensated, for example, by adding carbon nanotubes or other nanoparticles. However, in the number of cases, the opportunity for a quick structural health monitoring can be more critical than the priory known reduction in the strength of the material.

It is important to bear in mind that the described experiment was the first attempt to evaluate the effect of the integrated DVIS on the mechanical properties of the composite. General enhancement of the material, such as improvement of the safety exploitation and simplification of the structural NDT process, involved the degradation of another property. Thus, all relevant properties must be considered, and trade-offs must be made [141]. For example, the mechanical properties of the pure polymer matrix are reduced when microcapsules are added; however, the addition of carbon nanotubes significantly improved these mechanical properties [142]. A similar approach could be implemented for the composites with the integrated DVIS in future work.

### 3.2.3 Kinetics of colour change in the place of damage at room temperature

The kinetics of colour change was measured for samples after quasi-static tensile tests up to fracture of the sample and quasi-static indentation tests without fracture.

In the first case, after the fracturing of a sample with the integrated DVIS, the change of visual response in time was photo registered. The sample was immediately removed from grips, and the area of the shear plane was photographed at 5-second interval during the first minute, increasing the interval to 10 min for 30-150 min after a fracture. The visual response was determined by image processing using *Photoshop.* For a quantitative estimation, the *RGB* colour mode and parameter *Mean*, characterizing the average brightness of the image, were selected. Immediately after fracture, no colour change was observed, and therefore the first shot was used as a reference one $RGB_0$. The variation in the visual response was calculated as the difference between the *Mean* of the reference image and that of images taken at certain time intervals.

In the other case, the kinetic of colour response was estimated for the samples subjected to a quasi-static compression by a spherical indenter. Images of a sample before and after the test are shown in Figure 3.22. The figure clearly shows a darkening in the area of indentation. During these experiments, samples were not destroyed.

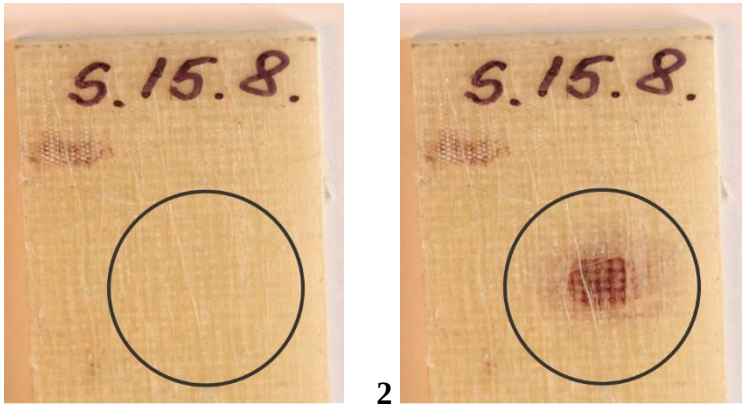


Figure 3.22. Sample with an integrated DVIS before (1) and after (2) quasi-static indentation test.

For the DVIS used as the damage indicator, it is necessary to estimate the time, when the visual response reaches its maximum brightness. The *Fractional conversion* $\alpha$ was used for estimating the brightness variation after damage. Parameter $\alpha$ quantitatively characterizes solid-phase reactions, i.e., reactions involving solid reactants or products. The value of $\alpha$ was found from

$$\alpha(t) = \frac{N_t}{N_0}, \tag{42}$$

where $N_0$ and $N_t$ are amounts of the reagent in the initial system and at a time $t$ from the beginning of the reaction, respectively [143].

The sequence of determination of the parameter $\alpha$ from the data obtained in processing the photos in the graphical editor followed:

- In all images, the place of the expected change in colour is determined. These areas must coincide upon superposition of all images.
- The average value of the brightness *RGB* of the selected area was determined for reference image $t = 0$ and each time $t$ when an image was taken.
- The degree of darkening was calculated as the difference between the brightness $RGB_0$ of the reference image, at $t = 0$, and at a definite instant of time $RGB_t$: $\Delta RGB(t) = RGB_0 - RGB_t$.
- The uncontrollable instability of lighting and imaging equipment introduces random errors into the measured value of the brightness *RGB*. To exclude the effect of these factors, the change in the brightness of image background for the reference image, $RGB_0^{bgr}$, at $t = 0$, and at a definite instant of time $RGB_t^{bgr}$, in a place where colour changes certainly were not expected (the area near the fracture of capsules) was evaluated by

$$\Delta RGB_{bgr} = RGB_0^{bgr} - RGB_t^{bgr}. \tag{43}$$

The degree of darkening after the reaction, considering the random errors, was evaluated as the difference between the intensity of darkening and its average deviation due to instability of the equipment

$$\Delta RGB^*(t) = RGB_0 - RGB_t - \Delta RGB_{bgr} . \quad (44)$$

For the instants of time when the darkening reached saturation and the brightness practically remained unchanged, the average brightness corresponding to the end of the reaction, $\Delta RGB_{max}$, i.e., at $\alpha = 1$, was calculated.

Thus, the value of parameter $\alpha$ during the reaction was determinates as

$$\alpha(t) = \frac{\Delta RGB^*(t)}{\Delta RGB_{\max}} . \quad (45)$$

For the describing the process of formation of the visual response, a one-step nucleation model was selected, meaning by this the process of turning of a small amount of reagent into a stable particle [144]. In the present work, the potential nuclei are considered as particles of the colour activator. They were randomly distributed over the surface of the layer, and they were stable initial solid components. On the destruction of the microcapsules, spreading or diffusion of the leuco dye on the layer occurs. The nuclei were activated when being exposed to activator particles. The first-order differential equation can describe the rate of nucleation as

$$\frac{dN}{dt} = k_1 (N_0 - N). \quad (46)$$

Its solution is

$$N(t) = N_0 \left[1 - exp(-k_1 t)\right], \quad (47)$$

where $N(t)$ is the amount of the activator particles contacting with the dye at an instant of time $t$ at a given point and causing a change $\Delta RGB(t)$ in colours, and $N_0$ is the amount of the reagent, i.e., the total number of potential centres of colouring.

It was assumed that in the case of $\Delta RGB(t) \to \Delta RGB_{max}$, all potential nuclei participate in the reaction and $N(t) \to N_0$. Therefore, the parameter $\alpha$ can be described by the Eq. (48)

$$\alpha = 1 - exp(-k_1 t). \quad (48)$$

Parameter $\alpha$ as a function of reaction time $t$ is shown in Figure 3.23.

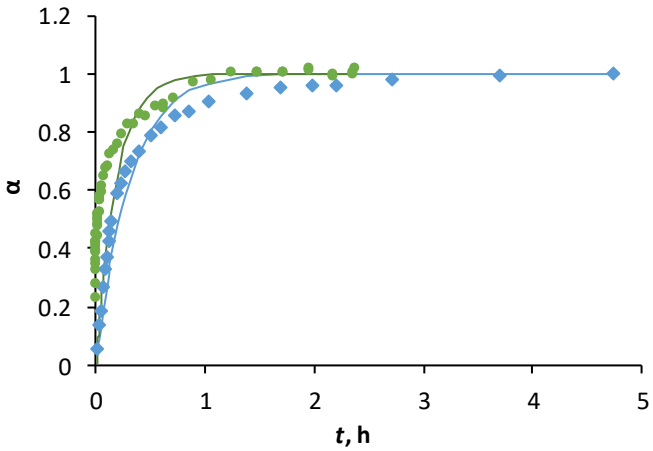


Figure 3.23. *Fractional conversion* vs the reaction time *t* after quasi-static tensile tests up to the fracture of the sample (♦) and quasi-static indentation tests without fracture (●). Experimental points (♦,●) and the approximation by Eq. (48) (—).

Figure 3.23 shows that Eq. (48) does not completely describe the relation $\alpha(t)$. For a more precise description of the experimental data, the following equation is more appropriate

$$\ln\left[\ln\left(1-\alpha\right)\right] = n\ln t + C\,, \tag{49}$$

which can also be written in the form

$$\alpha = 1 - exp\left(-k_1 t^n\right), \tag{50}$$

where the value of *n* is found empirically [144].

For practical use of the DVIS, it is necessary to determine the time when the visual response under the action of the applied load reaches a maximum value. Therefore, the kinetic equation (48) is suitable for describing the change in colour when $\alpha$ is close to 1. Approximation of the relation $\alpha(t)$ after the quasi-static tensile tests up to fracture of the sample and quasi-static indentation tests without fracture has revealed that reaction rate constants are $k_1 = 2.72$ and 5.47, respectively. It could be seen from Figure 3.23 that the parameter $\alpha$ reached saturation, i.e., the maximum visual response was observed after 1.5 h of quasi-static indentation tests and after 3.5 h of quasi-static tensile tests. Such a difference in the rate of parameter $\alpha$ may be due to the fact that during the indentation, the concentration of capsules remains unchanged. In turn, the shear fracture decreased the concentration of the capsules and activator particles per unit area of the DVIS. A sample after the quasi-static tensile tests up to fracture is shown in Figure 3.24. As seen, some portions of capsules and activator particles had remained on both parts of the sample [145].

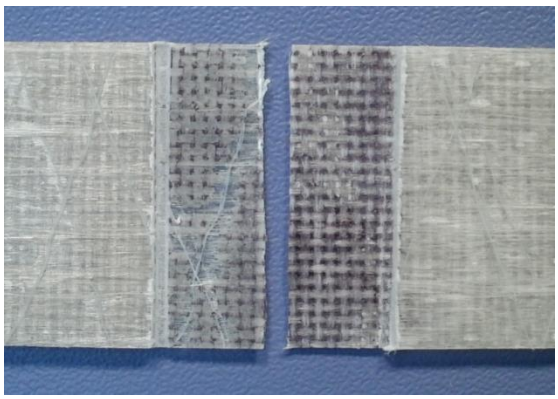

Figure 3.24. Sample with the integrated DVIS after the quasi-static tensile test.

## 3.3 Main results of Chapter 3

- Model composites with the integrated DVIS were developed and presented as two demonstrators: a) the DVIS integrated into a composite, b) the DVIS as a separate layer, which was placed on a surface of a composite.
- The DVIS as an external layer was developed as a prepreg. Exploitation parameters of the DVIS as a prepreg were defined, such as: type of fabric as a base, time and conditions of storage, and the ability to be removed from the surface after the use.
- A visual response using the DVIS on different substrates was evaluated. The visual response depended on the substrate material - with a stiffer substrate, a more intensive visual response was obtained. For the different size balls, but the constant energy, the diameter of the place with a visual response was similar. Increasing energy led to increasing in the diameter of the place with a visual response and increasing in the average brightness of visual response.
- For the DVIS as an internal layer, the correlation between the threshold of visualization of the load and protective epoxy coating thickness was defined.
- The effect of the integrated DVIS on mechanical properties of composite was estimated. It was defined that the DVIS reduced the interlaminar shear strength roughly twofold when integrated into a composite.
- Kinetics of colour change in the place of damage for composite samples with the integrated DVIS at the room temperature was measured. The maximal visual response could be observed in approximately 2 - 3 h, depending on the method of action on the composite sample – quasi-static indentation tests without fracture and quasi-static tensile tests up to fracture.
- The kinetics of darkening after the damage was described by a first-order differential equation of the reaction. The obtained values of reaction rate constants and allow to predict reaction’s run at room conditions.

## GENERAL CONCLUSIONS

The **damage visual indication system** for polymer composites **was developed and validated**.

In the frame of the work, all tasks were fulfilled.

Microcapsules for the DVIS were developed, their physical and mechanical properties were obtained experimentally and by analytical methods. Via in situ polymerization, two types of microcapsules were prepared with polyurethane and melamine formaldehyde shell materials. By varying synthesis parameters and amount of chemical components, microcapsules with different sizes and shell thickness were obtained. Laboratory synthesized and commercial microcapsules were compared by SEM images. By image analysis, shape regularity, smoothness of the surface, the presence of the remaining materials were compared, and as a result, for further work the commercial microcapsules were selected. Microcapsules size analysis was performed by dynamic light scattering, optical and SEM microscopy. Since microcapsules tend to agglomerate and additional sonication is needed before the measuring, image treatment in ImageJ in manual mode allowed to obtain the most precise results. Shell thickness was obtained from SEM images of manually broken microcapsules. Despite the stability of microcapsules till +350 °C defined by thermogravimetric analysis, stable colour response on the applied load was observed in the range -20 to +150 °C.

Nanoindentation by AFM allowed to define mechanical properties of single microcapsules. Applying Reisner equation for shallow spheres, the elastic modulus was defined. This value showed a good correlation with the results of effective elastic modulus obtained by various analytical models (Reuss and Voigt models, Hashin-Shtrikman, Counto, etc.), known from the mechanics of composite materials and applied for the description of compression of spherical inclusions in a polymer matrix. However, elastic modulus values obtained by direct measuring of pure shell material could not be compared with previous results due to the great influence of the manufacturing method on material properties.

Technologies for the manufacture of the DVIS as internal and external layers were developed and optimized. It was verified that in the manufacture of the DVIS it is possible to use two combinations of colour agent: microcapsules with leuco dye mixed with dye activator in microcapsules or as microparticles. For the quantitative estimation of the visual response on the damage, two algorithms of digital image analysis in the software Adobe® Photoshop® and Mathcad® were compared and used in the present work. By control of the fabric density after impregnation with microcapsules, the optimal impregnation procedure was developed. To make DVIS lighter by weight and decrease manufacturing costs, the quantity of microcapsules could be

decreased in two times, comparing to the nominal concentration of suspension. Fixation of microcapsules on the surface of the fabric could be realized by adding epoxy modified polyurethane-acrylic polymer which was polymerized by UV by mercury-quartz lamp with parameters 280-320 nm and 10.5 W/m$^2$ for at least 15 min.

For the DVIS as a separate layer, it was verified that it could be removed and exchanged after the use without any damage to the surface. Peel forces obtained for the DVIS prepreg with a glass fabric base (200-300 N/m) are in 2-3 times higher compared to that of with a nylon base (100 N/m), but at least twice smaller than the usual forces for removing peel plies used in the manufacturing process of reinforced composites.

DVIS allows indicate damage of the composite structure under compression and shear. The kinetics of darkening after the damage was investigated. The visual response was observed immediately after applied load (less than 1 s) and reaching the maximal response in 2-3 h. The kinetics of darkening after the damage was described by a first-order differential equation of the reaction. The reaction rate constants obtained allow one to predict its run at room conditions.

The presence of the DVIS in the composite reduced the interlaminar shear strength roughly twofold. Such a significant reduction in the strength of load-carrying structures must be compensated, for example by adding carbon nanotubes or other nanoparticles. However, in the number of cases, the opportunity for a quick structural health monitoring can be more important than the priory known reduction in the strength of the material.

The **scientific novelty of the work** could be described as follows:

- The concept of the DVIS was firstly applied to structural composite materials and presented in two ways: as internal and external layers.
- The DVIS was studied out from micro to macro levels, and fabrication technologies for both layers were developed.
- The DVIS as an external layer was tested on the ability to be glued to the surface and to be replaced after use.
- The DVIS as an internal layer was tested for the effect of this layer on the mechanical properties of the composite.
- Kinetics of colour change after the applied load, the effect of storage temperature and durability of the DVIS were tested.

**For the practical application** of the results of the research, Composite with the integrated DVIS was prepared as two demonstrators: a) the DVIS as a separate layer, which could be placed on a surface of existing construction or element, b) the DVIS integrated into a composite by vacuum bagging method. A Technology Readiness Level of the presented DVIS corresponds to TRL 4 – “Technology validated in lab” [146].

All experimental data and knowledge obtained during the work could be transformed into the **future work with** the next **preliminary plans**:

- To apply experimental data for modelling of composite structure with the integrated DVIS.
- To develop and test a composite structure with the integrated DVIS and with nanoparticles, thus compensating for the loss of mechanical properties.

The significant finding to emerge from this study is that **DVIS can improve exploitation safety and simplify the structural NDT process of polymer composites in constructions**. The present DVIS approach can be used as one method of non-destructive testing, but it can be attributed to a broader concept - structural health monitoring. The DVIS indicates the existing problem, but other NDT methods may also be used to aid the interpretation of it. Presented concept of the damage visual indication system for GFRP composites allows to minimise inspection time and simplify non-equipment permanent inspection of large surfaces, promote the safe operation of composites for various applications. The opportunity of in-time refit or replacement opens. But in general, the DVIS as an external layer can perform a function of the sensor, fixing applied load for any object and the DVIS concept is not limited to composite structures only.

## Theses to be defended

1. Effective elastic modulus of microcapsules can be evaluated using both Voigt and Reuss analytical models for the case of good bonding between microcapsules and matrix.
2. The effectiveness of the developed Damage visual indication system for polymer composite structures (DVIS) have been demonstrated. DVIS as an external layer could be placed on top of the structure and removed after use without damage to the structural integrity. DVIS as an internal layer allows indicating damage of the composite structure under compression and shear.
3. The visual indication efficiency of the DVIS have been demonstrated. Colour response is observed in seconds after the applied loads regardless of sample temperature in the range -20 to +150 °C. The kinetics of darkening after the damage can be described by a first-order differential equation of the reaction. The reaction rate constants obtained allow one to predict its run and finish at room conditions.

## APPROBATION OF RESULTS

The results of this work were published in 3 peer-reviewed scientific journals indexed in Scopus, 8 international conference proceedings, and 2 patent applications. These results were reported at 22 international scientific conferences; 14 of them were presented by the thesis author. Scientific results presented here were obtained during the work in 3 scientific projects and 2 individual grants. The research was performed in the Institute for Mechanics of Materials (before 2016 Institute of Polymer Mechanics), University of Latvia. Different parts of the work leading to these results were performed by the author in collaboration with colleagues from the following laboratories:

- Institute for composites and biomedical material, National research council, Naples, Italy;
- Department of Materials and Ceramic Engineering, University of Aveiro, Portugal;
- SMALLMATEK company, Aveiro, Portugal;
- SYNPO company, Pardubice, Czech Republic;
- Research Institute for Physical Chemical Problems, Belarusian State University.

**Scientific papers**

1. Aniskevich A., Kulakov V., Bulderberga O., Knotek P., Tedim J., Maia F., Leisis V., Zeleniakiene D. "Experimental characterisation and modelling of mechanical behaviour of microcapsules", Journal of Materials Science, 2020, Vol. 55 – P. 13457–13471.
2. Bulderberga O., Aniskevich A., Vidinejevs, S. "A Glass-Fiber-Reinforced Composite with a Damage Indication Function", Mechanics of Composite Materials. Springer US -2016. – Vol. 52(2) – P. 155-162.
3. Vidinejevs S., Strekalova O.[1], Aniskevich A., Gaidukov S. "Development of a composite with an inherent function of visualization of a mechanical action", Mechanics of Composite Materials. Springer US -2013. –Vol. 49 – P. 77-84.

**Patent applications**

1. Vidinejevs S., Bulderberga O., Aniskevics A. "Permanently attachable and detachable chromatic system for visual identification of shock" (P-18-97, 20.06.2020).
2. Vidinejevs S., Aniskevics A, Strekalova O. "Method of making an impact-indicating coating on a surface of an article made of composite materials" (EP 2 537 666 A1, 26.12.2012).

[1] Olga Bulderberga

**International Conference Proceedings**


1. Bulderberga O., Aniskevich A. “Damage visual indication system for polymer composite structures”. Proceedings of the 22nd International Conference on Composites Materials (ICCM-22), August 11-16, 2019, Melbourne, Australia. DOI 10.5281/zenodo.3375420.
2. Aniskevich A., Kulakov V., Bulderberga O., Knotek P., Zeleniakiene D. “Experimental characterization and modelling of mechanical behavior of microcapsules in composites”. Proceedings of the 22nd International Conference on Composites Materials (ICCM-22), August 11-16, 2019, Melbourne, Australia. DOI 10.5281/zenodo.3375396.
3. Bulderberga O., Starkova O., Glaskova-Kuzmina T., Knotek P., and Aniskevich A. “Polymer composite with inherent function of damage visualization: mechanical properties of microcapsules”. Proceedings of the 18th European Conference on Composite Materials- ECCM18, Athens, Greece, 24-28th June 2018, Code 155810.
4. Bulderberga O., Aniskevich A. “Polymer composite material with inherent function of damage visual indication”. Proceedings of the 21st International Conference on Composites Materials (ICCM-21), Xi’an, China, August 20-25, 2017. ICCM International Conferences on Composite Materials, Volume 2017, August 2017, Code 138793.
5. Bulderberga O., Aniskevich A., Vidinejevs S. “GFRP Composite with Damage Visualization Capability”. Proceedings of the 17th European Conference on Composite Materials- ECCM17, Munich, Germany, 26-30th June 2016, Excerpt from ISBN 978-3-00-053387-7, PO-6-06.
6. Zeleniakiene D., Leisis V., Griskevicius P., Bulderberga O., Aniskevich A. “A Numerical Simulation of Mechanical Properties of Smart Polymer Composite with Microcapsules for Damage Sensing Applications”. Proceedings of the 17th European Conference on Composite Materials- ECCM17, Munich, Germany, 26-30th June 2016, Excerpt from ISBN 978-3-00-053387-7, PO-3-02.
7. Strekalova O., Aniskevich A., Vidinejevs S. “GFRP composite with damage indicating layer”. 14th Baltic Polymer Symposium 2014, BPS 2014; Laulasmaa; Estonia; 24 - 26 September 2014; Code 113706. Proceedings of the Estonian Academy of Sciences, Vol. 64, Issue 1 S, 2015, p. 79.
8. Strekalova O., Vidinejevs S., Aniskevich A. “Polymer composite layer with damage indication ability”. Proceedings of the Fourth International Conference on Self-Healing Materials-ICSHM2013, Ghent, Belgium, June 16-20, 2013/ N. D. Belle et al (eds.), Magnel Laboratory for Concrete Research, Ghent, Belgium, 2013, P. 713-716.

**Presentations in international conferences** (speaker is underlined)

1. Bulderberga O., Vidinejevs S., and Aniskevich A. “Smart prepreg as damage visual indication system”. Baltic Polymer Symposium, September 18 - 20, 2019, Vilnius, Lithuania. Book of abstracts p. 112.
2. Aniskevich A., Kulakov V., Bulderberga O., Knotek P., and Zeleniakiene D. “Experimental characterization and modelling of mechanical behavior of microcapsules in composites”. 22nd International Conference on Composites Materials (ICCM-22), August 11-16, 2019, Melbourne, Australia.
3. Bulderberga O., Aniskevich A. “Damage visual indication system for polymer composite structures”. 22nd International Conference on Composites Materials (ICCM-22), August 11-16, 2019, Melbourne, Australia.
4. Bulderberga O., Starkova O., Glaskova-Kuzmina T., Knotek P., and Aniskevich A. “Polymer composite with inherent function of damage visualization: mechanical properties of microcapsules”. 18th European Conference on Composite Materials- ECCM18, Athens, Greece, 24-28$^{th}$ June 2018.
5. Bulderberga O., Aniskevich A. “Polymer composite material with inherent function of damage visual indication”. 2nd International Scientific Conference "Advanced Polymer Materials and Technologies", October 12-13, 2017, Kiev, Ukraine.
6. Dehtjars J., Gruškeviča K., Romanova M., Aniskevich A., Bulderberga O. “Material mechanical micro- nano- scaled features and their impact on human safety”. 3rd International Conference “Innovative Materials, Structures and Technologies”, September 27-29, 2017, Riga, Latvia.
7. Bulderberga O., Aniskevich A. “Polymer composite material with inherent function of damage visual indication”. 21st International Conference on Composites Materials (ICCM-21), August 20-25, 2017, Xi’an, China.
8. Bulderberga O., Aniskevich A. “Development and determination of properties of the polymer composite with damage indication ability”. 8th International Conference on Composites Testing and Model Identification - CompTest, April 5-7, 2017, Leuven, Belgium.
9. Dehtjars J., Aņiskevičs A, Bulderberga O., Romanova M., Gruškeviča K., Balodis A. “Material mechanical micro- nano- scaled features and their impact on human safety”. 57th International Scientific Conference of Riga Technical University, October 14-18, 2016, Latvia.

10. Bulderberga O., Aniskevich A., Vidinejevs S. “GFRP Composite with Damage Visualization Capability”. The 17th European Conference on Composite Materials-ECCM17, Munich, Germany, 26-30th June 2016.
11. Zeleniakiene D., Leisis V., Griskevicius P., Bulderberga O., Aniskevich A. “A Numerical Simulation of Mechanical Properties of Smart Polymer Composite with Microcapsules for Damage Sensing Applications”. The 17th European Conference on Composite Materials-ECCM17, Munich, Germany, 26-30th June 2016.
12. Bulderberga O., Aniskevich A. “Smart GFRP Composite with Damage Visualization Capability: Properties of Microcapsules”. 12th International Conference on Durability of Composite Systems, DURACOSYS 2016, Edited by: Ken Reifsnider, ISBN: 978-1-60595-318-2, Arlington, Texas, USA, June 12-15, 2016, Book of abstracts pp. 273-274.
13. Aniskevich A., Bulderberga O., Dekhtyar Y., Denisova V., Gruskevica K., Juhna T., Kozak I., Romanova M. “Coloured reactions and emission of electrons towards early diagnostics of polymer materials overloading”, 2nd International Conference „Innovative Materials, Structures and Technologies”, 30.09. - 02.10.2015, Riga, Latvia. Riga: RTU Press, 2015, 19.-19.lpp. ISBN 978-9934-10-742-9.
14. Zeleniakiene D., Leisis V., Griskevicius P., Bulderberga O., Aniskevich A., “A numerical study to analyse mechanical properties of polymer composites with smart microcapsules for high performing sensing applications’’. Baltic Polymer Symposium 2015, September 16-18, 2015, Sigulda, Latvia, Book of abstracts, p. 71.
15. Aniskevich A., Bulderberga O., Vidinejevs S. “Polymer composites with ability of visual damage indication’’. Euro Nano Forum 2015, June 10 – 12, 2015, Riga, Latvia.
16. Bulderberga O., Aniskevich A., and Vidinejevs S.. “Visual indication of mechanical damages in polymer composites”. Open Readings 2015, March 24-27, 2015, Vilnius, Lithuania, Book of abstracts, p. 155.
17. Strekalova O., Aniskevich A., and Vidinejevs S. “GFRP composite with damage indicating layer”. Baltic Polymer Symposium 2014, September 24-26, 2014, Laulasmaa, Estonia, Book of abstracts, p. 78.
18. Strekalova O., Vidinejevs S., and Aniskevich A. "GFRP composite with integrated damage indication layer". XVIII International Conference on Mechanics of Composite Material, June 2-6, 2014, Riga, Latvia, Book of abstracts, p. 177.
19. Strekalova O., Vidinejevs S., Aniskevich A. “Polymer composite layer with damage indication ability”. Self-Healing Materials (ICSHM2013), June 16–20, 2013, Ghent, Belgium, Book of abstracts, p. 328.

20. Strekalova O., Vidinejevs S., and Aniskevich A. “Self-Monitoring Fibre Reinforced Composites: Visual Response to the External Indentation”. XVII International Conference on Mechanics of Composite Material, May 28-June 1, 2012, Riga, Latvia, Book of abstracts, p. 208.
21. Strekalova O., Vidinejevs S., Aniskevich A. „Critical loading visualization capability in glass fibre reinforced epoxy composite”. Baltic Polymer Symposium 2011, September 21-24, 2011, Pärnu, Estonia, Book of abstracts, p. 95.
22. Vidinejevs S., Strekalova O., Aniskevich A. „Biomimetic fiber reinforced composite with damage visualization capability”. Third International Conference Self-Healing Materials, June 27-29, 2011 Bath, United Kingdom, Book of abstracts p. 153.

**Scientific projects**

1. Latvian Council of Science project LZP-2018/1-0084, DUROCAPS, “Durability and environmental stability of microcapsule-filled polymer composites with smart-interaction capability”, 08.2018 - 07.2021, Project Leader: A. Aniskevich.
2. Horizon-2020, MSCA, RISE, project SMARCOAT, GA 645662 “Development of Smart Nano and Microcapsulated Sensing Coatings for improving of Material Durability/Performance”, 01.01.2015 - 31.12.2018.
3. Latvia state research programme "Innovative materials and smart technologies for environmental safety, IMATEH", 07.2014 - 12.2017.

**Individual grants**

1. Italian government Bursaries for foreign and I.R.E. students 2013-2014, research project “Composites with damage indication function”. Institute for composites and biomedical material, National research council, Naples, Italy, 03.2014. - 08.2014.
2. Research Grant under the FP7 Project “Smart Intelligent Aircraft Structures”. Department of Materials and Ceramic Engineering, University of Aveiro, Portugal, 11.2013 - 02.2014.

**Other scientific projects, where the author took part**

1. European Regional Development Fund Project Nr. 1.1.1.1/19/A/031 “Decision Tool for Optimal Design of Smart Polymer Nanocomposite Structures Produced by 3D Printing”, 01.07.2020 - 30.06.2023, Project Leader: A. Aniskevich.
2. Horizon-2020, MSCA, RISE, project NANO2DAY, GA 777810 “Multifunctional polymer composites doped with novel 2D nanoparticles for advanced applications”, 01.05.2018 - 30.04.2022, Project Leader: A. Aniskevich.
3. M-ERA.Net, Grant No. 1.1.1.5/ERANET/18/02, Research Council of Latvia, “Advanced polymer composites filled with novel 2D nanoparticles”, 02.07.2018 - 01.07.2021, Project Leader: A. Aniskevich.

4. European Regional Development Fund Project Nr. 1.1.1.1/16/A/141 “Development of nano-modified polyolefin multilayer extrusion products with enhanced operational properties”, 01.03.2017- 29.02.2020, Project Leader: A. Aniskevich.
5. European Regional Development Fund Project Nr. 2010/0213/2DP/2.1.1.1.0/10/APIA/VIAA/049 „Development of new anchoring systems for pultruded composite materials and its application in structural elements with an increased load-carrying capacity”, 03.12.2012-13.12.2013, Project Leader: A. Aniskevich.

# LIST OF FIGURES

# LIST OF TABLES

## REFERENCES


1. Sathishkumar, T.P., S. Satheeshkumar, and J. Naveen, *Glass fiber-reinforced polymer composites – a review.* Journal of Reinforced Plastics and Composites, 2014. **33**(13): p. 1258-1275.
2. *Nondestructive Testing.* NDT Resource Center (available - https://www.nde-ed.org/index_flash.htm).
3. Gholizadeh, S., *A review of non-destructive testing methods of composite materials.* Procedia Structural Integrity, 2016. **1**: p. 50-57.
4. Ciang, C.C., J.-R. Lee, and H.-J. Bang, *Structural health monitoring for a wind turbine system: a review of damage detection methods.* Measurement Science and Technology, 2008. **19**(12).
5. Schubel, P.J., et al., *Review of structural health and cure monitoring techniques for large wind turbine blades.* Renewable Energy, 2013. **51**: p. 113-123.
6. C., N.S., et al., *Non-destructive Inspection of Multi-layered Composite Using Ultrasonic Signal Processing.* IOP Conference Series: Materials Science and Engineering, 2011. **17**(1).
7. Bhat, M.R. and M.P. Binoy, *Non-destructive evaluation of porosity and its effect on mechanical properties of carbon fiber reinforced polymer composite materials.* AIP Conference Proceedings, 2012. **1430**.
8. *X-rays for NDT of composites.* Composites World (available - https://www.compositesworld.com/articles/x-rays-for-ndt-of-composites).
9. Gostautas, R.S., et al, *Acoustic Emission Monitoring and Analysis of Glass Fiber-Reinforced Composites Bridge Decks.* Journal of Bridge Engineering, 2005. **10**(6).
10. Dahmene, F., S. Yaacoubi, and M. EL Mountassir, *Acoustic Emission of Composites Structures: Story, Success, and Challenges.* Physics Procedia, 2015. **70**: p. 599-603.
11. Chrysafi, A.P., N. Athanasopoulos, and N.J. Siakavellas, *Damage detection on composite materials with active thermography and digital image processing.* International Journal of Thermal Sciences, 2017. **116**: p. 242-253.
12. Li, Y., et al., *Investigation on the damage evolution in the impacted composite material based on active infrared thermography.* NDT & E International, 2016. **83**: p. 114-122.
13. Meola, C., et al., *Nondestructive evaluation of carbon fibre reinforced composites with infrared thermography and ultrasonics.* Composite Structures, 2015. **134**: p. 845-853.
14. Garnier, C., et al., *The detection of aeronautical defects in situ on composite structures using Non Destructive Testing.* Composite Structures, 2011. **93**(5): p. 1328-1336.
15. Wang, B., et al., *Non-destructive testing and evaluation of composite materials/structures: A state-of-the-art review.* Advances in Mechanical Engineering, 2020. **12**(4): p. 1-28.
16. Vavouliotis, A., A. Paipetis, and V. Kostopoulos, *On the fatigue life prediction of CFRP laminates using the Electrical Resistance Change method.* Composites Science and Technology, 2011. **71**(5): p. 630-642.
17. Keulen, C., et al., *Embedded fiber optic sensors for monitoring processing, quality and structural health of resin transfer molded components.* Journal of Physics: Conference Series, 2011. **305**: p. 012135.
18. Gao, L., et al., *In situ sensing of impact damage in epoxy/glass fiber composites using percolating carbon nanotube networks.* Carbon, 2011. **49**(10): p. 3382-3385.
19. Todoroki, A., et al., *Piezoresistivity of unidirectional carbon/epoxy composites for multiaxial loading.* Composites Science and Technology, 2009. **69**(11-12): p. 1841-1846.
20. García Márquez, F.P., et al., *Condition monitoring of wind turbines: Techniques and methods.* Renewable Energy, 2012. **46**: p. 169-178.
21. Rana, S., et al., *A review on smart self-sensing composite materials for civil engineering applications.* AIMS Materials Science, 2016. **3**(2): p. 357-379.

22. Han, B., et al., *Nanotip-induced ultrahigh pressure-sensitive composites: Principles, properties and applications.* Composites Part A: Applied Science and Manufacturing, 2014. **59**: p. 105-114.
23. Jin, X., et al., *A novel concept for self-reporting materials: stress sensitive photoluminescence in ZnO tetrapod filled elastomers.* Adv Mater, 2013. **25**(9): p. 1342-7.
24. Baaran, J., *Final Report of European Aviation Safety Agency - Research Project/2007/3 "Study on visual inspection of composite structures"*. 2009, Institute of Composite Structures and Adaptive Systems, DLR Braunschweig, Germany. p. 114.
25. Sun, X.C. and S.R. Hallett, *Barely visible impact damage in scaled composite laminates: Experiments and numerical simulations.* International Journal of Impact Engineering, 2017. **109**: p. 178-195.
26. Zoltan, M. and H. Peter, *Final Report of European Aviation Safety Agency - Research Project EASA.2010.C13 "Composite Damage Metrics and Inspection"*. 2012, Bishop GmbH - Aeronautical Engineers, Germany. p. 106.
27. Singh, A.V., et al., *Bio-inspired approaches to design smart fabrics.* Materials & Design (1980-2015), 2012. **36**: p. 829-839.
28. *Bruise (pathology).* Online ENCYCLOPEDIA BRITANNICA (available - https://www.britannica.com/science/bruise).
29. Eastham, J., *Detectionof damage in materials.* UK Patent Application GB 2194062 A, 1988: p. 5.
30. Gilles, A., C. Andre, and H. Hubert, *Process and device for revealing impact(s) received by a substrate.* Patent US 5242830, 1993: p. 10.
31. Rush, G.A., *Impact indicator for athletic helmets.* . US 6332226 B1, 2001: p. 5.
32. Richard, T.M. and J.D. Anthony, *Polymer composite materials.* UK Patent Application GB2469735 A, 2010: p. 28.
33. Smith, E.M. and J.C. Marsh, *Pressure sensitive work indicator.* Patent US 7,649,469 B2, 2010: p. 12.
34. Thomas, D. and D. Thomas, *Stress indicating materials.* Patent US 2008/0083286 A1, 2008: p. 6.
35. Koene, B.E. and M.E. Rogers, *Method for detecting damage.* Patent US 2007/0197383 A1, 2007: p. 8.
36. Koene, B.E. and M.E. Rogers, *Method for detecting damage* Patent WO 2006/105290, 2006: p. 22.
37. Hu, M., et al., *Monitoring crack appearance and healing in coatings with damage self-reporting nanocapsules.* Materials Horizons, 2018. **5**(1): p. 51-58.
38. Hopmann, C., M. Kerschbaum, and K. Küsters, *Processing of microencapsulated dyes for the visual inspection of fibre reinforced plastics.* 2014: p. 449-453.
39. Odom, S.A., et al., *Visual indication of mechanical damage using core-shell microcapsules.* ACS Appl Mater Interfaces, 2011. **3**(12): p. 4547-51.
40. Li, W., et al., *Autonomous Indication of Mechanical Damage in Polymeric Coatings.* Advanced Materials, 2016. **28**(11): p. 2189-2194.
41. *Damage Indicating Paints.* Sensor Products Inc. (available - http://www.sensorprod.com).
42. *Thermochromic, photochromic and scented microcapsules production.* Gem'innov (available - http://www.geminnov.com).
43. *Microcapsules for a range of different applications and industries.* Koehler Innovative Solutions (available - https://www.koehlerinnovative.com).
44. *Design and manufacture of microcapsules* Calyxia (available - https://www.calyxia.fr/).
45. Li, Y., et al., *Microcapsule encapsulated with leuco dye as a visual sensor for concrete damage indication via color variation.* RSC Advances, 2020. **10**(3): p. 1226-1231.
46. Zheng, X., et al., *Microcapsule-Based Visualization Smart Sensors for Damage Detection: Principles and Applications.* Advanced Materials Technologies, 2019. **5**(2): p. 1900832.

47. Zheng, X., et al., *Fabrication of self-reactive microcapsules as color visual sensing for damage reporting.* Journal of Materials Science, 2020. **55**(21): p. 8861-8867.
48. Zheng, X., Wang, Q., Li, Y., Luan, J., & Wang, N., *Microcapsule-Based Visualization Smart Sensors for Damage Detection: Principles and Applications.* Advanced Materials Technologies, 2019. **1900832**.
49. *Leuco Dyes.* Kolorjet, Chemicals PVT. LTD (available - http://www.dyes-pigment.com/leuco-dyes.html).
50. Jyothi, S.S., et al., *Microencapsulation: A review.* International Journal of Pharma and Bio Sciences, 2012. **3**(1): p. 23.
51. Sopena, F., C. Maqueda, and E. Morillo, *Controlled release formulations of herbicide based on micro-encapsulation.* Ciencia e investigación agraria, 2009. **35**(1): p. 27-42.
52. N., S.M., et al., *Microencapsulation: a promising technique for controlled drug delivery.* Research in Pharmaceutical Sciences, 2010. **5**(2): p. 65-77.
53. Estevinho, B.N., et al., *Microencapsulation with chitosan by spray drying for industry applications – A review.* Trends in Food Science & Technology, 2013. **31**(2): p. 138-155.
54. Ghosh, S.K., *Functional Coatings and Microencapsulation.* Functional Coatings, 2006: p. 28.
55. Peanparkdee, M., S. Iwamoto, and R. Yamauchi, *Microencapsulation: a review of applications in the food and pharmaceutical industries.* Reviews in Agricultural Science, 2016. **4**: p. 56-65.
56. *Smart Fibres: Microencapsulation.* Technology Online (available - http://technology.tki.org.nz/Resources/Case-studies/Technologists-practice-case-studies/Resistant-materials-textiles/Smart-Fibres/Microencapsulation)
57. Casanova, F. and L. Santos, *Encapsulation of cosmetic active ingredients for topical application – a review.* Journal of Microencapsulation, 2015. **33**(1): p. 1-17.
58. *Chemical Based Microencapsulation Technologies.* Microencapsulation innovations (available - http://www.microencapsulationinnovations.com).
59. Jeong-Sook, C., K. Aehwa, and C. Chang-Gi, *Microencapsulation of octadecane as a phase-change material by interfacial polymerization in an emulsion system.* Colloid and Polymer Science, 2002. **280**(3): p. 260-266.
60. Jun-Seok, H., et al., *Preparation and Characterization of M-F Resin Microcapsules containing fragrant oil.* Biotechnology and Bioprocess Engineering, 2006. **11**(4): p. 332–336.
61. Yuan, L., et al., *Synthesis and characterization of microencapsulated dicyclopentadiene with melamine–formaldehyde resins.* Colloid and Polymer Science, 2007. **285**(7): p. 781-791.
62. Tiarks, F., K. Landfester, and M. Antonietti, *Preparation of Polymeric Nanocapsules by Miniemulsion Polymerization.* Langmuir, 2001. **17**(3): p. 908–918.
63. Thi, T.H.L. and T.C. Luu, *Synthesis of microcapsules from prepolyurethanes.* Journal of Science and Technology, 2017. **55**(1B): p. 138-144.
64. Ghodrati, S. and M. Khatibzadeh, *How do synthesis processing parameters influence the colorimetric, morphology, and particle size distribution of leuco dye-based thermochromic inks microcapsules?* Conference Paper, 13th AUTEX World Textile Conference, May 22nd to 24th 2013, Dresden, Germany. , 2013.
65. *Carbonless Copy Paper.* NIOSH HAZARD REVIEW (available - https://www.cdc.gov/niosh/docs/2001-107/pdfs/2001-107.pdf).
66. *ImageJ.* Image Processing and Analysis in Java (available - https://imagej.nih.gov/ij/index.html).
67. Lavrenova, A., et al., *Visualization of Polymer Deformation Using Microcapsules Filled with Charge-Transfer Complex Precursors.* ACS Applied Materials & Interfaces, 2015. **7**(39): p. 21828-21834.

68. Alic, B., U. Sebenik, and M. Krajnc, *Microencapsulation of butyl stearate with melamineformaldehyde resin: Effect of decreasing the pH value on the composition and thermal stability of microcapsules.* eXPRESS Polymer Letters, 2012. **6**(10): p. 826–836.
69. Weyermann, C., et al., *Evaluation of the Photodegradation of Crystal Violet upon Light Exposure by Mass Spectrometric and Spectroscopic Methods.* Journal of Forensic Sciences, 2009. **54**(2): p. 339-345.
70. Oda H., *New developments in the stabilization of leuco dyes: effect of UV absorbers containing an amphoteric counter-ion moiety on the light fastness of color formers.* Dyes and Pigments, 2005. **66**: p. 103-108.
71. Zhu, D.Y., M.Z. Rong, and M.Q. Zhang, *Self-healing polymeric materials based on microencapsulated healing agents: From design to preparation.* Progress in Polymer Science, 2015. **49-50**: p. 175-220.
72. Keller, M.W. and N.R. Sottos, *Mechanical Properties of Microcapsules Used in a Self-Healing Polymer.* Experimental Mechanics, 2006. **46**(6): p. 725-733.
73. Staresinic, M., B. Šumiga, and B.B. Podgornik, *Microencapsulation for textile applications and use of SEM image analysis for visualisation of microcapsules*. Vol. 54. 2011. 80-103.
74. Poncelet, D. and R.J. Neufeld, *Shear breakage of nylon membrane microcapsules in a turbine reactor.* Biotechnology and Bioengineering, 1989. **33**(1): p. 95-103.
75. Neubauer, M.P., M. Poehlmann, and A. Fery, *Microcapsule mechanics: from stability to function.* Adv Colloid Interface Sci, 2014. **207**: p. 65-80.
76. Fery, A. and R. Weinkamer, *Mechanical properties of micro- and nanocapsules: Single-capsule measurements.* Polymer, 2007. **48**(25): p. 7221-7235.
77. Giro-Paloma, J., et al., *Physico-chemical and mechanical properties of microencapsulated phase change material.* Applied Energy, 2013. **109**: p. 441-448.
78. Su, J.-F., X.-Y. Wang, and H. Dong, *Micromechanical properties of melamine–formaldehyde microcapsules by nanoindentation: Effect of size and shell thickness.* Materials Letters, 2012. **89**: p. 1-4.
79. Giro-Paloma, J., et al., *Preparation and Characterization of Microencapsulated Phase Change Materials for Use in Building Applications.* Materials (Basel), 2015. **9**(1).
80. Mettu S., e.a., *Ultrasonically synthesized organic liquid-filled chitosan microcapsules: part 2: characterization using AFM (atomic force microscopy) and combined AFM–confocal laser scanning fluorescence microscopy.* Soft Matter, 2018.
81. Bando, K. and Y. Yamaguchi, *Mechanical Characterization of APA Microcapsules by Parallel-Plate Compression.* Journal of Membrane and Separation Technology, 2017. **6**: p. 40-47.
82. Liu, K.K., D.R. Williams, and B.J. Briscoe, *Compressive deformation of a single microcapsule.* Physical Review E, 1996. **54**(6): p. 6673-6680.
83. Muller, E., et al., *Characterization of the mechanical properties of polymeric chromatographic particles by micromanipulation.* J Chromatogr A, 2005. **1097**(1-2): p. 116-23.
84. Bando, K., K. Ohba, and Y. Oiso, *Deformation analysis of microcapsules compressed by two rigid parallel plates.* Journal of Biorheology, 2013. **27**(1-2): p. 18-25.
85. Mercade-Prieto, R. and Z. Zhang, *Mechanical characterization of microspheres - capsules, cells and beads: a review.* J Microencapsul, 2012. **29**(3): p. 277-85.
86. Hu, J., X. Zhang, and J. Qu, *Investigation on the mechanical properties of polyurea(PU)/melamine formaldehyde (MF) microcapsules prepared with different chain extenders.* Journal of Microencapsulation, 2018. **35**(3): p. 219-228.
87. Sun, G. and Z. Zhang, *Mechanical properties of melamine-formaldehyde microcapsules.* J Microencapsul, 2001. **18**(5): p. 593-602.
88. Sun, G. and Z. Zhang, *Mechanical strength of microcapsules made of different wall materials.* International Journal of Pharmaceutics, 2002. **242**(1-2): p. 307-311.

89. Hu, J., H.Q. Chen, and Z. Zhang, *Mechanical properties of melamine formaldehyde microcapsules for self-healing materials.* Materials Chemistry and Physics, 2009. **118**(1): p. 63-70.
90. Liu, M., *Understanding the Mechanical Strength of Microcapsules and Their Adhesion on Fabric Surfaces.* PhD thesis. The University of Birmingham, 2010.
91. Ghorbanzadeh Ahangari, M., et al., *Effect of nanoparticles on the micromechanical and surface properties of poly(urea–formaldehyde) composite microcapsules.* Composites Part B: Engineering, 2014. **56**: p. 450-455.
92. Ahmed, A., et al., *A practical methodology for modeling and verification of self-healing microcapsules-based composites elasticity.* Composite Structures, 2018. **184**: p. 1092-1098.
93. Lv, L., et al., *Micromechanical Properties of a New Polymeric Microcapsule for Self-Healing Cementitious Materials.* Materials, 2016. **9**.
94. Guangming, Z., et al., *Determination of the rupture stress of microcapsule and the Young's modulus of its shell materials by nanoindenter.* 2015.
95. Chen, P.W., J. Brignoli, and A.R. Studart, *Mechanics of thick-shell microcapsules made by microfluidics.* Polymer, 2014. **55**(26): p. 6837-6843.
96. Lee, J., et al., *Micromechanical behavior of self-healing epoxy and hardener-loaded microcapsules by nanoindentation.* Materials Letters, 2012. **76**: p. 62-65.
97. Mercadé-Prieto, R., et al., *Determination of the elastic properties of single microcapsules using micromanipulation and finite element modeling.* Chemical Engineering Science, 2011. **66**(10): p. 2042-2049.
98. Yan, Y., et al., *Mechanical characterization of agarose micro-particles with a narrow size distribution.* Powder Technology, 2009. **192**(1): p. 122-130.
99. Kim, K., et al., *Investigation of mechanical properties of soft hydrogel microcapsules in relation to protein delivery using a MEMS force sensor.* J Biomed Mater Res A, 2010. **92**(1): p. 103-13.
100. Berry, J.D., S. Mettu, and R.R. Dagastine, *Precise measurements of capsule mechanical properties using indentation.* Soft Matter, 2017. **13**: p. 1943-1947.
101. Glaubitz, M., et al., *A novel contact model for AFM indentation experiments on soft spherical cell-like particles.* Soft Matter, 2014. **10**(35): p. 6732-6741.
102. Kucerova, J., et al., *PEGylation of magnetic poly(glycidyl methacrylate) microparticles for microfluidic bioassays.* Materials Science and Engineering: C, 2014. **40**: p. 308-315.
103. Aniskevich, A., et al., *Experimental characterisation and modelling of mechanical behaviour of microcapsules.* Journal of Materials Science, 2020.
104. Konnerth, J., W. Gindl, and U. Muller, *Elastic Properties of Adhesive Polymers.* Journal of Applied Polymer Science, 2007. **103**: p. 3936–3939.
105. Glaeser, G., H. Stachel, and B. Odehnal, *The Universe of Conics. From the ancient Greeks to 21st century developments.* 2016: Springer Spektrum.
106. Choudhury, I., et al., *Effect Of TETA Microcapsules On Self-healing Ability Of Dual Component Epoxy System.* Advanced Materials Letters, 2016. **7**(10): p. 836-843.
107. Guadagno, L., et al., *Evaluation of the Mechanical Properties of Microcapsule-Based Self-Healing Composites.* International Journal of Aerospace Engineering, 2016. **2016**: p. 1-10.
108. Bourkas, G., et al., *Estimation of Elastic Moduli of Particulate Composites by New Models and Comparison with Moduli Measured by Tension, Dynamic, and Ultrasonic Tests.* Advances in Materials Science and Engineering, 2010. **2010**: p. 1-13.
109. Pal, R., *New models for effective Young's modulus of particulate composites.* Composites Part B: Engineering, 2005. **36**(6-7): p. 513-523.
110. Loos, M., *Carbon Nanotube Reinforced Composites.* ISBN: 978-1-4557-3195-4, 2015.
111. Fu, S.-Y., et al., *Effects of particle size, particle/matrix interface adhesion and particle loading on mechanical properties of particulate–polymer composites.* Composites Part B: Engineering, 2008. **39**(6): p. 933-961.

112. Bergstrom, J.S. and M.C. Boyce, *Mechanical Behavior of Particle Filled Elastomers.* Rubber Chemistry and Technology, 1999. **72**(4): p. 633-656.
113. Alger, M., *Polymer science dictionary*. 1996: Springer Science & Business Media. 640.
114. Mooney, M., *The viscosity of a concentrated suspension of spherical particles.* Journal of Colloid Science, 1951. **6**(2): p. 162-170.
115. Kim, H.S., S.I. Hong, and S.J. Kim, *On the rule of mixtures for predicting the mechanical properties of composites with homogeneously distributed soft and hard particles.* Journal of Materials Processing Technology, 2001. **112**(1): p. 109-113.
116. *Effective Medium Models.* Effective Medium Theories (available - https://pangea.stanford.edu/courses/gp262/Notes/9.EffectiveMediumTheories.pdf).
117. Alexander, M. and S. Mindess, *Aggregates in Concrete*. Modern Concrete Technology. 2005: CRC Press 448.
118. Young, B.A., et al., *Effective elastic moduli of core-shell-matrix composites.* Mechanics of Materials, 2016. **92**: p. 94-106.
119. Lakes, R., *Introduction to viscoelastic composites* Viscoelastic Composite Materials (available - http://silver.neep.wisc.edu/~lakes/VECmp.html).
120. Hurang, H., O. Landon, and A. Ayo, *Characterizing and Modeling Mechanical Properties of Nanocomposites-Review and Evaluation.* 2010.
121. Yoshitake, I., et al., *A Prediction Method of Tensile Young's Modulus of Concrete at Early Age.* Advances in Civil Engineering, 2012. **2012**: p. 1-10.
122. ADOBE® PHOTOSHOP. Help and tutorials.
123. *Histogram.* PhotoshopMaster (available - https://photoshop-master.ru/lessons/practice/gistogramma.html).
124. *Mathcad: user's guide Mathcad 6.0, Mathcad plus 6.0*. 1997, Филинъ. p. 712.
125. Vidinejevs, S., et al., *Smart polymeric coatings for damage visualization in substrate materials.* Journal of Intelligent Material Systems and Structures, 2012. **23**: p. 1371-1377.
126. *Probability and distributions.* Normal distribution (available - http://www2.stat.duke.edu/~tjl13/s101/slides/unit2lec3.pdf)
127. Bulderberga, O. and A. Aniskevich, *Polymer composite material with inherent function of damage visual indication.* Conference Paper, 21st International Conference on Composite Materials, ICCM 2017; Xi'an; China, 20-25 August, 2017. , 2017.
128. Vidinejevs, S., et al., *Development of a composite with an inherent function of visualization of a mechanical action.* Mechanics of Composite Materials, 2013. **49**(1): p. 77-84.
129. *Prepreg.* Fible Glast Development Corporation (available - https://www.fibreglast.com/product/about-prepregs/Learning_Center).
130. *Trade secret thinning epoxy: Best practice guidance for reducing the viscosity of west system epoxy.* Epoxycraft (available -https://epoxycraft.com/westsystem/thinning-epoxy-best-practice-reducing-viscosity-west-system-epoxy/).
131. Loos, M., et al., *The effect of acetone addition on the properties of epoxy.* Polimeros, 2008. **18**(1): p. 76-80.
132. *Storage and Handling of Prepregs.* The Fibre Reinforced Plastic & Composite Technology Resource Centre (available - http://www.fibre-reinforced-plastic.com/2010/03/storage-and-handling-of-prepregs.html).
133. *ASTM D6862 - 11(2016).* Standard Test Method for 90 Degree Peel Resistance of Adhesives (available - https://www.astm.org/Standards/D6862.htm).
134. Buchmann, C., et al., *Analysis of the removal of peel ply from CFRP surfaces.* Composites Part B, 2016. **89**: p. 352-361.
135. *Peel Ply.* Fible Glast Development Corporation (available - https://www.fibreglast.com/product/econostitch_peel_ply/Vacuum_Bagging_Films_Peel_Ply_Tapes).

136. Kanerva, M. and O. Saarela, *The peel ply surface treatment for adhesive bonding of composites: A review*. International Journal of Adhesion and Adhesives, 2013. **43**: p. 60-69.
137. *Standard ASTM D 3846-02*. In-plane Shear Strength of reinforced plastics.
138. Markham, M.F. and D. Dawson, *Interlaminar shear strength of fibre-reinforced composites*. Composites, 1975. **6**(4): p. 173-176.
139. Tarnopolskii, Y.M. and T.J. Kincis, *Methods of Static Tests for Reinforced Plastics (in Russian)*. Khimia, 1981.
140. Bulderberga, O., A. Aniskevich, and S. Vidinejevs. *GFRP Composite with Damage Visualization Capability*. in *ECCM17 - 17th European Conference on Composite Materials*. 2016. Munich, Germany.
141. Christensen, R.M., *Mechanics of composite materials*. 1979: Wiley.
142. Ahangari, M.G. and A. Fereidoon, *Micromechanical properties and morphologies of self-healing epoxy nanocomposites with microencapsulated healing agent*. Materials Chemistry and Physics, 2015. **151**: p. 112-118.
143. Trat'yakov, Y.D., *Solid-phase reactions (in Russian)*. Sorosovskii Observatelnyi Zhurnal, 1999. **4**: p. 35-39.
144. Braun, M., D. Dollimor, and A. Halway, *Reactions of Solid Bodies*. Mir, 1983.
145. Bulderberga, O., A. Aniskevich, and S. Vidinejevs, *A Glass-Fiber-Reinforced Composite with a Damage Indication Function*. Mechanics of Composite Materials, 2016. **52**(2): p. 155-162.
146. *Technology readiness levels*. HORIZON 2020, Work Programme 2018-2020 (available - https://ec.europa.eu/research/participants/data/ref/h2020/other/wp/2018-2020/annexes/h2020-wp1820-annex-ga_en.pdf).